Doctoral Dissertation
Doctoral Program in Materials Science and Technologies (31st Cycle)

Carbon materials and their role as reinforcement in composite materials

Luca Lavagna
* * * * * *

Supervisor
Prof. Matteo Pavese

Doctoral Examination Committee:
Dott. Adriano Troia, Referee, INRIM, Torino, Italy
Dott. Enzo Laurenti, Referee, Università degli Studi di Torino, Torino, Italy
Dott. Simone Musso, Referee, Aramco Services Company, Houston, USA
Prof. Claudio Gerbaldi, Referee, Politecnico di Torino, Torino, Italy
Prof. Claudio Francesco Badini, Referee, Politecnico di Torino, Italy

Politecnico di Torino
2018

I hereby declare that, the contents and organisation of this dissertation constitute my own original work and does not compromise in any way the rights of third parties, including those relating to the security of personal data.

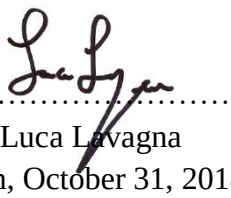

……

Luca Lavagna

Turin, October 31, 2018

Summary

The study of composite materials goes far in time, and their applications are plentiful in almost all fields of engineering. Wattle and daub is one of the oldest man-made composite materials, at over 6000 years old, while some of the most up-to-date applications involve the use of carbon allotropes, that are being extensively studied in the recent years. In fact, carbon fibers, graphene and carbon nanotubes can significantly improve the mechanical, electrical and thermal properties of the matrix in which they are used. These materials have brought tremendous progress in the field of technology. In cement matrix, composites with carbon fibers and carbon nanotubes allows a self-monitoring of the structure. In polymers, the use of graphene can increase not only the mechanical properties but also the thermal ones.

From various studies analyzed over the years, it has emerged that there is a key role of the dispersion of reinforcement in the matrix. In some cases, a bad dispersion can even create a defect in the structure causing a worsening of the properties of materials. Another important point is the interaction between matrix and reinforcement: only with a high interaction there will be a significant increase in properties.

In recent years, it was demonstrated that a chemical treatment on the reinforcement surface can increase the dispersion and the interaction with the matrix. In this work, we studied the effect of chemical treatments on the surface of the reinforcement, with the goal of improving both dispersion and interaction with the matrix. For this goal, we used different matrices, different reinforcement and various approaches. On one side, we tried to understand what is the best chemical treatment for reinforcements that can improve both mechanical and electrical properties of a cement-matrix composite. On the other hand, we tried to demonstrate that a hierarchical arrangement of nano and micro reinforcement can bring to better mechanical properties, overcoming interaction problems between a

polymer matrix and carbon-based reinforcement. In fact, we showed that grafting the nanotubes onto the carbon fibers considerably improves their interface interaction with the matrix, effectively doubling their apparent strength. At the same time, the addition of nanotubes to microfibers reinforcement helps to improve the composite toughness, reaching more than twice the value obtained for the conventional, non-hierarchically reinforced composites.

Acknowledgment

The work presented in this dissertation has been conducted at Department of Applied Science and Technology of Politecnico di Torino. I would like to express my gratitude to all those who helped me to make it possible.

I would like to acknowledge my supervisor Prof. Matteo Pavese for the opportunity to work on this very interesting and promising research topic. Special gratitude to all my friends and colleagues at DISAT, Elisa, Giulio, Alberta, Giorgio, Simone, Alessandro, Gloria, Giulio, Hamed, Mario, Claudio and Eleonora for the support, kindness, patience and good time together. Particular mention for Roberto that supported me all the time in the last period on research and laboratory activities.

I would like to express my gratitude to Dott. Simone Musso for the collaboration and the essential support for the research activity and for having given me the opportunity to start my research in the first period.

Last but not least, my loved family, all my friends for the encouragement and support and a very warm thanks to Valentina for all her love and for everything she did for me.

Contents

List of Tables

List of Figures

Chapter 1

Introduction

1.1 Carbon nanotubes

Carbon is a non-metallic chemical element having symbol C and atomic number 6; it is one of the most abundant elements on earth and is found in nature both in the free state and in numerous compounds. The carbon atom in the compounds can occur in one of the three hybridization forms sp^3, sp^2 and sp; thanks to them the carbon is able to coordinate respectively other 4, 3 and 2 atoms with bond angles equal to: 109.5°, 120° and 180°.

The carbon has an electronic configuration $1s^2\ 2s^2\ 2p^2$, from which it is possible to notice that the complete ionization of carbon is thermodynamically disfavored, both as anion and as a cation; moreover, the value of electronegativity equal to 2.5 causes covalent bonds to form [3]. The thermodynamic stability and the availability to form covalent bonds makes the carbon able to form long chains of atoms fundamental in the development of organic molecules. Carbon is naturally present under two main allotropic forms: graphite and diamond. The cubic diamond and hexagonal graphite have been identified and characterized by X-Ray diffraction in 1912. The “amorphous carbons” was studied only in the middle of the last century with new carbon polymorphic phases. Russian scientists discovered one dimension chain like carbon structures, called carbynes (Donnet et al. 2000; Li et al. 2000); in 1985 fullerene starts to be studied (Kroto et al. 1985); finally in 1991 Iijima identified a curved form of graphene and called it carbon nanotube (Iijima 1991; Bethune et al. 1993; Iijima and Ichihashi 1993).

However, the carbon nanotubes (CNTs) were observed in the previous decades, mostly by Russian researchers. The date of 1991 remain in the history of this materials since their discovery seem to be the starts of a new technological application. This was due both to the technological development that allowed at that time a more facile studies of nano-sized materials. The previous observations of similar materials could not be complete and were generally neglected to the apparent little interest in such a material (Monthioux and Kuznetsov 2006).

Table 1: Schematic classification of the different forms of carbon (Loiseau et al. 2006)

Crystalline form	Diamond	Graphites	Carbynes*	Fullerene Nanotubes
Hybridization	sp^3	sp^2	sp^1	sp^{2+3}
Coordinance z	4	3	2	3
Physical dimensionality D	3	2	1	0 and 1
Bond length (Å)	1.54	1.40	1.21	1.33 to 1.40
Bond energy (eV/mole)	15	25	35	>25

*Also mixed sp^1 and sp^3 hybridizations (α form)

Allotropic forms of elemental carbon are divided into thermodynamically stable and metastable phases. It has been elaborated after several decades of experimental works (Bundy 1996).

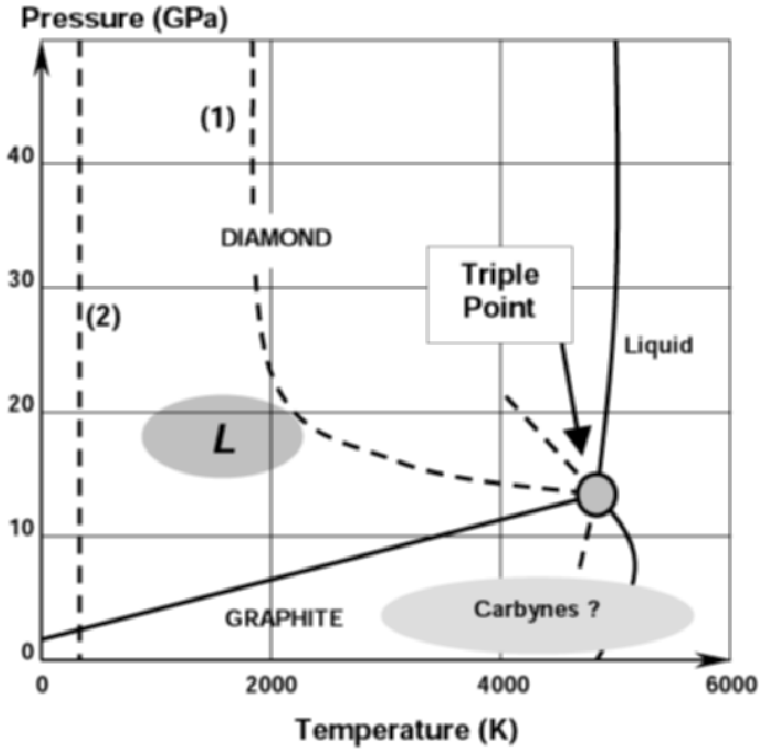

Figure 1: Thermodynamic phase diagram of the carbon element. Solid lines represent equilibrium phase boundaries and dotted lines the kinetic transformations; L isfor lonsdaleite phase (Bundy 1996)

At ambient temperature and pressure, graphite with hexagonal structure is the stable phase that coexist with a polytype and rhombohedral structure. If we move in the graph to more high pressure we can find the cubic diamond that is an hexagonal phase known as lonsdaleite. The carbyne phase should exist at high temperature, below the melting line of graphite. All the transformations from a form to another are considered theoretically reversible. Under this frame it does not appear evident to include in the same diagram the new molecular carbon phases, fullerenes and nanotubes which are not classical extended solids but can form themselves crystalline structures.

New carbon species with particular properties had developed several theoretical model during last decades (Cohen 1994, 1998).

In carbon nanotubes, the total cohesion energy can be decreased by curving the graphene sheets and forming closed structures as cylinders. A topological classification for curved surfaces, in non-Euclidian geometry, was proposed by Schwarz (Schwarz 1890). A simple approach is to define a mean (H) and a Gaussian (K) curvatures proportional to the inverse of a length and a surface, respectively. As proposed by Mackay and Terrones (MACKAY and TERRONES 1991), the following geometrical shapes may exist:

– K >0 (spheres) as fullerenes

– K = 0 (planes or cylinders if H = 0), as nanotubes

– K <0 (saddle): “Schwarzites”.

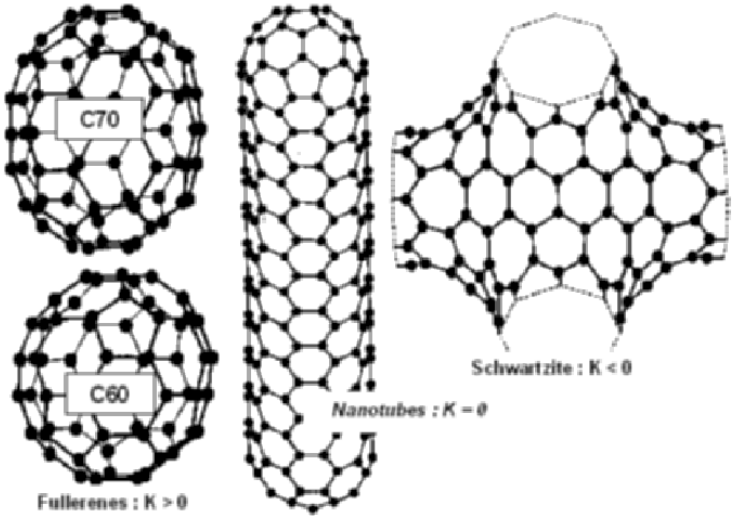

Figure 2: Examples of curved graphene varieties classified through their gaussian curvature K

Negatively curved carbon networks belong to the class of periodic minimal surfaces and they have been called “Schwarzites”, in honour of Karl Hermann Amandus Schwarz that was a German mathematician, known for his work in complex analysis. This curvature is made possible by introducing seven or eight member rings in addition to the usual six member for planar surfaces. In spite of different attempts, these big unit cells have not been observed experimentally. The same holds for a positive curvature owing to a five member ring (case of C_{60}).

Single-wall nanotubes are cylindrical shaped with carbon atoms organized in a honeycomb lattice. Due to their structure, they introduce some s-p ibridation and their Coordination number is three (z = 3). Single-wall carbon nanotubes (SWCNTs) are normally describe as a rolling a graphene sheet. Because of this construction it is possible to characterize the CNT structure with a pair of integers (n,m). These indices define the so-called “chiral vector”:

$$\vec{C} = n\overrightarrow{a_1} + m\overrightarrow{a_2}$$

which joins two crystallographically equivalent sites of the nanotube on the graphene sheet, $(\overrightarrow{a_1},\overrightarrow{a_2})$ being the graphene basis where $a = |\overrightarrow{a_1}| = |\overrightarrow{a_2}| \approx 2.49$ Å. The conventional basis chosen in crystallography for a graphene sheet is a basis $(\overrightarrow{a_1},\overrightarrow{a_2})$ where the angle between the vectors is 120° (Hamada et al. 1992). The angle between reciprocal vectors $\overrightarrow{a_1}^*$ and $\overrightarrow{a_2}^*$ is 60° and allows one to use the well-known (h, k, $l = -h - k$) notation: the wave-vectors are equivalent for circular permutations of the h, k, l indices which describe three-fold rotations. However, the basis which is the most frequently used in nanotube literature is the one with $(\overrightarrow{a_1},\overrightarrow{a_2}) = 60°$ (Robertson et al. 1992).

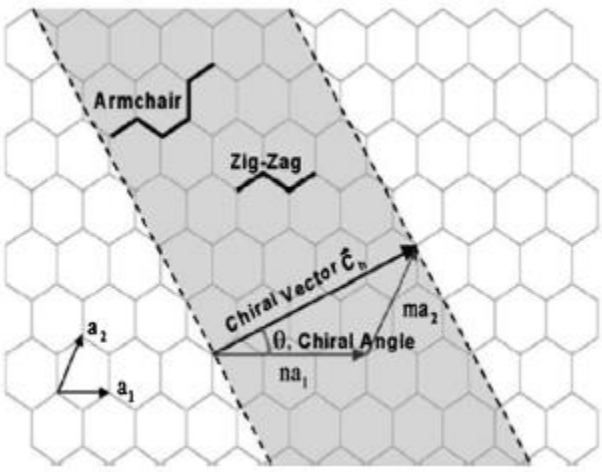

Figure 3: Schematic diagram showing how a hexagonal sheet of graphene is rolled to form a CNT with different chiralities (Thostenson et al. 2001)

The nanotube is obtained by cutting a ribbon of perpendicular basis $\overrightarrow{C}$ in the sheet and by rolling it up, as shown in figure 4 (Dresselhaus et al. 1995). The tube circumference could be written as:

$$\vec{C} = \left|\vec{C}\right| = a\sqrt{n^2 + m^2 + nm}$$

The hexagons orientation on the tube surface is characterized by the "chiral angle" θ:

$$\theta = \arctan\left(\sqrt{3}m/(2n + m)\right)$$

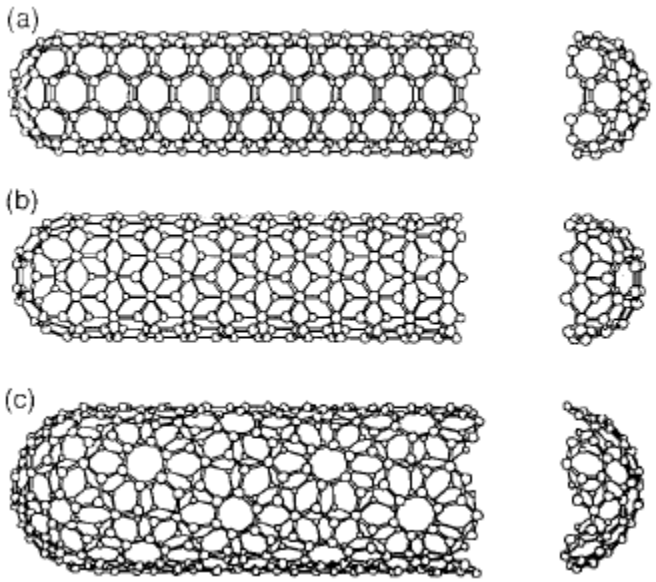

Figure 4: A schematic theoretical model for single-wall carbon nanotube with different chiralities (Dresselhaus et al. 1995)

Carbon nanotubes has different chiral angles in function of their chiralities and are classified in different structure. A schematic theoretical model for a single-wall carbon nanotube is shown in figure 4, with the tube axis normal to: (a) the $\theta = 30°$ direction (an "armchair" tubule), (b) the $\theta = 0°$ direction (a "zigzag" tubule), and (c) a general direction B with $0° < |\theta| < 30°$ (a "chiral" tubule). The actual tubules shown in the figure correspond to (n,m) values of: (a) (5,5), (b) (9,0), and (c) (10,5).

1.1.1 Carbon nanotubes synthesis methods

The Electric Arc Discharge Technique

This method is based on an arc discharge generated between two graphite electrodes placed face to face in the instrument chamber under a partial pressure of helium or argon (typically 600 mbar). The temperature of 6000 °C of this instrumentation allows the graphite to sublimate. Carbon atoms are ejected from the electrodes forming a plasma due to the fact that a very high pressure it is necessary during the process,. These atoms move toward colder zones within the chamber, and a nanotube deposit on the cathode follows.

Iijima used an apparatus of this kind in his early experiments. He produced multiwall nanotubes in the soot. Later, single-wall carbon nanotubes were grown with the same set-up by adding to the electrodes suitable catalyst particles, e.g. of Fe, Co, Ni or rare-earth metals (Loiseau et al. 2006)

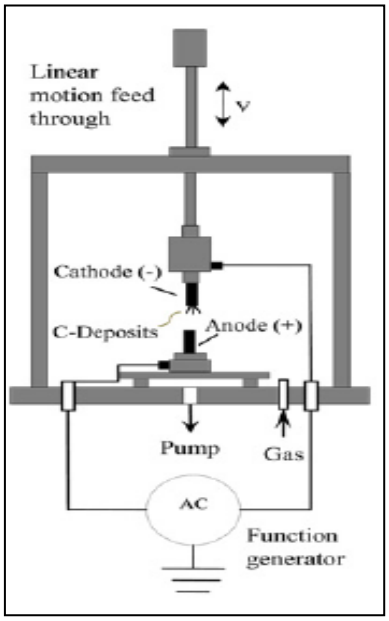

Figure 5: A typical arc-discharge apparatus (Merchan et al. 2010)

The working conditions hugely influence the carbon nanotubes properties: in presence of small amounts of transition metals such as Fe, Co, Ni in the graphitic anode material (and leaving the cathode as pure graphite) single-wall carbon nanotubes results the main product. A hydrocarbon gas introduced into the arc discharge is more favourable to yield CNTs than fullerenes (Ando 1994). In absence of such catalysts, the formation of multiwall carbon nanotubes is favoured.

Laser Ablation

The process is based on the sublimation of a mix made of graphite and metallic catalyst induced by laser impulses. The synthesis is done in a quartz tube inserted in furnace at 2700-3200 °C in He or Ar atmosphere; the gas flux allows the deposition of carbon atoms and catalyst particles on a collector at lower temperature as is sketched in figure 6. By varying the temperature of the collector and the gas flow rate it possible to control the growth of the nanotubes (Alfredo M. Morales and Charles M. Lieber 1998).

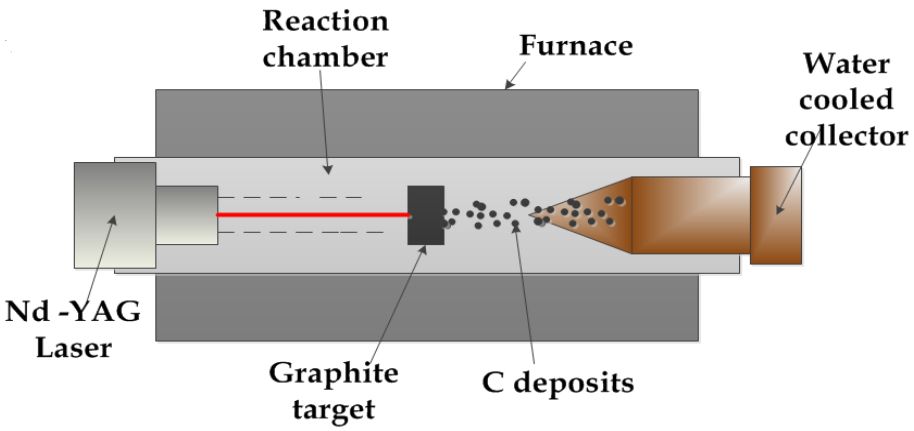

Figure 6: Laser ablation apparatus for the production of CNTs (Gore and Sane 2011)

Vaporisation induced by a solar beam

This technique consist in a solar furnace in which the sunlight is focused on a graphite sample to vaporize the carbon. The vapour is then condensed in a cold dark zone of the reactor. The sunlight ray is concentrated by a flat tracking mirror and reflected towards a parabolic mirror which focuses the radiation directly on the graphite target (figure 7). Under clear-sky conditions, temperatures of around 3273 °C can be reached at the 2-kW set-up of the solar station and the evaporation process can start. At the beginning only fullerenes were produced with this technique (Laplaze et al. 1994), but since 1998 also nanotubes were obtained, just by changing the target composition and adjusting the experimental conditions (Laplaze et al. 1998).

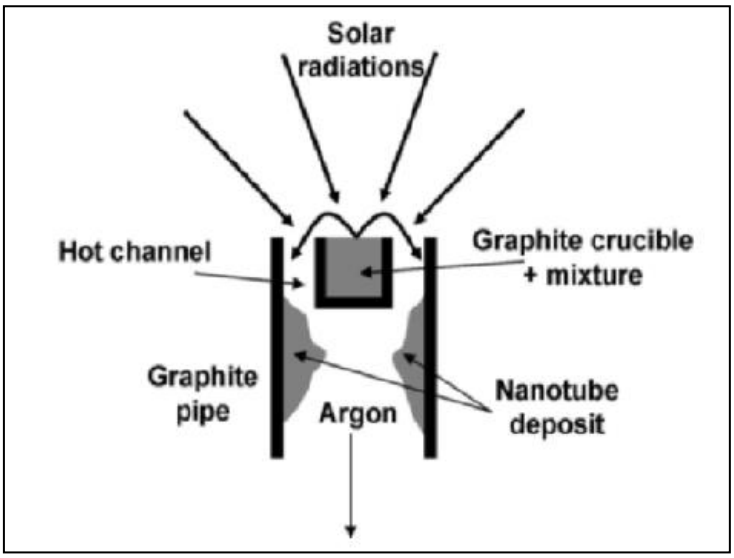

Figure 7: Principle of the solar furnace technique (Loiseau et al. 2006)

1.1.2 Synthesis of MWCNTs and SWCNTs via medium-temperature routes Chemical Vapor Deposition

In this case, the nanotubes are produced by the decomposition of a gas containing carbon, where the carbon atoms would rearrange themselves in a CNTs structure. This technique is easier to be performed, and so it is suitable for industrial production but leads to the formation of lower quality nanotubes (Valentin N. Popov 2004). In a CVD process it is possible to have an effective control on the nanostructures growth by regulating process variables such as temperature, gas flow rate and the chemical nature of reactants and catalysts; in this way the nanotube growth can be favored with respect to the production of other carbon allotropes. During this process an organic precursor, usually methane, is transported by a flow of inert gas on a metallic catalyst (Fe, Co, Ni) (Alan M. Cassell et al. 1999). A scheme of a CVD apparatus is given in figure 8.

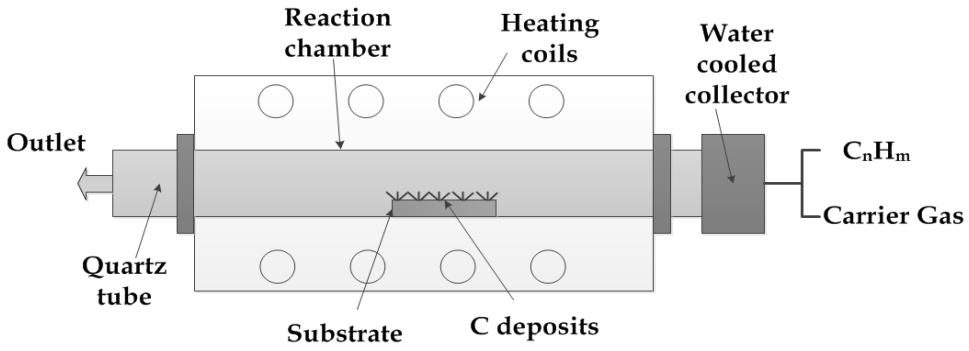

Figure 8: Scheme of a chemical vapor deposition apparatus (Gore and Sane 2011)

The morphology of the catalyst affects the morphology of the product, in particular, it has been proven that catalyst in the form of thin film can lead to a lower diameter CNTs, usually the catalyst thin film has a thickness of 20 nm and it is produced by electron beam deposition. The synthesis occurs in a hydrogen-argon atmosphere at 700-1200 °C for SWCNT while for MWCNT 400-700 °C are reached. The key steps of the process are the diffusion of the precursor in order to reach the substrate, the adsorption on the catalyst surface, and the chemical reactions that lead to the growth of the nanostructures. The steps described above are reversible ones so it is possible to observe also the desorption of the species from the catalyst and their diffusion through the substrate and their diffusion in the vapor phase. Being CVD a multiple-step process it is crucial to identify the

kinetically controlling one and adjust the process parameter in order to maximize the kinetic of the overall process (Alan M. Cassell et al. 1999).

1.1.3 Properties of CNTs

Electrical properties

Single-walled carbon nanotubes (SWCNTs) may be either metallic or semiconducting depending on how the graphite layer is wrapped into a cylinder (Mintmire et al. 1992; Hamada et al. 1992) as shown in figure 4. Carbon nanotubes with the hexagons orientated in the configuration labeled armchair (hexagons are lined up parallel to the axis of the nanotube) have electrical properties similar to metals. The electrical resistivity through the same graphite cylinder in a MWCNT is much lower than that between the shells (Hone et al. 2000). In conventional graphite, the electrical resistivity is in the order of 2.5–5×10^{-6} Ω m in the direction perpendicular to the basal plane and approximately 3×10^{-3} Ω m in the direction parallel to the basal plane (Pierson 1993). The resistivity of MWCNTs is in the range of 5×10^{-8}–6×10^{-2} Ω m, spanning from metallic to semiconducting (Ebbesen et al. 1996). Using the needle of a scanning-force microscope as electric contact, Dai et al.(Dai et al. 1996) found the resistivity of MWCNTs produced by catalytic process to be in the range of 8–20×10^{-6} Ω m. In comparison, a high quality carbon fibre has an electrical resistivity of approximately 1×10^{-6} Ω m (de Pablo et al. 1999) and amorphous carbon 5–8×10^{-4} Ω m (Dasgupta et al. 1991). Structural defects in a SWCNT or in the same shell of a MWCNT can cause an increase of electrical resistivity, and subjecting the CNTs to annealing can reduce their resistivity (Wang et al.; Dai et al. 1996).

The other two possible chiral orientations of carbon nanotubes share electrical properties similar to semiconductors. Those with the hexagons oriented in a circle around the nanotube have a configurations labeled zigzag. Those with a twist to the nanotube so the hexagons do not form any line are called chiral. These last two chiral configurations may only conduct an electric current when an high energy in the form of light or an electric field is applied to free electrons from the carbon atoms(Lu and Chen 2005).

Mechanical properties

Table 2. Main mechanical properties of different kinds of CNTs and comparison with graphite and steel.

Table 2: Mechanical properties of CNTs adapted from (Callister 2001)

	Young Modulus [GPa]	Tensile Strength [GPa]	Density [g/cm^3]
MWNT	1200	150	1.34
SWNT	1054	75	1.3
Bundle of SWNT	563	150	1.3
Carbon Fibers	350	2.5	2.1
Steel	208	1	7.8

The study of physical and mechanical properties of CNTs arouse a remarkable interest since their discovery, many studies have been conducted theoretically, experimentally and by computer simulation. The outstanding tensile properties are the results of the σ bonds between the carbon atoms, which are the strongest bonds existing in nature, moreover thanks to the refolding of the graphene sheets in a tubular structure the mechanical properties are remarkably increased in the axial direction. Both experimental data and theoretical calculation showed that Young modulus of SWCNT depends on the diameter of the tubes and not their chirality, the highest value of about 1 TPa is obtained by CNTs with a diameter of 1-2 nm. Another interesting property is the ability of CNTs to stand high levels of plastic deformation without breaking; they can stand an axial deformation of 16% without breaking. These characteristics combined with their low density seems to constitute the real force with respect to carbon fibers used nowadays (Valentin N. Popov 2004).

The use of carbon nanotubes as a reinforcing material in composites would lead to an increase in the mechanical resistance of the system as a whole. However, the achievement of this result would depend on the possibility of dispersing effectively the nanotubes in the matrix generating a good adhesion

between the matrix and the filler in such a way that the stress would be transferred evenly and without shearing phenomena.

The critical issue is then the scarce wettability of CNTs due to high number of Van der Waals interaction that limits their potential in many applications (Marchisio Silvia 2013).

1.2 Graphene

Graphene is a planar film composed of carbon atoms with sp^2 hybrid orbital and has a honeycomb-like lattice structure. It is a two-dimensional (2D) material of only one atomic layer thickness. Fullerene (0-dimensional), carbon nanotube (1-dimensional), and graphite (3-dimensional) can be formed from this basic constituent element, and can be regarded as infinite aromatic molecules (figure 9). Since its discovery in 2004, graphene has received considerable scientific interest for its unique mechanisms and excellent thermal, electrical, optical, and other properties (Novoselov 2004; Geim and Novoselov 2007; Castro Neto et al. 2009; Balandin 2011).

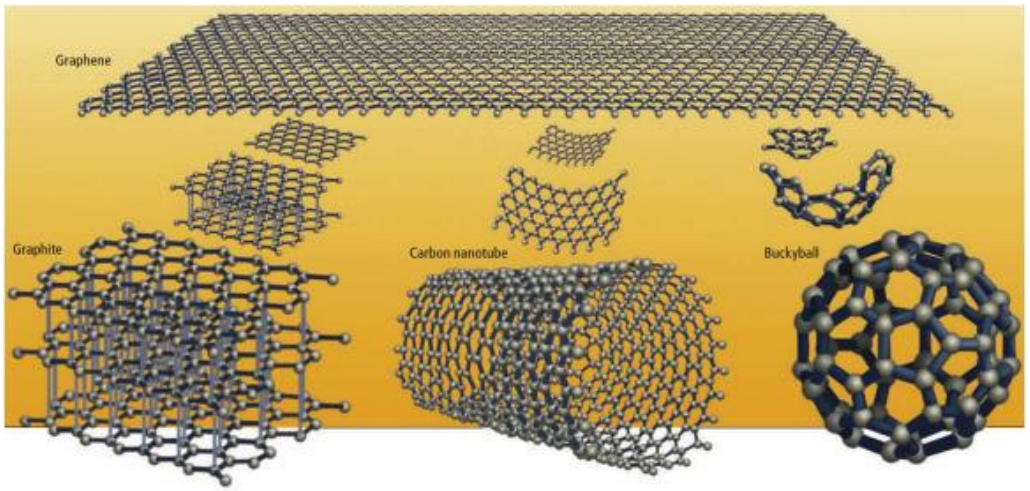

Figure 9: Graphene is the basic unit of various carbon compounds (GEIM and KIM 2008)

1.2.1 Graphene synthesis

There are innumerable method and articles where is describe “how to produce graphene”, many of them are repetition of these three classical method that are classified in function of the methodology. For a real idea of overall methods, take notice of the Table 3 at the end of this chapter.

Micromechanical cleavage

In 2004, the nobel prize Novoselov published a paper detailing electronic measurements made on single- and few-layer graphene (Novoselov 2004). They obtained this graphene by removing layer of graphite from a pencil using a tape. This technique was called micromechanical cleavage.

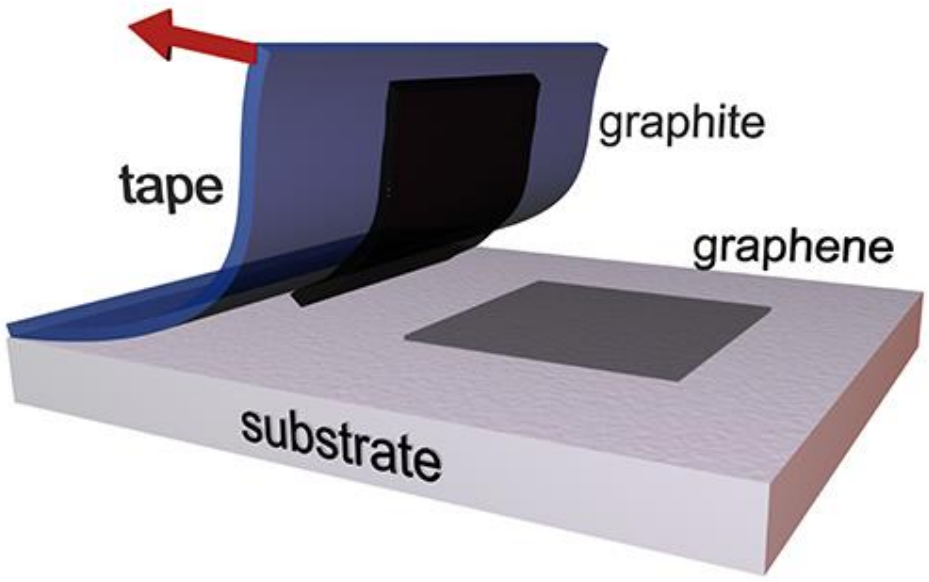

Figure 10: Micromechanical cleavage, a.k.a. the scotch tape method (Badini et al.)

This method was not a novelty; several researcher used the same method to obtain suitable surfaces for atomic force microscopy and scanning tunneling microscopy for many years. The novelty of this methodology was in realizing that the thin flakes obtained by micromechanical cleavage could be further cleaved into successively thinner samples. With this breakthrough, Novoselov could perform experiments demonstrating the unique electronic structure of single-layer graphene, namely the observation of the anomalous quantum Hall effect, confirming the Dirac-fermionic behavior of the charge carriers in graphene.

Liquid-phase mechanical exfoliation

As it is known carbon is insoluble in standard condition. This observation has been a major obstacle for studying carbon nanotubes, as the tubes tend to

aggregate in bundle and do not solvate by any commonly available solvents. Various approaches have been used to circumvent this problem and isolate individual carbon nanotubes as is explain later in this work. These approaches generally pursue one of two strategies. In the first strategy, nanotubes are mixed with a solution of water and surfactant and are sonicated; the hydrophobic group of the surfactant interacts with the hydrophobic nanotube, while the hydrophilic group of the surfactant stabilizes the individual nanotubes in solution. In the second strategy, the nanotubes are sonicated directly in a solvent that can solvate the nanotubes. The solvent used must have a surface tension near to the surface energy of the carbonaceous material. The decreases the energetic penalty between nanotubes and solvent allowing the separation of nanotubes from their bundles and enables a fraction of weakly dispersed nanotubes to persist in solution. For the exfoliation of graphene, in high quantity, can be used the same methods explained before. The sonication of graphite powder in N-methylpyrrolidone and centrifugation create a dispersion of unexfoliated graphite pieces with concentrations of few layer of graphene lower than 1 $\%_{wt}$. This dispersion showed remarkable stability toward aggregation over a period of weeks to months (Hernandez et al. 2008). Surfactant-assisted graphene exfoliation is another well-established technique, with many surfactants being employed (Lotya et al. 2009, 2010).

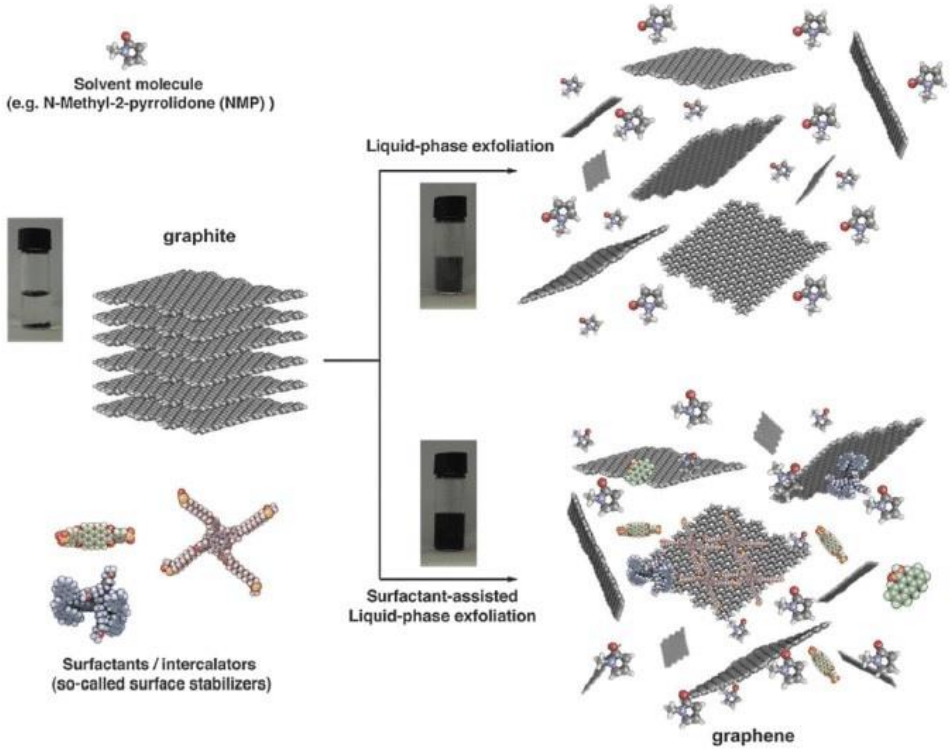

Figure 11: Schematic representation of the liquid-phase exfoliation process of graphite in the absence (top-right) and presence (bottom-right) of surfactant molecules (Ciesielski and Samorì 2014)

Chemical cleavage and exfoliation

In 1859, in an attempt to measure the atomic weight of carbon, Benjamin Brodie performed some of the first experiments on the chemical reactivity of graphite (Brodie and F. R. S. 1859). In their experiment, graphite can be oxidized using a mixture of nitric acid and potassium chlorate for several days. At the end of this experiments, they obtained "…a substance of a light yellow colour, consisting of minute transparent and brilliant plates." They went on to evaluate many properties of what they called "graphic acid," which we today call graphene oxide (GO). Nearly a century later, the Hummers and Offeman method was used to obtain graphene in a "significantly" safer synthesis. In this method graphene oxide is obtained from graphite using a solution of sodium nitrate, sulfuric acid, and potassium permanganate (Hummers Jr and Offeman 1958). This method is most used for the production of graphite oxide in the lab. Recently more green method are developed to overcome the use of heavy strong acid and sodium that is an impurity in the graphite lattice and it is difficult to remove from graphene oxide after his production (Chen et al. 2013).

Table 3: Different method to produce graphene from graphite structure and from other carbon (Whitener and Sheehan 2014)

Production method		Advantages	Disadvantages
From graphite	Mechanical cleavage	• Simple, inexpensive • Usable with many different layered materials • Suitable for demonstrations	• Too inefficient for mass production • Yields mainly few-layer to many-layer graphene • Dimensions constrained by size of initial crystal
	Liquid-phase exfoliation	• Simple and inexpensive • Faster than mechanical cleavage • Less damaging than chemical exfoliation	• Dimensions constrained to size of initial crystal • Not high-yielding
	Graphite oxide/fluoride reduction	• Inexpensive • Industrial-scale production • Reducible to rGO/rGF • Allows for expanded chemistry on graphene	• Processing degrades electronic properties • Not completely reversible • Dimensions constrained to size of initial crystal
	Intercalation compound exfoliation	• Cleaner than GO production and reduction • Exfoliation is very efficient	• Requires special processing techniques • Dimensions constrained to size of initial crystal
Not from graphite	Epitaxial silicon carbide decomposition	• Large-area single layer and few layer graphene • Growth directly on insulating substrate • Easily transferrable to arbitrary substrates	• Requires specialized equipment and apparatus • Very expensive to produce • Single crystal size limited to SiC terrace size
	CVD growth	• Arbitrarily large area graphene • Self-limiting to a single or few layers • Large single-crystal growth • Easily transferrable to arbitrary substrates	• Still somewhat expensive compared to GO • Transfer can contaminate and damage graphene sheet
	Bottom-up chemical synthesis	• Atomically precise • Simple chemical process	• Very low yield • Field is too new for confident predictions

1.2.2 Properties of graphene

Electrical properties

There are three σ bonds in each elementary cell of graphene. The p orbitals of all carbon atoms are perpendicular to the hybridization plane of sp^2 and form a delocalized π bond in a shoulder-by-side fashion, which runs through the whole graphene, so that π electrons are free to move in the plane (Hamada et al. 1992; Yan et al. 2009; Dresselhaus et al. 2010). Graphene has a good conductivity, and, at room temperature, it exhibits semi-integer quantum Hall effect, bipolar electric field effect, superconductivity, high carrier rate, and excellent electrical properties. At room temperature, its carrier mobility can reach 15,000 $cm^2/V{\cdot}s$. The electrons in the band conduction and the holes in the band valence are collectively referred to as the electron-hole pairs, and the electrons and holes are free to move into free carriers. Together, they create an electrical conduction under the action of external electric field to form macroscopic currents.

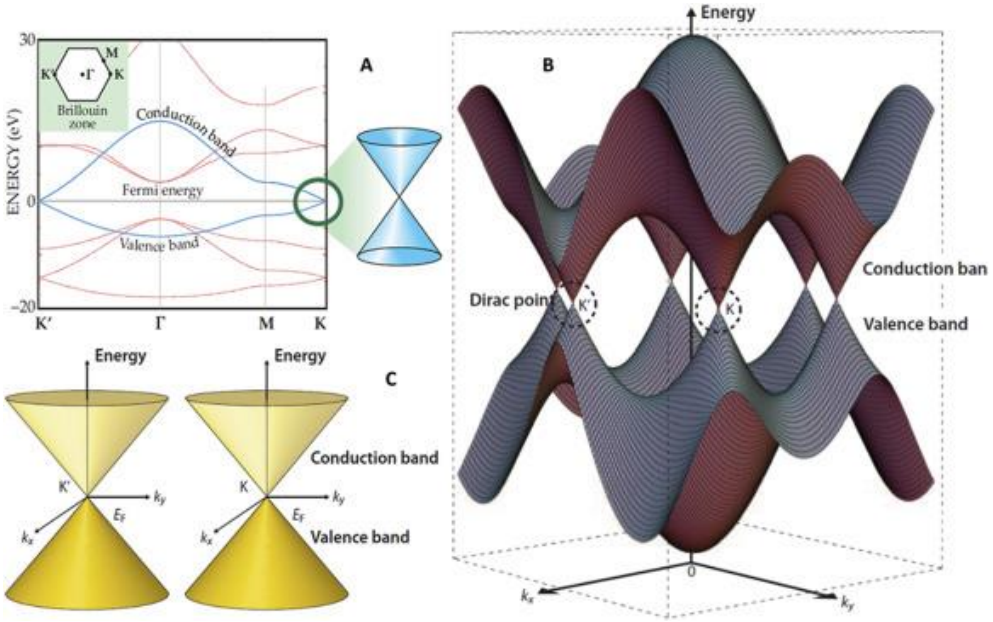

Figure 12: Band structure near the Fermi level of graphene. (A) 2D schematic diagram (Bodenmann and MacDonald 2007), (B) 3D schematic diagram, and (C) Dirac cone of K and K′, which correspond to the Fermi level of (B) (Ando 2009)

Most of the experimental research on graphene focuses on the electronic properties. The tune effect of graphene with its properties of transistor is extensively studied. This effect is most pronounced in the thinnest samples whereas samples from multiple layers show much weaker gate dependence due to screening of the electric field by the other layers. With an high magnetic field and at low temperatures the quantum hall effect for both electrons and holes can be observed(Novoselov et al. 2005; Zhang et al. 2005). The graphene quantum hall effect is little bit different from conventional quantum Hall effect. In this typology, the plateaus occur at half integers of $4e^2/h$ rather than the typical $4e^2/h$.

Unfortunately, graphene has no band gap and correspondingly resistivity changes are small. Therefore, a graphene transistor by its very nature is plagued by a low on/off ratio. To overcome this problem it is possible carve graphene into narrow ribbons. By shrinking, the ribbon the momentum of charge carriers in the transverse direction becomes quantized which results in the opening of a band gap, proportional to the width of the ribbon. This effect is evident in carbon nanotubes where a nanotube has a band gap proportional to its diameter. The studies about opening of a band gap in graphene ribbons are addressed on wide ribbon devices lithographically patterned from large graphene flakes (Han et al. 2007) and in narrow chemically synthesized graphene ribbons (Li et al. 2008b).

Mechanical properties

"Graphene is the strongest material ever tested"; with this sentence Lee et al. (Lee et al. 2008) declared the extraordinary properties of this material with an intrinsic tensile strength of 130.5 GPa and a Young's modulus of 1 TPa. The impressive mechanical properties of graphene are one of the reasons that make graphene one of the most used materials as a reinforcing agent in composites. The reason of its exceptional mechanical properties lies in the stability of the sp^2 bonds that form the hexagonal lattice and oppose a variety of in-plane deformations (Papageorgiou et al. 2017). The maximum stress was obtained using the equation:

$$\sigma_m^{2D} = \left(\frac{FE^{2D}}{4\pi R}\right)^{1/2}$$

where E^{2D} is the second order elastic stiffness, R is the tip radius and F is the applied force. However, the breaking strength of 55 N m^{-1} which can be obtained by this equation cannot be considered accurate, due to the fact that the model used ignores non-linear elasticity. The breaking force obtained experimentally and from simulation was almost identical and the experimental value of the second order elastic stiffness was equal to E^{2D} = 340 ± 50 N m^{-1}. This value corresponds to a Young's modulus of E = 1.0 ± 0.1 TPa, assuming an effective thickness of 0.335 nm (Lee et al. 2008).

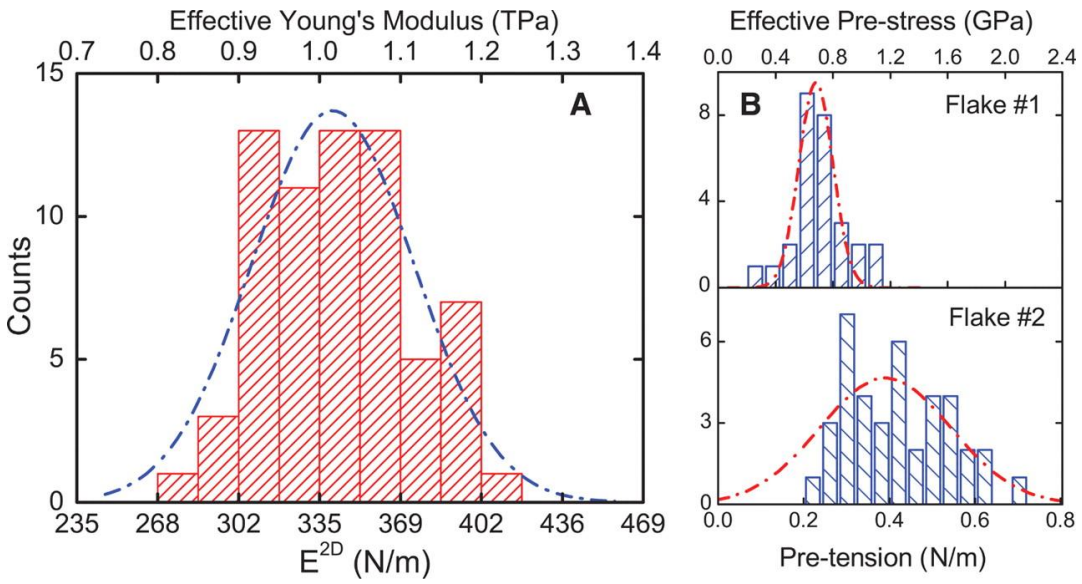

Figure 13: Elastic response test results. (A) Histogram of elastic stiffness. (B) Histogram of film pretensions. Dashed lines in both plots represent Gaussian fits to data. The effective Young's modulus and prestress were obtained by dividing the graphite interlayer spacing.(Lee et al. 2008)

Zandiatashbar et al.(Zandiatashbar et al. 2014) have studied the effect of defects on the intrinsic strength and stiffness of graphene. Interestingly, the strength and the stiffness of graphene is maintained also with a defective structure. The breaking strength, in this case, is only 14% lower than the pristine graphene. Once the material passes into the vacancy-defect regime however, its strength drops significantly.

The toughness of graphene is similar to most fibers and membranes and depends on their weakest link where failure initiates. Additionally, in the numerous attempts to scale up of the production of large graphene sheets, the accomplishment of this venture will probably result in a material that contains more defects, and therefore possesses inferior mechanical properties (Papageorgiou et al. 2017).

1.3 Carbon fibers

Carbon fibers (CF) are defined by IUPAC as fibers containing at least 92% of carbon by mass fraction. The first example of such material dates back 1879 when Thomas Edison used charred cotton threads to conduct electricity in a light bulb (Bacon and Moses 1986). In the 1950 researchers started to use regenerated cellulose to produces continuous carbon fibers in the attempt of obtaining a light

and stiff material for aerospace applications; the idea came from the fact that the C-C bond is the strongest existing in nature, so a fiber containing a lot of these bonds would provide a valuable reinforcement (Bacon and Moses 1986). Nowadays CFs are widely used in advanced composites and are product in a large variety of forms, which can be categorized according to:

- the starting material;
- the performance;
- the tow size, i.e. the number of filaments contained in a newly produced bundle.

According to tow size the historical classification sorts CF tows of 3000, 6000, 12000, 24000 filaments.

The performance based classification divides CFs in:

- Low modulus ($E < 200$ GPa)
- Standard modulus ($E \approx 230$ GPa)
- Intermediate modulus ($E \approx 300$ GPa)
- High modulus ($E > 350$ GPa)
- Ultra high modulus ($E > 600$ GPa).

Finally, basing on the starting material it is possible to distinguish between CFs obtained by carbonization of a precursor fiber and CFs synthetized directly from a hydrocarbon gas. By carbonization process it is possible to obtain carbon fibers from Rayon, PAN and Pitch residues, the starting material affects the production process and the final performance of the fiber itself (J. G. Lavin 2001).

1.3.1 Carbon fibers synthesis

Rayon based carbon fibers

These kind of fibers showed a low modulus due to the scarce organization of the atomic structure of carbon. This is related to the fact that cellulose possess only 24%$_w$ of carbon atoms, so, the material obtained upon removal of heteroatoms will possess a high number of structural defects. This material shows scarce mechanical properties that limits its use in high performance applications, but its natural porosity combined with low production cost makes it an interesting precursor for activated carbon fibers used in filtration and environmental applications (A. Ferri 2015).

PAN based carbon fibers

These fibers were firstly produced in 1960, nowadays the 90% of produced carbon fibers are obtained polyacrilonitrile precursor whose molecular structure and polymerization route are described in figure 14 [78].

The greatest advantage of starting from PAN consist in the fact it contains around the 67%$_w$ of carbon and this allows obtaining a fiber with 90%$_w$ of carbon without defects.

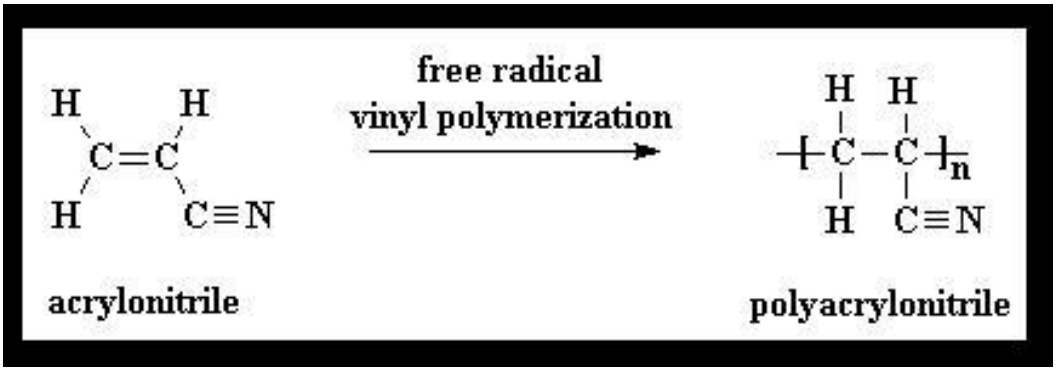

Figure 14: Molecular formula and polymerization route of PAN

The production process consists in two main steps: the spinning of the PAN and the carbonization of the obtained fiber. Since the PAN does not melt before 300 °C, the solution spinning technique is used; the spinning apparatus is sketched in figure 15.

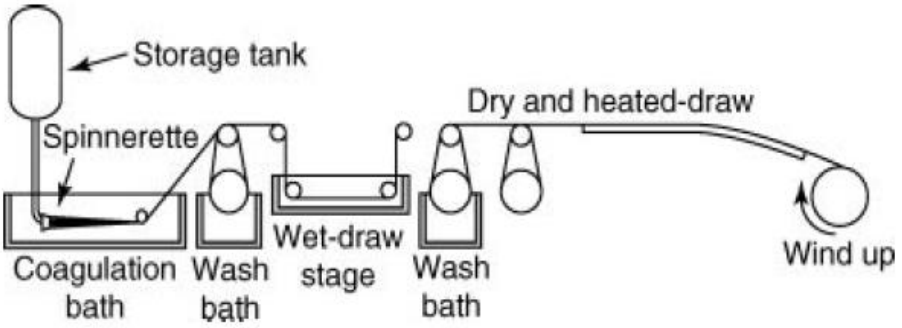

Figure 15: Wet spinning apparatus to produce PAN fibers (A. Ferri 2015)

A concentrated solution containing 93–95 wt% of polyacrylonitrile is obtained by using dimethylacetamide (DMA) as solvent and it is put in the storage tank. The solution is filtered to minimize impurities and passed through a spinneret. The fibers emerge through the small capillary holes directly into a

coagulation bath containing ethylene glycol that extracts the solvent from the fiber. The rate of solvent removal allows control the shape and the texture of the fiber. As soon as it emerges from the coagulation bath the fiber undergoes a sequence of post spinning steps such as washing drawing and drying (J. G. Lavin 2001).

The next processing step consists in the carbonization of the spun fibers as sketched in figure 16.

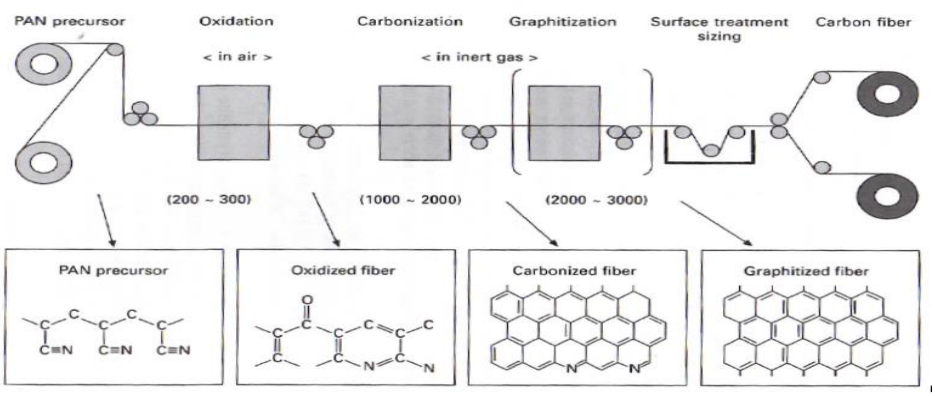

Figure 16: Graphitization process for carbon fibers production (A. Ferri 2015)

The first critical step in the production of carbon fibers from PAN fibers is to react the nitrile functional groups to form cycles. This reaction must be thermally activated and it is highly exothermic; the fibers have to be made infusible by oxidation in air at 200-300 °C for ten minutes, this will allow the material to stand the higher temperatures.

After oxidation, the fibers are carbonized at about 1000 °C in an inert atmosphere (normally nitrogen) for a few hours. During this process, the non-carbon elements are removed to give carbon fibers with a yield of about 50% of the mass of the original PAN.

Depending on the type of fiber required, a graphitization step is carried out at temperatures between 1500-3000 °C, this allows an improvement of the ordering and orientation of the crystallites in the direction of the fiber axis(J. G. Lavin 2001).

Even though PAN based CFs are conventionally called graphite fibers their structure cannot achieve the order of graphitic lattice, instead the large aromatic sheets are randomly oriented in a turbostratic structure (turbulent and stratified); the graphene planes are uneven and wavy with a mean interplanar spacing

significantly greater than the 0.335 nm of graphite as sketched in figure 17 (J. G. Lavin 2001).

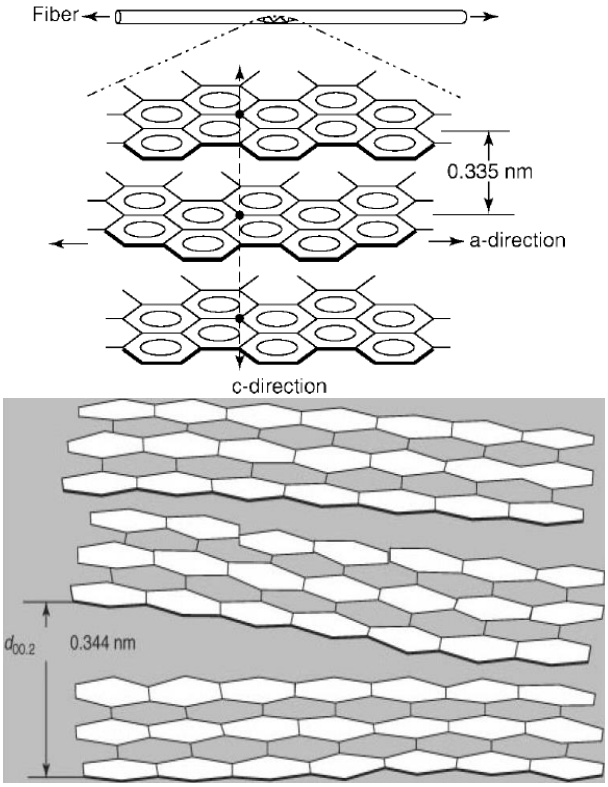

Figure 17: Representation of graphitic planes inside the carbon fibers (A. Ferri 2015)

Since the heat treatment causes a weight loss of 50%, the final structure will contain many longitudinal voids that will lead to a lower density (1.8 g/cm^3) than the pure graphite (2,28 g/cm^3) (J. G. Lavin 2001). Carbonized PAN shows a fibrillar microstructure that may be viewed as undulating ribbons with high flexibility, the fiber surface consists of planar microcrystallites aligned parallel to the fiber axis; the absence of functional groups on the surface makes this material quite chemically inert (J. G. Lavin 2001).

Pitch based carbon fibers.

While in PAN based fibers the starting material is a very pure polymer with high molecular weight, here the starting material is a by-product with unknown and variable composition. Pitch consists of an heavy fraction of aromatic hydrocarbons residues of oil refining processes, coal processing and steel industry; even though the exact composition of pitch has never been identified the carbon mass fraction of this material ranges from 80 to 90% making it an

interesting material for the purpose of CFs production (A. Ferri 2015). A general sketch of a pitch molecule is given in figure 18.

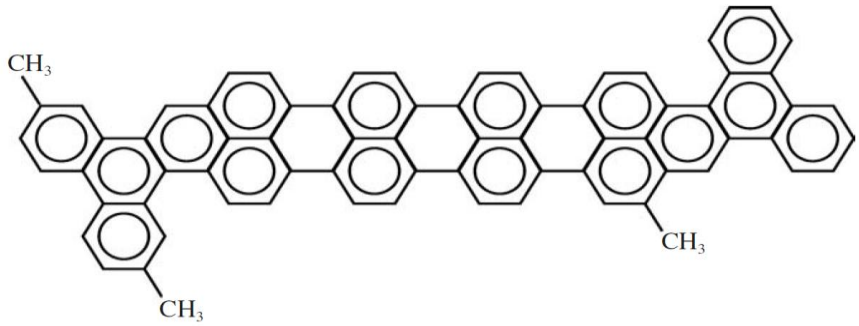

Figure 18: General represantation of a pitch molecule (A. Ferri 2015)

Isotropic pitches are glassy solids that can be softened upon heating achieving at 280 °C a low enough viscosity to be drawn (J. G. Lavin 2001). The pitch, then, is spun either by centrifugal spinning or by melt blowing obtaining short fibers (3-200 mm). The carbonized isotropic pitch fibers are not graphitized leading to inferior mechanical properties of the final fibers also called general purpose fibers (J. G. Lavin 2001). On the other hand, high performance fibers can be obtained from mesophase pitch in which the molecular structure has a degree of order typical of the liquid crystals (LC). During the thermal treatment of aromatic hydrocarbons, between 400 and 550 °C, it is observed the formation of a LC phase of spheroids with a mosaic structure within the continuous isotropic phase. As the pyrolysis progresses the spherules grow and coalesce and finally the phase inversion occurs making the mesophase to become the continuous phase. The mesophase molecules show an higher degree of orientation with respect to isotropic ones (A. Ferri 2015). The formation of the mesophase can be influenced by numerous factors such as the presence of insoluble particles, presence of oxygen and sulfur, applied pressure and temperature of the heat treatments. Mesophase pitch can be produced either by heat soaking or by solvent extraction. Heat soaking process require heating at 400 °C , during the process the higher density mesophase is precipitated and collected at the bottom of the vessel, the process allowing a 50% yield (J. G. Lavin 2001).

In solvent extraction process, part of the isotropic pitch is removed by a solvent such as benzene or toluene, the remaining part is pyrolized for 10 min at 230 °C obtaining a mesophase product with a yield of 75% (J. G. Lavin 2001).

The obtained mesophase is then spun by mean of a melt spinning apparatus; however, the rheological behavior of pitch is far more complex than the one of common polymers. The viscosity is very sensitive to temperature and this causes the fiber to achieve the final diameter as spun without the possibility of further drawing, this means that the spinneret must have very tiny holes (Edie D.D. and Dunham M.G. 1989).

After spinning, the fiber must be stabilized allowing oxygen to react with side-groups creating cross-links and allowing the material to withstand the carbonization temperatures (A. Ferri 2015). The carbonization process is similar to the one of PAN based CFs but the pitch fibers experience a much more significant graphitization during which the dislocations in the turbostratic carbon stacks are gradually annealed resulting in the formation of a three dimensional lattice (A. Ferri 2015).

1.3.2 Properties of carbon fibers

Electrical properties

The main thermal and electrical properties for different kinds of carbon fibers are shown in the table below.

Table 4: Physical properties of carbon fibers (A. Ferri 2015)

	Density, g/cm^3	Electrical resistance, 10^{-3} Ω m	Specific heat C_p, J g^{-1} K^{-1}	Thermal conductivity λ, W m^{-1} K^{-1}
PAN-based HT	1.76–1.81	1.5–2.4	0.71	8–20
PAN-based HM	1.82–2.00	0.6–1.0	0.71	60–100
Anisotropic pitch-based	2.00–2.15	0.4–1.1	0.93	110–375
Isotropic pitch-based	1.60	5–10	0.56	10–17

Mesophase pitch fibers possess the highest electrical conductivity and the lowest resistivity, they are often used to impart electrical conductivity to non-conductive bulk materials.

Even though in CFs the mechanisms for conduction of heat and electricity are similar, heat and electricity are transferred by electron diffusion and holes. There is a strong connection between the two such that thermal conductivity can be estimated by an electrical resistance measurement; more over also mechanical properties are correlated with electrical resistance. (Lavin J.G. et al. 1993)

Mechanical properties

The high tensile strength and modulus made the CFs an interesting choice in replacing conventional materials, mechanical properties of commercial CFs are shown in Table 5.

Table 5: Mechanical properties of carbon fibers (A. Ferri 2015)

Type	Manufacturer	Product name	Tensile strength (GPa)	Young's modulus (GPa)	Strain to failure (%)
PAN	Toray	*T300*	3.53	230	1.5
		T1000	7.06	294	2.0
		M55J	3.92	540	0.7
	Hercules	*IM7*	5.30	276	1.8
GP-Pitch	Kureha	*KCF200*	0.85	42	2.1
HP-Pitch	BP-Amoco	*Thornel P25*	1.40	140	1.0
		Thornel P75	2.00	500	0.4
		Thornel P120	2.20	820	0.2

Tensile strength depends on the number and size of defects, instead tensile modulus is dominated by the size and alignment of the crystals along the fiber direction. Carbon fibers are elastic materials thanks to the high number of covalent bonds (J. G. Lavin 2001). A property that sets CFs apart from other material is the outstanding creep resistance. Creep studies were conducted at 2300 °C at stresses of 800 MPa (Sines G. et al. 1989). The apparent activation energy was determined to be 1082 Kj/mol.

For what concerns compressive strength, dominant factors are both the presence of defects and the crystallites size; so reducing the crystallite size while keeping an effective alignment would allow to improve compressive strength without decreasing the tensile one (A. Ferri 2015).

Chapter 2

Method of dispersion and functionalization of carbon materials

2.1 Dispersion techniques

Due to their outstanding mechanical, electrical and thermal properties, carbon nanotubes, graphene and carbon fibers are considered good fillers material for the production of functional and structural composites.

However, the production of such materials is limited by the problems encountered in obtaining a uniform and effective dispersion in the matrix, leading to a non-efficient exploitation of their properties and to a poor performance of the material as a whole (Junrong Yu et al. 2007).

Achieving a correct dispersion is a critical issue in composite manufacturing. In facts, the presence of a bundle of fillers not only would not improve the performance of the matrix but also will act as defect leading to a lower resistance of the matrix itself. A low volume of the filler is usually preferred in order to avoid the cost of the overall material to rise and to avoid the incorporation of air bubbles that would act as defects (Linda Vaisman et al. 2006). Many different techniques have been proposed in order to obtain an effective dispersion: ultrasonication, calendaring, ball milling, physical functionalization, and oxidation. Most are based on two different approaches. The mechanical one consists in dispersing the nanotubes into a solvent by applying only physical or mechanical forces such as ultrasounds, while in the chemo-physical dispersion

bonds of various intensity are formed between the CNTs surface and a chemical agent (Linda Vaisman et al. 2006).

2.1.1 Mechanical dispersion: mechanical milling

This approach consists in achieving a dispersion in the medium by the mechanical force exerted by a milling machine. One example of a machine used in this technique is the three rolls mill (figure 19), that exploits the force created by the rollers to mix, disperse and homogenize the nanoparticles and a viscous material matrix. This technique allows an effective dispersion of CNTs or graphene sheet, but it has the drawback to be implementable only with viscous matrices (Marchisio Silvia 2013). In this case, however, the nanomaterials are severely damaged during the dispersion.

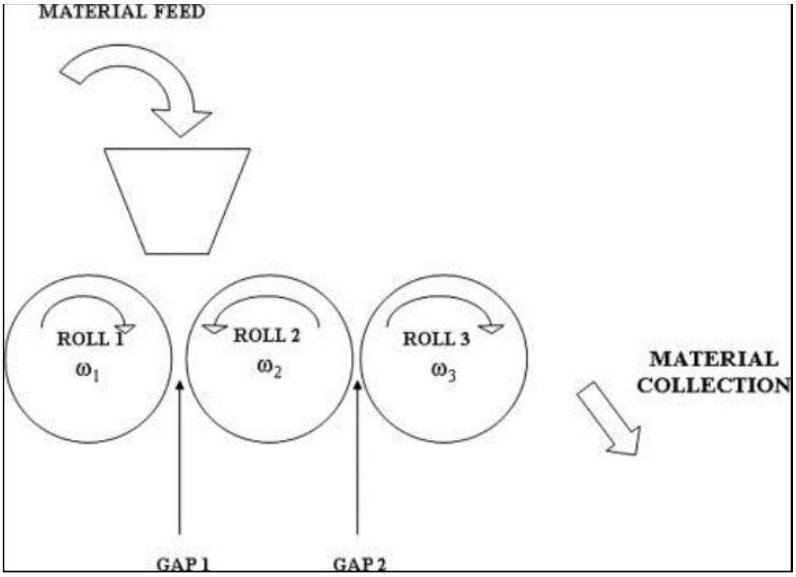

Figure 19: Scheme of a three rolls mill (Marchisio Silvia 2013)

2.1.2 Mechanical dispersion: Ultrasonication

The most commonly used technique to disperse all the carbon materials in a solution consists in the use of an ultrasonic probe or bath. The cavitation induced by the ultrasonic waves cause the breakage of the bundles with a particularly good efficiency in non-viscous media. The main limits of this technology lies into the excessive heating of the solution, this leads to the necessity of having a cooling apparatus; moreover if ultrasounds are used for a long time or with too high energy the carbon materials surface will be damaged (Linda Vaisman et al. 2006). Moreover, it is necessary to take into account that if the fluid is left still after the

sonication the nanotubes will tend to aggregate again. For what concerns the damage on the nanotubes or graphene, in the literature this effect is sometimes deemed as a positive issue as long as the structure is not compromised, this is because the introduction of defects on the surface will create points of higher reactivity that can improve the adhesion with the matrix (Lavagna et al. 2018b).

2.2 Functionalization

2.2.1 Dispersion by using surfactants

Recent studies aim to improve the carbon materials dispersion and interaction with the matrix by exploiting the surface properties, the goal of the surface treatment is to obtain an increase in the hydrophilicity. Studies has shown the contact angle decrease if hydroxyl and carboxyl groups are present on the surface of materials as impurities or defects (Linda Vaisman et al. 2006; Zhang et al. 2008; Bagri et al. 2010).

In order to obtain defects the oxidation in strong acids such as HNO_3 or H_2SO_4 can be exploited: the sulfuric acid causes the breakage of the C-C bonds, then the nitric acid promotes the oxidation and the formation of the –COOH groups, an example of such reaction is given in figure 20 regarding carbon nanotubes (A. Laachachi et al. 2007). The presence of these groups improves the dispersion in polar media and enhance the surface interaction with polar matrices leading to an improvement in the load transfer mechanism. This functionalization process requires a modification in the hybridization state of some carbon atoms from sp^2 to sp^3 since some functional groups are added to the structure.

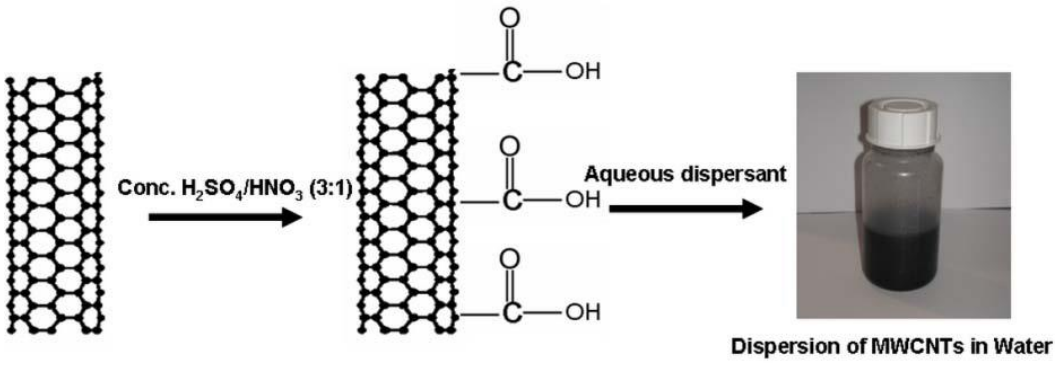

Figure 20: Chemical functionalization of CNTs

Even though this kind of functionalization improves the dispersion some drawbacks exists. Firstly, the strong oxidation causes the creation of defects on the surface and if it is too strong the tubes will be broken and lose all their

characteristic properties (Linda Vaisman et al. 2006); moreover a series of problems connected with strong acids has to be faced, from safety to environmental issues. An interesting alternative could be the non-covalent functionalization, in order to not interfere with the chemical equilibrium of the nanotubes. It consists in the use of polymers that can increase the interaction with the matrix and improve the dispersion by an effect of steric repulsion. Quite good results have been reached by wrapping the nanotubes with polymers such as polystyrene (Linda Vaisman et al. 2006).

The use of surfactants have been studied to facilitate the dispersion process, once they are adsorbed at the carbon-matrix interface, they can lower the surface tension improving the matrix filler interaction and preventing the formation of bundles or aggregate. The effectiveness of a surfactant depends greatly on the solution and on the nature of the surfactant itself (anionic, cationic and non-ionic). The use of surfactants is always coupled with a mechanical dispersion technique such as ultra-sonication, the idea is that firstly ultrasounds separate the aggregates, then the surfactants bind with surface avoiding the re-coagulation (Linda Vaisman et al. 2006) as it is described in figure 21.

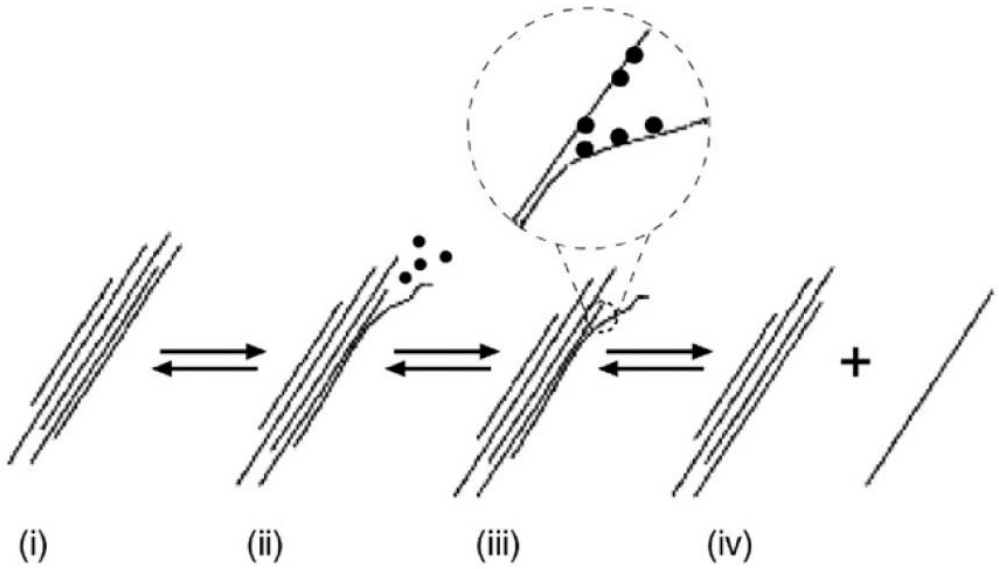

Figure 21: Scheme of CNTs dispersion enhanced by surfactants (Linda Vaisman et al. 2006)

2.2.2 Dispersion without the use of surfactants

A universal solution seems to be the chemical functionalization of carbon materials. In the literature, several functionalization methods can be easily found (Zhang et al. 2008; Vázquez et al. 2014), although, wet functionalization via

acidic oxidation seems the most common. An acidic treatment is used not only for functionalization, but also to remove the amorphous carbon from the surface.

The most used is the nitric acid, in this case the treatment should be used both to functionalize the surface and to remove the residual metals present in the lattice of carbon nanotubes. Typically, through harsh nitric acid treatments, the pristine carbon surface can be effectively purified and oxygen-containing groups, mainly carboxyl and hydroxyl, have been found to decorate the graphitic surface (Wu et al. 1995). Aviles et al. (Avilés et al. 2009), showed that a small concentration of nitric acid could improve the presence of these groups on the surface of carbon. Functionalization in presence of nitric acid can enhance the dispersion in polar solvent. The time of soaking or refluxing in acid is important in this type of treatment. As shown by Rosca et al. (Rosca et al. 2005), a treatment for long time in nitric acid could strongly damage the structure and cover the surface by amorphous carbon. However, hot nitric acid leads to an efficient elimination of metal impurities and amorphous graphitic platelets. The treatment with only sulfuric acid does not permit a good oxidation of the external lattice in the case of carbon nanotubes and graphene, and the oxygen contained in treated carbon nanotubes is similar to the pristine ones. If hydrogen peroxide is added, this permit to have not only carboxylic functionalities, but also hydroxyl groups. The presence of oxygen is high and the structure of carbon nanotubes seems not be destroyed. Datsyuk et al. (Datsyuk et al. 2008; Lavagna et al. 2018b) shows that the functionalization with sulfuric acid/hydrogen peroxide mixture (piranha solution) guaranteed a good dispersion in not only polar solvent but also in non-polar media. These functionalities guaranteed a good structure for the solvation by water. Concerning the oxidation reaction of piranha solution with CNTs, Ziegler et al. (Ziegler et al. 2005) have shown that the one-dimensional nanostructures can be cut in a controlled manner under specific conditions. At high temperatures, piranha was found to attack existing damage sites, generating vacancies in the graphene sidewall and consume the oxidized vacancies to yield shorter nanotubes. The detailed observation and analysis of Zhang et al. (Zhang et al. 2003) showed that the defects on the surface, original or newly created, play a crucial role in the oxidation process. Following the defect-generating and defect-consuming steps, they explored the possible oxidation reactions and predicted the intermediate and final products. Dispersion after an acidic treatment was evaluated by Osorio et al.

(Osorio et al. 2008) who treated carbon with three different combinations of acids: nitric acid, sulfonitric acid and sulfonitric combined with hydrochloric acid. The best stability of the water dispersion was obtained for the last two treatments; this is due to the high percentage of functional groups absorbed on the surface. An investigation on the effect of sulfonitric acid on the surface of CNTs was made by Chiang et al. (Chiang et al. 2011). They demonstrate that the graphitic structure did not suffer from severe destruction except for some thinning and cutting into short tubes. The sulfonitric oxidation attacks only the active site and generates new defect sites with the incorporation of functional groups containing oxygen. This treatment reduce the thermal stability of CNTs due to the high presence of oxygen. Pavese et al. (Pavese et al. 2008) made the same evaluation in their study of wettability of CNTs after sulfonitric treatment. The study was performed on vertically aligned (VA) CNTs, and showed how the interaction with water was enhanced. The presence of carboxyl and sulfonic groups started after a treatment of 6 hours. After the treatment, the contact angle between water and VA-CNTs was very low and showed a transition from a hydrophobic to hydrophilic behavior. Obviously, the increase in wettability was due to the high presence of oxygen on the surface. The use of concentrated acid at different temperature enhanced the presence of oxygen (Ramanathan et al. 2005). Concerning the use of carbon structures as reinforcements in composite materials, the incorporation of oxygen-containing functionalities onto the graphitic surface is a very crucial step for the enhancement of interfacial adhesion. Saleh et al. (Saleh 2011) demonstrated that the amount of oxygen is increased when the acidic treatment is performed at high temperature. On the other hand, the structure of the external lattice is strongly damaged. CNTs in this case have a reduction in size and are not as efficient in performance as the pristine. It can be summarized that the extent of oxygen content into the CNTs surface is sensitive to both the oxidant used and the treatment temperature. A facile approach to the surface oxidation with an enhancement of polar groups on the surface is also presented by Xing et al. (Xing et al. 2005). The use of sonication during the acid treatment promotes the formation of a high quantitative of grafted functional groups. This method guarantees a continuous breakage of CNTs bundles during the process.

2.2.3 Oxidation without the use of acid

Oxidation with other oxidant agents was studied in different ways. Peng and Liu (Peng and Liu 2006) showed the effect of hydrogen peroxide for long contact times. The oxygen content results lower than in the case of an acid treatment, however the damaging of the external lattice seems to be much lower than with an acid treatment. The hydrogen peroxide reacts with amorphous carbon forming –OH groups on the surface removing disordered carbon. Wepanick et al. (Wepasnick et al. 2011) tried to analyze the degree of oxidation, using common oxidants. They showed that also a non-acidic treatment is sufficient to decorate the surface with functional groups. The use of $KMnO_4$ is a good solution to have a high number of carboxylic groups and functionalities usable for other chemical reaction. On the other hand, the use of ammonium persulfate $(NH_4)_2S_2O_8$ does not guarantee a good oxygen content (Wepasnick et al. 2011) on the surface and this kind of oxidant can attack only the defects present on the external lattice. This oxidation create acidic functional group such as carboxyl, lactone and phenolic acid (Moreno-Castilla et al. 2000). These studies suggests this route also as an "eco" friendly idea to avoid the use of acid to functionalize CNTs.

There is very little information on the structural alteration of graphitic material under basic oxidative treatments. Datsyuk et al. (Datsyuk et al. 2008) and previously Kim et al. (Kim et al. 2005) treated MWCNTs with an ammonium hydroxide/hydrogen peroxide mixture. As already seen before, in the case of hydrogen peroxide, this mixture allows an oxidation without heavily damaging the external lattice; the nanotubes were decorated with epoxy and could be used in composites for enhancing electrical conductivity.

Summarizing: more aggressive oxidants produced a larger fraction of highly oxidized functional groups, in line with the expectations of basic chemical principles. In Table 6 and figure 22 are presented some literature results on the final oxygen content of CNTs treated with different oxidative mixtures, together with the main functional groups formed.

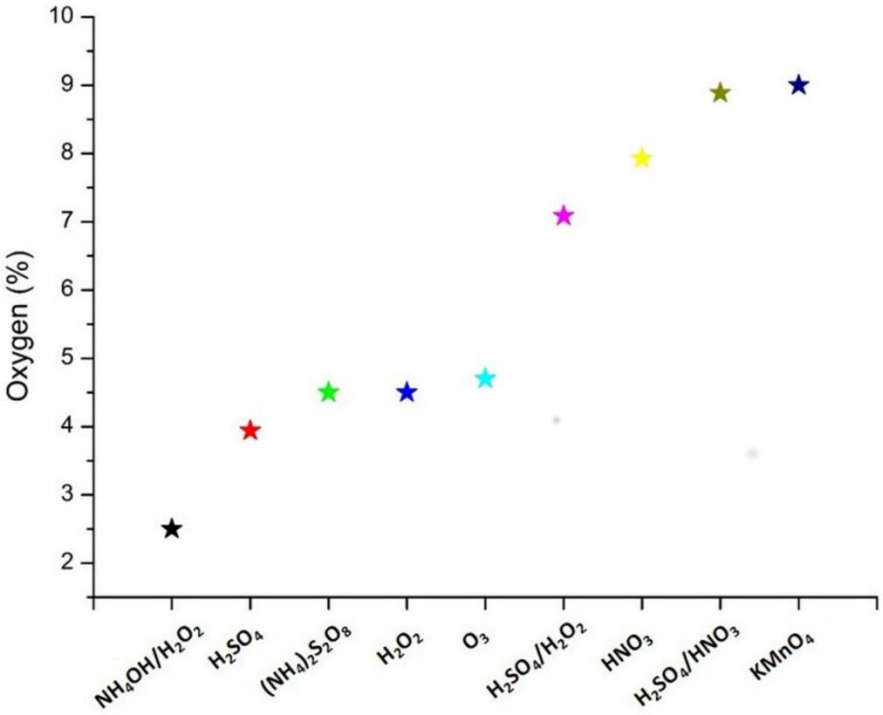

Figure 22: Percentage oxygen present on the surface of carbon materials as a function of chemical treatment applied on the surface from the literature cited in the chapter 2.2

Table 6: Different chemical groups formed on the surface in function of oxidant used

Type of oxidation	References	Chemical groups formed
H_2SO_4	(Avilés et al. 2009)	$-SO_3H$
HNO_3	(Rosca et al. 2005; Tchoul et al. 2007; Datsyuk et al. 2008; Osorio et al. 2008; Avilés et al. 2009; Wepasnick et al. 2011; Saleh 2011)	-COOH; -C=O
H_2SO_4/ HNO_3	(Xing et al. 2005; Datsyuk et al. 2008; Pavese et al. 2008; Osorio et al. 2008; Avilés et al. 2009; Wepasnick et al. 2011; Saleh 2011)	-COOH; -OH; $-SO_3H$
H_2SO_4/ H_2O_2	(Datsyuk et al. 2008)	-OH; -COOH
$KMnO_4$	(Wepasnick et al. 2011)	-COOH; -C=O
$(NH_4)_2S_2O_8$	(Moreno-Castilla et al. 2000; Wepasnick et al. 2011)	-OH; -COOH
H_2O_2	(Wepasnick et al. 2011)	-C=O; -OH
NH_4/H_2O_2	(Datsyuk et al. 2008)	-COOH; -OH

2.2.4 Oxidation in flux of gas and vapour

An alternative method to oxidize CNTs consists in fluxing through dry CNTs an oxidant gas or vapor. This methodology guarantees a substantial reduction in waste production and a more homogenous functionalization. Xia at al. (Xia et al.

2009) developed a gas-phase route for the oxidation and functionalization of CNTs. The HNO_3 vapor treatment was observed to be more efficient in introducing oxygen-containing functional groups on CNT surfaces than conventional treatment with liquid HNO_3. In addition, the use of HNO_3 vapor treatment was more advantageous since it allowed to avoid the filtration, washing, and drying steps. An alternative oxidant gas is ozone (O_3), that can be fluxed on carbon nanotubes at room temperature or at high temperature. The reaction between the gas and the carbon produces two distinct surface bound functional groups, esters and quinones, as well as gas phase CO_2 and CO (Mawhinney et al. 2000). The rate of formation of these species diminishes at higher O_3 exposures as the number of active sites on the SWNT diminishes (Wepasnick et al. 2011). If is a UV radiation is used during the ozone treatment, carboxylic groups content showed a steady rise with increasing the exposure (Sham and Kim 2006). The treatment with ozone guaranteed a stable dispersion of CNTs for days after a short time sonication, as is shown by Li et al. (Li et al. 2008a). A different gas used for oxidize the surface is CO_2. Actually, it is used to eliminate the metallic residues present in the nanotubes after the synthesis. Due to the acidity of the gas, the amorphous carbon is oxidized and the stability of CNTs goes down at medium temperature. The evaluation of the damaging of the surface is well explained by Chiang et al. (Chiang et al. 2001)**.** The variation of the surface oxidation is well visible also by SEM and TEM and the structure of nanotubes after the treatment seems damaged, in particular the dimension of CNTs is reduced. The oxidation by an air treatment is diffusely used to purify CNTs after their synthesis (Hou et al. 2008). Normally a slight oxidation with a small quantitative of oxygen permits to eliminate the residual amorphous carbon and the metals (Park et al. 2001) present on the external lattice of CNTs. The treatments in air are variable in temperature (Sen et al. 2003; Li et al. 2004), time (Andrews et al. 2001) and percentage of oxygen (Chiang et al. 2001) used. To have an annealing beyond the treatment in air, is necessary also a treatment in vacuum (Huang et al. 2003).

Chapter 3

Composite materials

Composites are defined as those materials obtained as a combination of multiple conventional materials. The two phases by which the composite is made are commonly defined as matrix and reinforcement, the matrix is the continuous phase that encloses the filler granting the cohesion of the system. The filler is the disperse phase and aims to impart peculiar properties to the system.

The final properties of a composite are different from the ones of the starting materials and often are not observable in any traditional material.

The matrices can be metallic, ceramic, and polymeric while the filler can be in the form of fibers or particles.

3.1 Cement matrix composite

Since Biblical times, approximately 3500 years ago, brittle building materials, e.g. clay sun baked bricks, were reinforced with horse-hair, straw and other vegetable fibres. In the recent years several materials were tested to analyse the compatibility of cement paste with reinforcement. There are many examples about the use of wood and cellulose fibres in cement composites (Jorge et al. 2004). Many studies focus their attentions in the use of waste plastics (Riley and Razl 1974) and rubber from tyres (Sofi 2017) to embrace not only the mechanical properties but also the ecological point of view in buildings technology. The concept of fibre reinforcement was developed in modern times and brittle cement-based paste was reinforced with asbestos fibres when in about 1900 the so called Hatschek technology was invented for the production of plates for roofing, pipes,

etc.. Nowadays the use of different fibres as reinforcement for cement composite was extensively studied (Brandt 2008). In general, concrete and particularly concrete with dispersed fibre reinforcement is becoming a high-tech material that provides excellent performance but requires competent design and execution. With nanotechnology it is possible to increase the quality and characteristics of the existing products, and create new composite materials that can complete specifics functions. The application of nanotechnologies to cement materials has aroused in the last decade considerable research interest; the purpose of these studies is to improve properties cement both in mechanical, such as strength, durability and ductility, and in electrical properties. A significant part of the current civil infrastructure is partially or completely built with cementitious materials such as concrete. The use of glass or steel fibers to reinforce the cement and reduce the formation of cracks is not new. Instead, the excellent mechanical, thermal, electrical properties of carbon nanotubes (CNTs) and nanofibers (CNF) have motivated the creation of advanced nanocomposites with exceptional and multifunctional properties that have opened a new field regarding the reinforcement of nanometric dimensions inside the concrete (Yu et al. 2000b). Among the many nano-materials, the CNTs were chosen by virtue of their mechanical and electrical properties (Yu et al. 2000a; Li 2004). The application of nanotubes and carbon fibers lies in the combination of the nanometric dimensions with very strong mechanical properties; allows a uniform distribution of reinforcement over the entire matrix using a relatively small amount of fillers. In this technological application both a good dispersion of the filler and a good interaction filler-matrix are essential to obtain a performing composite material (Larson et al. 1990; Hertel et al. 1998; Nasibulina et al. 2012). It appears that the effect of carbon nanotubes on the properties of cement is still not completely clear, and several issues related to dispersion are still to be solved (Mendoza Reales and Dias Toledo Filho 2017). With carbon fibers, literature suggests that the use of a dispersant, such as sodium naphthalene sulphonate or sodium dodecyl sulfate, can be a good solution to enhance the dispersion of the fibers (Yang 2002; Wang et al. 2008, 2014; Lestari et al. 2013; Chuang et al. 2017).

The possibility of creating a structural material able to self-monitor the applied tension represents a turning point in the engineering of control and safety structural. The incorporation of nanometric fibers would allow nano-scale control

of matrix cracks allowing the creation of a new generation of "crack-free materials" (Musso et al. 2009; Konsta-Gdoutos et al. 2010). The advantages of this self-detection capability compared with the use of connected sensors are: the low cost, long life, large detection volume without losing mechanical properties. Self-assembled cement-based materials take piezoresistive properties due to the fact that fibers can conduct electricity (Shah et al. 2009). There are many researches on the use of carbon fibers, carbon black, carbon nanotubes or combinations of them in order to import piezoelectric properties to the cement matrix (Inam et al. 2014; Gong et al. 2015). The cement composites materials have been tested by recording the electric resistivity variations while the sample was loaded cyclically. By soliciting the material, the conductive network in the sample could be deformed. These changes in the position of the elements of the conductive lattice (during a compressive stress approach, for example), cause a consequent change of electrical resistivity. The hope is to be able to assess the state of tension through the electrical resistivity allowing, thus, the real-time monitoring of the structure. Theoretically, the use of nanotubes would give a more reliable response than fibers carbon or other materials, thanks to the unique electromechanical properties of the nanotubes. Yu and Kwon (Yu and Kwon 2009) in 2009 tried to build a monitoring sensor by controlling the dispersion of carbon nanotubes in cement. They tried to prepare two samples using two different ways to disperse the nanotubes, discovering that the technique of treatment and preparation can influence the piezoresistive response of the material. The piezoresistive properties of the cement containing carbon nanotubes are particularly good when the surface of the nanotubes is not covered by surfactants but is in contact direct with cement (Sihai Wen and D. D. L. Chung 2005). Azhari and Banthia studied in 2012 the possibility of creating a sensor based on cement using both carbon nanotubes and carbon fibers (Azhari and Banthia 2012). This idea is particularly interesting as it combines the cost effectiveness of carbon fibers with the unique electro-mechanical characteristics of the CNTs. The fibers are able to decrease the electrical resistivity of the cement nanotubes and are able to give life to a conductive network which gives a remarkable electromechanical behavior to the cement. The exceptional mechanical properties of the fibers could also improve the mechanical properties such as fracture strength and deformation capacity.

3.2 Polymer matrix composites

Polymer-matrix composites (PMCs) consist of a polymer resin as the matrix, with particles or (preferentially) fibers as the reinforcement medium. These materials are used in the greatest diversity of composite applications, as well as in the largest quantities, in light of their room-temperature properties, ease of fabrication, and cost (Callister and Callister 2001). Many types of fibers can be used as reinforcement. In literature is possible find three typology of composite: composite with glass fibers (Sathishkumar et al. 2014), composite with carbon fibers (Coleman et al. 2006) and with aramid fibers (John et al. 2001). In this chapter, we focus our attention on PVB matrix composites reinforced by carbon nanotubes and fibers.

Polyvinyl butyral is a polymer belonging to the class of polyvinyl acetals, this material was firstly employed by Monsanto in the 1930s as the key ingredient for automotive safety glass interlayers. Acetals are formed by the reaction between aldehydes and two molecules of alcohol. Polyvinyl acetals are prepared from aldehydes and polyvinyl alcohols. Polyvinyl alcohols are high molecular weight resins containing various percentages of hydroxyl and acetate groups produced by hydrolysis of polyvinyl acetate. The conditions of the acetal reaction and the concentration of the particular aldehyde and polyvinyl alcohol used are closely controlled to form polymers containing predetermined proportions of hydroxyl, acetate, and acetal groups (Eastman and Chemical Company 2013). The reaction mechanism and the product structure are shown in figure 23.

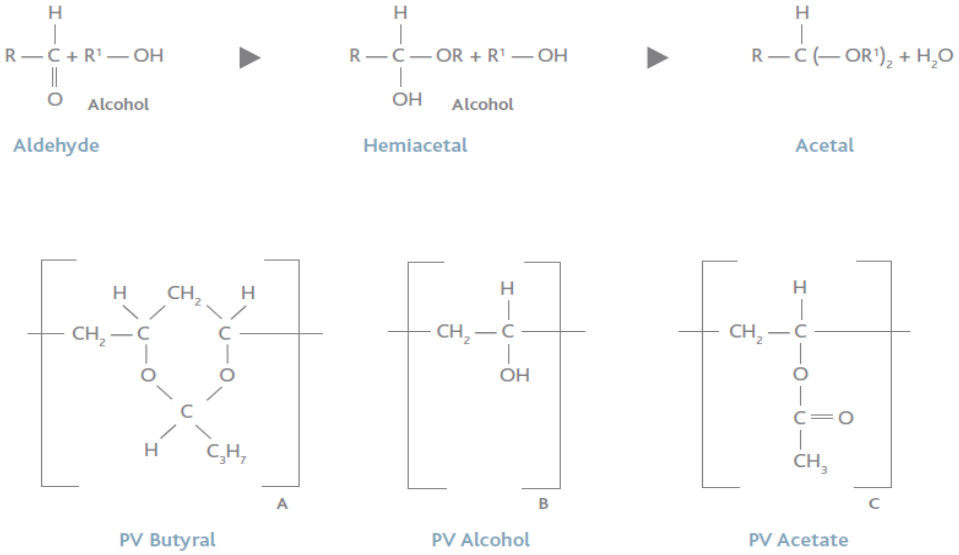

Figure 23: Reaction scheme for PVB production (Eastman and Chemical Company 2013)

PVB is available on the market in many forms and with different properties and molecular weights; a key characteristic in defining the polymer variety is the amount of PV alcohol and PV acetate residues present in the polymeric chains. In the experimental work PVB 76 was used, which contains 88% butyral residues, the remaining is composed by 10-12% alcohol and 0-2% acetate respectively. The properties of PVB 76 at ambient temperature are listed in Table 7.

PVB is compatible with different solvents, the viscosity trends of PVB in ethanol solution are shown in figure 24.

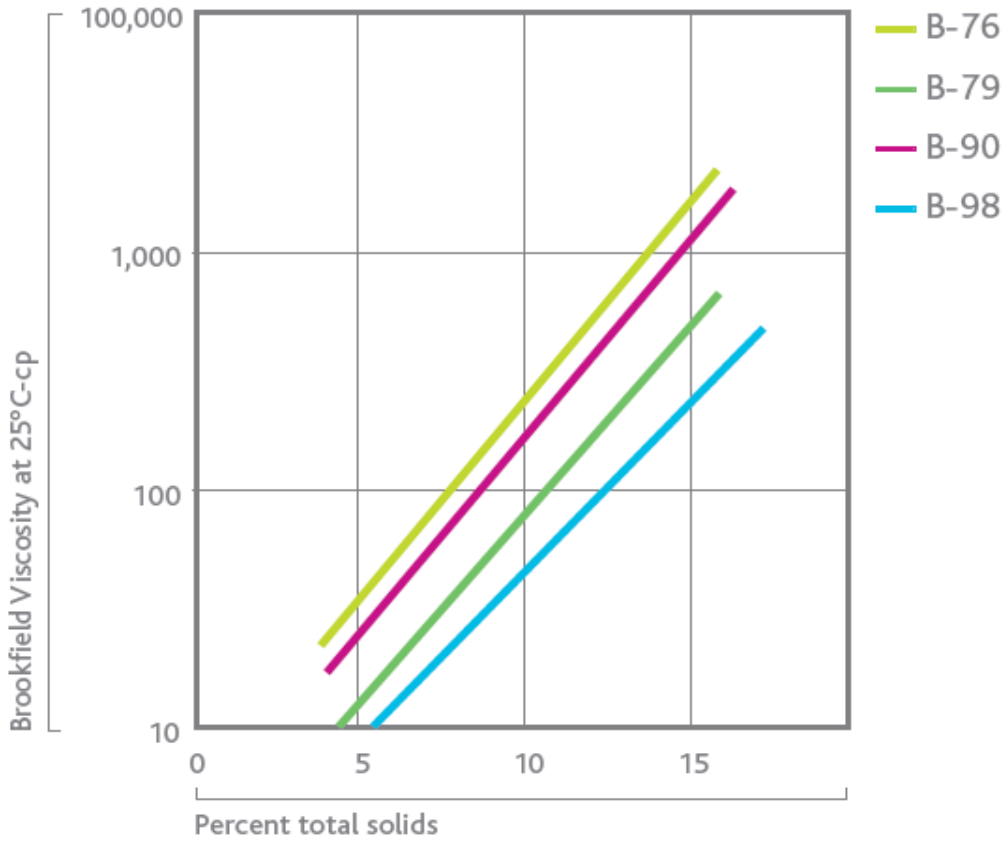

Figure 24: Viscosity profiles for different PVBs in ethanol solution (Eastman and Chemical Company 2013)

The use of fibers as fillers is because materials in bulk form tend to fail at lower load than fibrous ones; this is because, when failure occurs due to the presence of random defects, then the failure will be limited to a restricted number of fibers while the other ones will maintain their characteristics.

Moreover, in composites, the mechanical performance strongly depends on how the loads are transferred between the matrix and the reinforcing system, and this transfer strongly depends on the interfacial area between the filler and the resin; this is the reason why the fibers with their high surface to volume ratio are considered as the ideal material for plastic reinforcement. The properties of a fiber reinforced polymer depends on the properties of the fiber, the ones of the matrix, the ratio of fiber to resin in the matrix, and on the geometry and orientation of fibers in the composites. An idea of how the properties of the composites will lie between the ones of the resin and the ones of the fibers is given in figure 25.

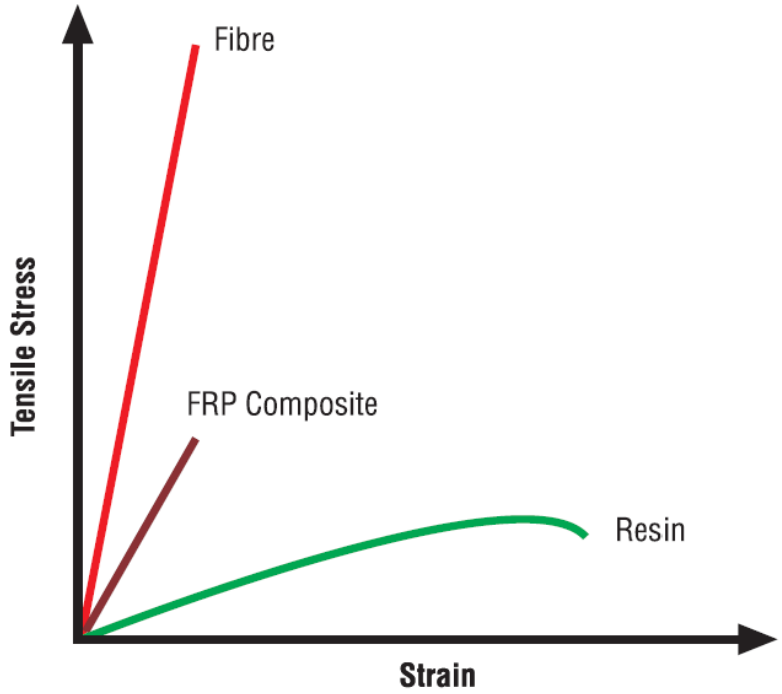

Figure 25: Stress/strain curve for matrix, filler and composite (A. Ferri 2015)

Since the properties of fibers are superior to the one of the resins the higher the amount of fibers in the composite the better the mechanical properties. However, there are some technological limits to this rule: firstly, the fibers must be completely coated by the polymer in order to be effective; moreover, the manufacturing process must allow a uniform dispersion of the fibers into the matrix. Another important parameter is the geometry with which the fibers are distributed: this is because their properties are the best along their length, so the orientation of the fibers will provide high anisotropy to the composite. The anisotropic properties of the fibers can be advantageous since they make possible to apply the reinforcement only in the direction where it is required. For this purpose, many fabrics are available. Unidirectional fabrics are straight and uncropped; most of the fibers run in the same direction and are held together by the resin. They allow placing the reinforcement only where it is needed it is also possible to place several unidirectional layers with different directions in order to obtain a quasi-isotropic configuration as shown in figure 26.

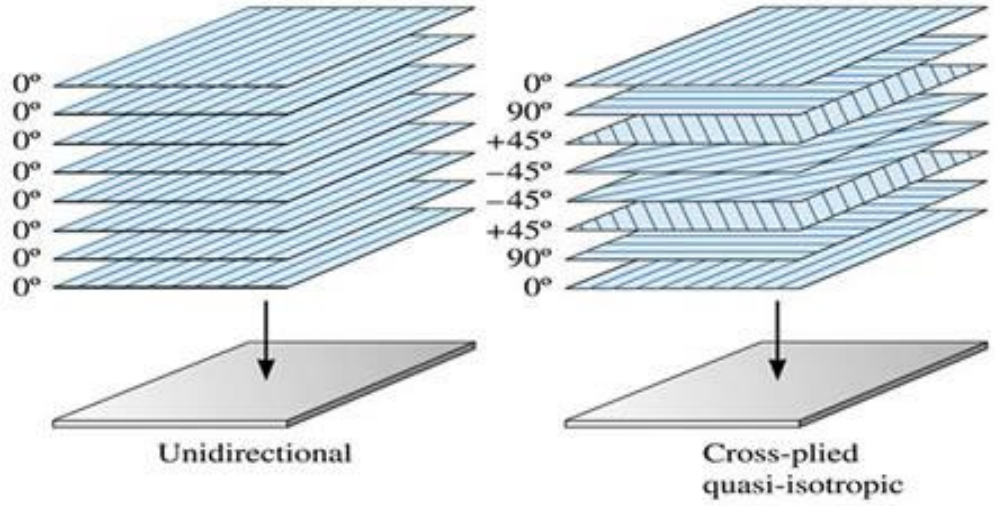

Figure 26: Unidirectional and quasi-isotropic laminates (Callister and Callister 2001).

0/90° fabrics instead are used in those applications where more than one fiber orientation is required; they are mostly woven products in which warp and weft are interlaced with arrangements. Plain weave is the most crimped and symmetrical one, it provides good stability but lower mechanical performances. Twill weave presents lower crimp and smoother surface that lead to higher mechanical properties without losing the stability of the plain one. Satin weave consists in a twill weave with fewer warp/weft intersections; this induces better mechanical performances in one direction but leads to an instability and asymmetry. Different weaves are shown in figure 27.

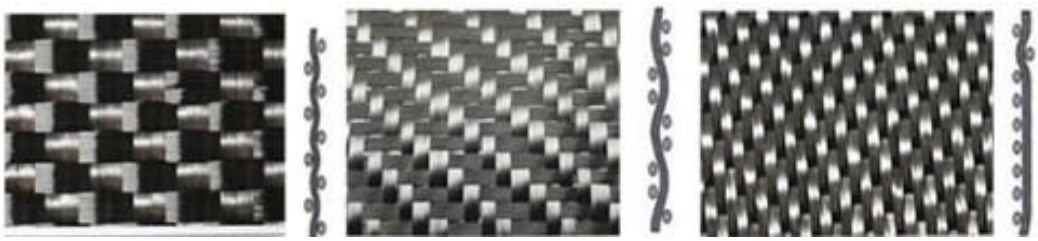

Figure 27: Carbon weaves, from left to right: plain, twill and satin weave.(Callister and Callister 2001)

Since surface-to-volume ratio is increased by two-three orders of magnitude when passing from carbon fibers to carbon nanotubes, this nano-sized carbon form could seem the best possible choice for improving the properties of a polymer. However several challenges arise when dealing with nano-reinforcement. The main one is to properly transfer the properties of the nano-filler to the macro-scale composite by choosing the best combination of material and processing method.

The mechanical properties of the nanocomposites depend on the load transfer mechanism and on the CNTs dispersion. The presence of CNTs into the polymer matrix has shown significant effects on the fracture mechanism, as a matter of facts they are able to stop a crack propagation by bridging the two crack faces. CNTs can improve the out of plane and inter laminar properties both by increasing the matrix strength and by linking the different laminar layers (Andrews R, et al. 2002). Thermal and electrical conductivity can be imparted to polymers by addition of CNTs thanks to their very high aspect ratio. The key factors influencing the mechanical and electrical properties of the composites are the processing technique, matrix properties and the nanotubes types. The addition of CNTs has showed to increase the glass transition temperature (O. BREUER and UTTANDARAMAN SUNDARARAJ 2004).

The use of short reinforcement, such as CNTs, within the PMCs leads to an increase in the tensile strength of the composites directly correlated to the amount of nanotubes loaded into the composite. However, it is observed that the theoretical predictions of mechanical properties and the experimental findings often differ due to a number of issues including the presence of voids, lack of perfect orientation, poor filler dispersion and insufficient load transfer due to the lack of interfacial adhesion. The use of long fibers in PMC such as carbon fibers increases the tensile strength of the polymer matrix (as shown in figure 25), but leads to a reduction in the toughness, in contrast with what happen when using carbon nanotubes.

Chapter 4

Materials and methods

4.1 Materials

The carbon fibres (CFs) used throughout all the work were purchased from TOHO-Tenax; as reported by the manufacturer, the CFs are 6 mm long and sized with PU (polyurethane) up to 2.5% in weight, the bulk density is declared to be 530 g/dm^3, probably meaning the density of the nanotube powder.

MultiWalled Carbon Nanotubes (MWCNTs) were acquired from Nanocyl, produced by catalytic chemical vapour deposition, and display the following characteristics: 9.5 nm average diameter, 1.5 µm average length, 90% purity and 250-300 m^2/g surface area, as stated by the producer.

Graphene nanoplatelets (GNPs), COOH-functionalized graphene nanoplatelets (GNP-COOH) were purchased by Cheaptubes, reduced graphene oxide (RGO) and graphene oxide (GO) were purchased by Graphenea. The oxygen content of these materials is, respectively, 0%, 5%, 20%, 45.5%, as declared by the producers.

All the reactant for chemical treatment were purchased from Merck. For the oxidation and grafting treatments, sulfuric acid (H_2SO_4) 98% v/v, nitric acid (HNO_3) 65% v/v, sodium hydroxide (NaOH) with 97% v/v purity, and acetone with assay > 99.9% v/v were used. For the chemical oxidation of carbon nanotubes and carbon fibers: sulfuric acid 98% v/v (H_2SO_4), nitric acid 65% v/v

(HNO_3) and hydrogen peroxide 30% v/v (H_2O_2). Sodium hydroxide 97% v/v (NaOH). For dissolving PVB was used ethanol 97% v/v.

Table 7: Properties of PVB 76 adapted from source (Eastman and Chemical Company 2013)

Property	PVB-76
Molecular weight [Da]	90000-120000
Tensile strength at yield [MPa]	39-47
Tensile strength at break [MPa]	32-39
Elongation at yield [%]	8
Elongation at break [%]	110
Glass transition temperature T_g [°C]	62-72

The cement-based system selected for this thesis is based on the American Petroleum Institute (API) oil-well cement Class G (Lafarge North America).

4.2Characterization of carbon materials

4.2.1 IR

All the FTIR spectra were recorded in transmission mode in a Bruker Tensor 27 Fourier Transform Infrared spectrometer equipped with Globar source, MCT detector and working with 128 scans at 4 cm^{-1} of resolution in the 4000-500 cm^{-1} range. FTIR analysis was carried out on KBr diluted pellets.

4.2.2 Raman

The Raman spectra of crystalline samples were obtained with a Horiba Jobin Yvon HR800 instrument equipped with an Olympus BX41 microscope. The samples were excited with a red HeNe laser (wavelength 633 nm, power 20 mW) and a Nd solid state green laser (wavelength 532 nm, power 250 mW) with a magnification ratio of 50× with 30 acquisition of 30 seconds.

4.2.3 Thermogravimetric analysis

Thermogravimetric analysis was conducted by mean of a TGA instrument

Mettler Toledo 1600. The analysis was generally performed in air atmosphere in order to observe the possible interactions between the oxygen containing surface groups and the air.

4.2.4 SEM

The morphology of the samples was inquired by mean of a FESEM Zeiss Merlin. Samples were prepared for each multiscale fibers batch. Various micrographs have been taken at different magnifications and in different areas of the samples in order to observe the average morphology of the different samples.

4.2.5 DLS

The hydrodynamic size and zeta potential of the carbonaceous nanomaterials were measured by using a DLS Zetasizer Nanoseries ZS90, Malvern Instruments, UK. Samples were prepared by dispersing the powders in distilled water and the measurements were carried out at a controlled temperature of 25.0 ± 0.1 °C in a thermostatic cell; analyses were done in triplicate and the average value was considered.

4.2.6 TEM

TEM was used in collaboration with dott. Simone Musso at Massachusetts Institute of Technology.

4.3 Characterization of composites

4.3.1 Mechanical characterization
Cement matrix composites

The mechanical properties of the cement composites were measured with a three point bending test (ASTM C348) controlled by crack mouth opening displacement (CMOD) on notched specimens with size 75x20x20 mm. The specimens were tested with a single-column Zwick-Line z050 flexural testing machine with a load cell having a maximum capacity of 1 kN. As described in literature (Jenq and Shah 1986; Shah 1990), this measurement requires the samples to be notched in the middle, the notch having a width of 2 mm and a depth of 5 mm, equal to one fourth of the width of specimen. CMOD was

controlled at a fixed displacement rate of 0.003 mm/min by placing an extensometer on the two sides of the notch (figure 28).

Figure 28: Prismatic sample of cement composite tested with the single-column ZwickiLine z050 flexural testing machine having maximum load capacity of 1 kN. The CMOD (Crack Mouth Opening Displacement) control mode was selected and the displacement rate was fixed as 0.003 mm/min for all the specimens

Polymer matrix composites

Tensile tests were performed on the samples using a ZwickLine z050 testing machine with a 50 kN load cell. The test was conducted at room temperature in displacement control at a velocity of 0.5 mm/min (corresponding to a strain rate of about 0.015 $\%s^{-1}$) and applying a preload of 5 N. All measurements were also subsequently repeated and verified using a universal testing machine MIDI 10 by Messphysik Materials Testing, at a velocity of 0.6 mm/min, corresponding to a strain rate of about 0.025 $\%s^{-1}$. The samples were rectangular specimens, cut from the fabricated tapes, 57 x 9 or 40 x 9 mm^2 in size with variable thickness.

The tape casting method is based on a suspension of a mix of ceramic powders, nanomaterials, micromaterials etc. and organics components (dispersant, binder and plasticizer) in a proper solvents, which is spread or “cast” on a flat moving support. After the actual casting step the solvents are slowly evaporated to obtained a “green ceramic tape” in form of a thin sheet. The thickness reported in tape casting go from 5 microns to some millimetres(Mistler and Twiname 2000).

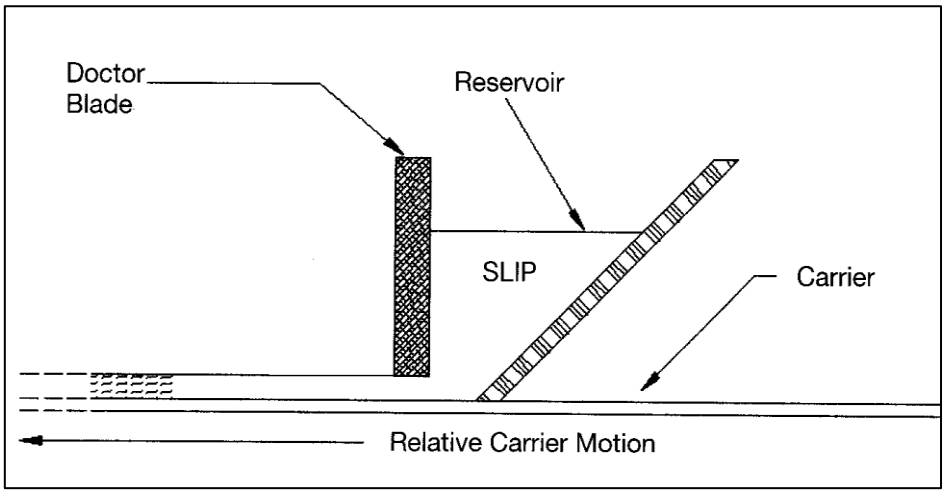

Figure 29: Diagram of typical tape casting apparatus

4.3.2 Electrical characterization

Electrical properties were evaluated by using a WAYNE KERR impedance analyzer (Precision Component Analyzer 6425). The electrical contact between the copper electrodes and the sample was optimized with a conductive gel produced by Ardet s.r.l..

Chapter 5

Results and discussion

5.1 Thermal oxidation of carbon materials

As is well known, nanotubes are purified when they are brought to a high temperature under a strong flow of oxidizing gas (Hou et al. 2008). This type of methodology is often applied to CNTs synthesized in the laboratory. The commercial's nanotubes, instead, contain a significant quantity of amorphous carbon, that is instead preferentially eliminated by carrying the CNTs at high temperature (Ajayan et al. 1993), since it is preferred to transform it to graphitic carbon instead of risking to damaging the nanotubes structure with a strong oxidation.

In this work, the thermal oxidation of carbon nanotubes was used to functionalize the surface of the nanotubes without disrupting the external lattice structure.

In fact, if the oxidation treatment is carried out inside a thermogravimetric analysis (TGA) instrument, it is possible to estimate the point of degradation of carbon nanotubes, thus allowing to identify the point at which oxygen begins to interact with the material. In the presence of air under a flow of 50 ml/min, with a ramp of 10 °C/min, as shown in figure 30, the degradation of CNTs starts around 450 °C.

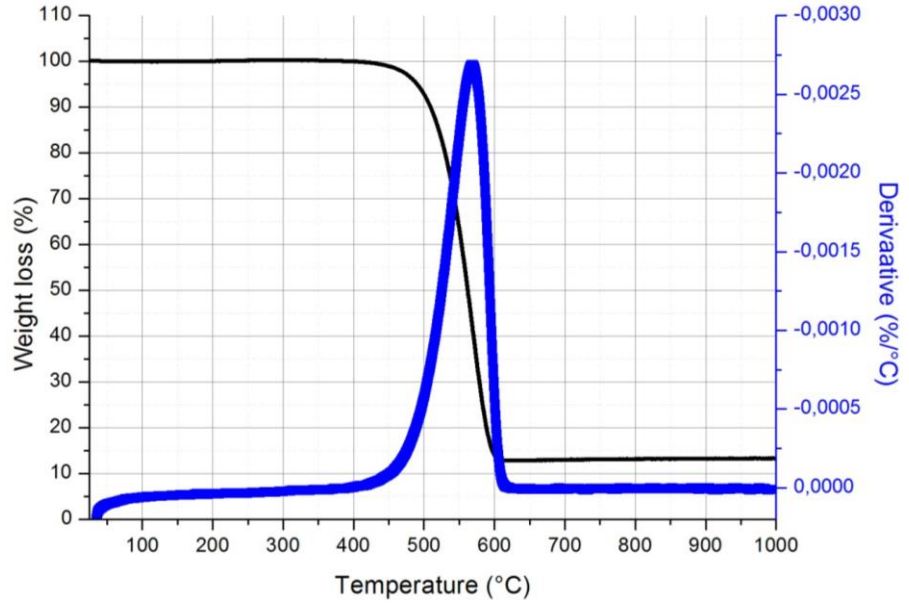

Figure 30: Thermal gravimetric analysis in 50 ml/min air at 10 °C/min of pristine CNTs

The interaction between oxygen and nanotubes starts already at temperatures below 450 °C, but at high oxygen content, the transition between slight surface oxidation (functionalization) and CNTs degradation is too steep. Instead, by reducing the percentage of oxygen in the oxidizing gas, it is possible to pass gradually from the oxygen functionalization of the surface to the full oxidative degradation.

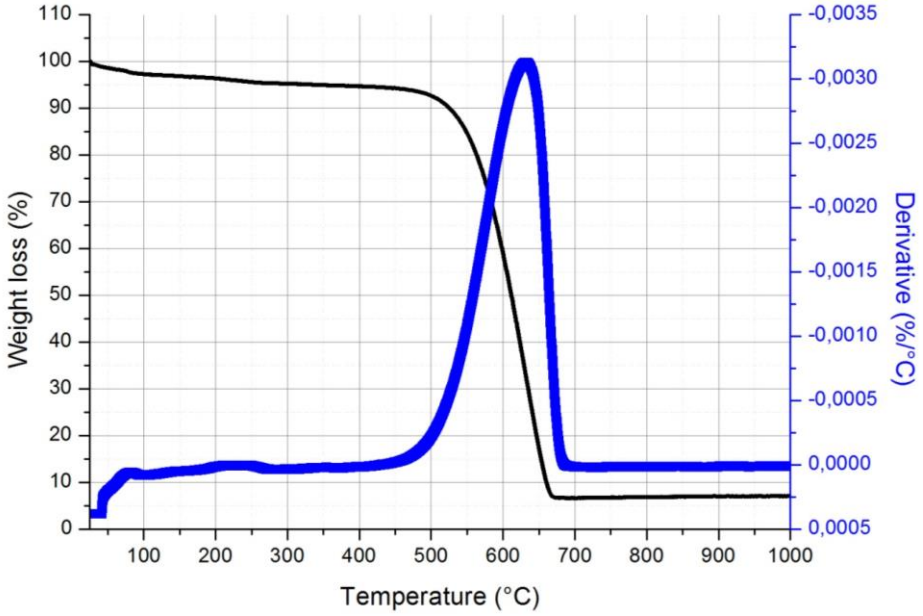

Figure 31: Thermal gravimetric analysis in 2 % oxygen at 10 °C/min

Thus, since the phenomenon of degradation is slowed down, it is possible to find a temperature where the maximum interaction between amorphous carbon

and oxygen is observed, without damaging the nanotube by removing high quantities of carbon by oxidation.

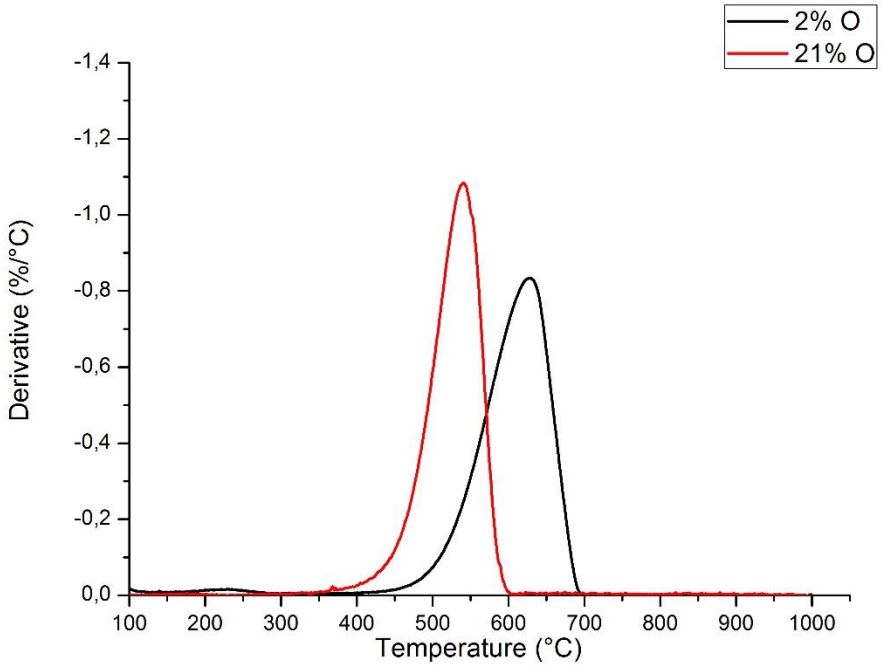

Figure 32: Derivative difference between 21% of oxygen and 2% of oxygen during at 10 °C/min

In figure 32 the comparison between the derivative weight loss of carbon nanotubes in 2% and 21% oxygen is presented. It is clear how the peak obtained at 2% oxygen is wider and shifted to higher temperature than the one obtained at 21% oxygen. In order to find the temperature at which the CNTs are not degraded, but at the same time functionalization occurs, some isothermal analyses were performed, keeping the oxygen percentage at 2%. The reason was not only to slow down the degradation process but also to minimize the presence of defects that can form on the carbon nanotubes structure during the process. It is evident from figure 33 that 450 °C is too high a temperature for this kind of oxidation: the full degradation of the carbon nanotube structure starts below this temperature. Instead, 350 and 400 °C were acceptable temperatures: only a slight weight loss is observed, probably due to the oxidation of the most defective carbon.

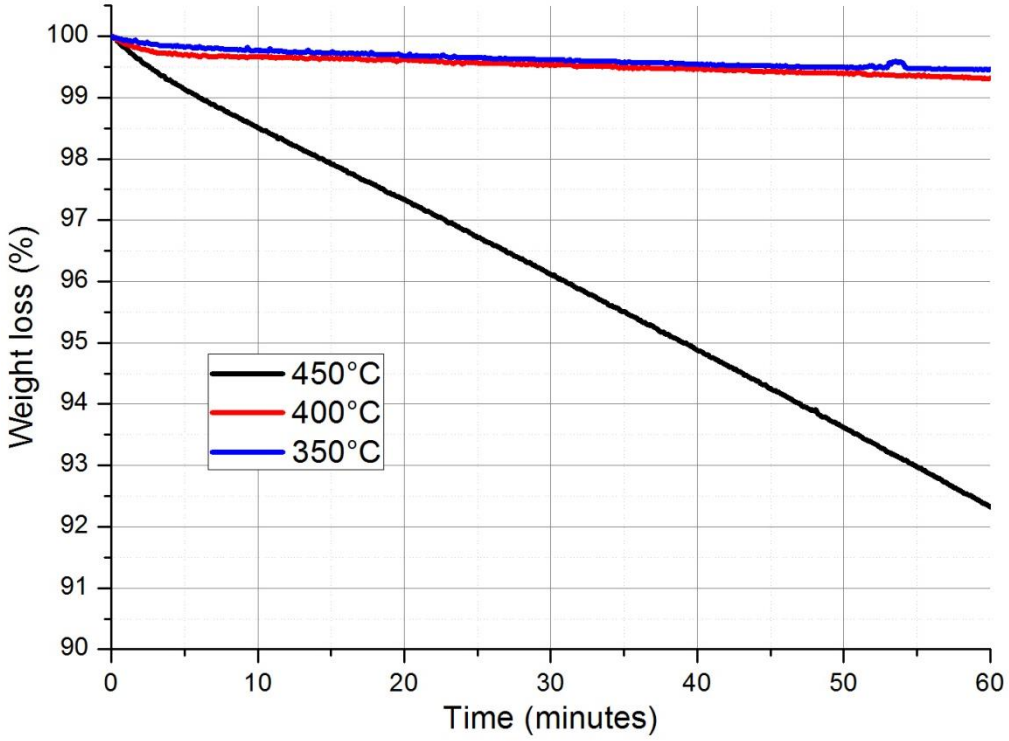

Figure 33: Thermal gravimetric analysis in 2 % oxygen in isothermal condition at different temperature

After these treatments, carbon nanotubes were placed in ultrapure water and sonicated at a power of 70 W (35 % amplitude) for 10 minutes. Dispersion of nanotubes was found to be excellent for those treated at 350 °C and with an oxygen percentage of 2%. At higher or lower temperature, the dispersion was not as efficient, probably due to the establishing of different chemical equilibrium: at temperatures below 350 °C the energy supplied is insufficient to ensure the formation of C-O bond while at higher temperatures the reaction brings to less stable functionalities, that are removed instead of remaining on the surface. This is not visible on the TGA curve probably due to the very low amount of functionalities, which do not alter significantly the weight loss curve, more influenced instead by defective carbon that is slowly completely degraded both at 350 and at 400 °C.

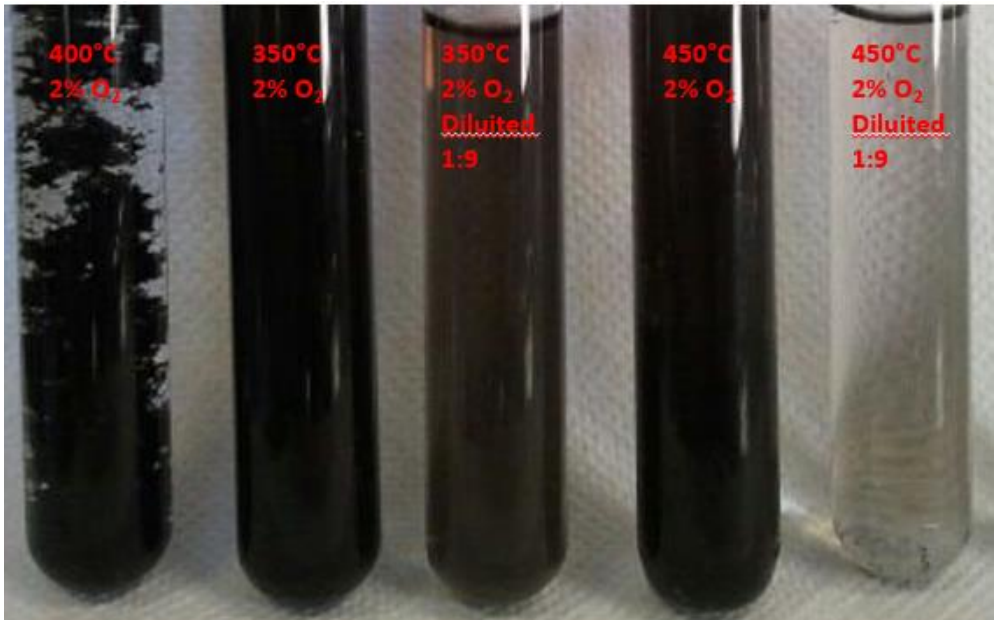

Figure 34: Dispersion of CNTs after the thermal treatment in water, and diluited 1:10 to better observe the degree of dispersion

The carbon nanotubes oxidized at 350 °C for 60 minutes were observed at the SEM and compared with the pristine ones. No significant difference was observed, save that the treated nanotubes appear to be slightly less conductive than the pristine ones.

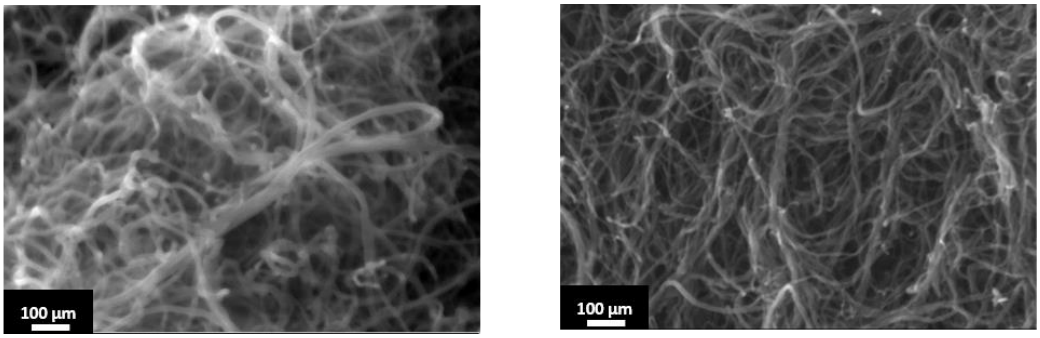

Figure 35: SEM images of pristine (left) and oxidized (right) CNTs

From an IR analysis take in ATR mode, some bands appear, as shown in figure 36.

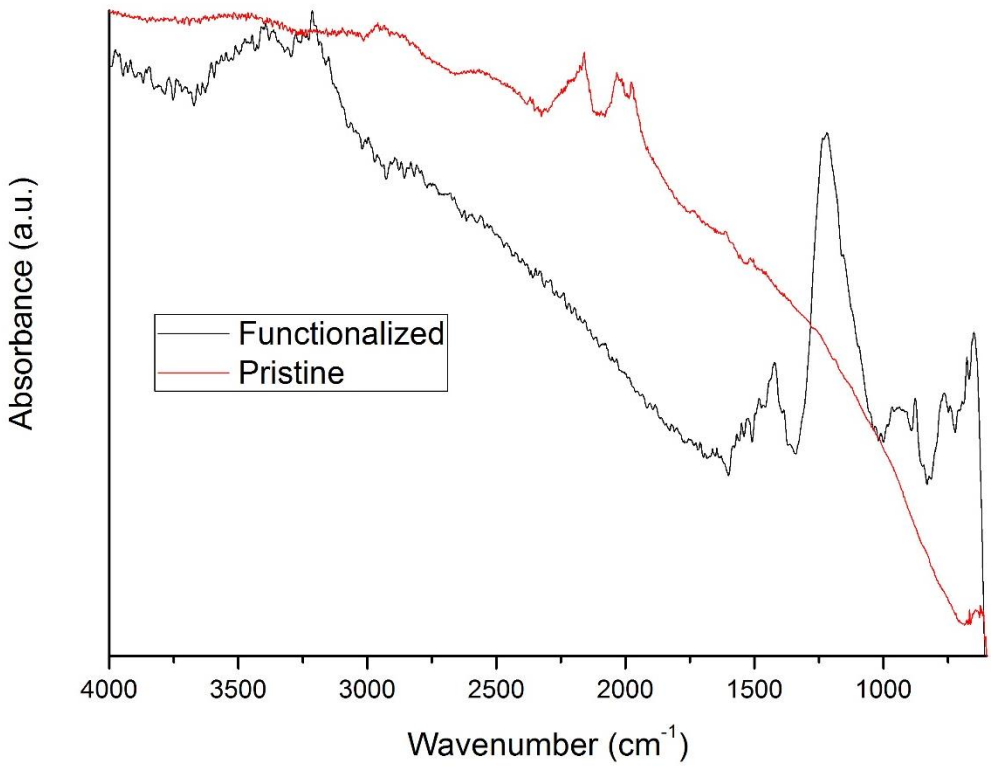

Figure 36: FT-IR spectrum of pristine (red line) and functionalized (black line) CNTs

The large band around 3400 cm^{-1} is due to the presence on the surface of –OH functional groups. At lower wavenumber we can find peak at 1427 cm^{-1} due to stretching of C-O bond and deformation of O-H bond of carboxylic acid; instead the high peak at 1224 cm^{-1} is probably due to stretching of acidic dimer or asymmetric stretching of saturated aliphatic ester. Currently it is still too early to determine with certainty the type of group that is formed with this kind of oxidation, but the clear presence of oxygen containing groups explain why CNTs are well dispersed in water without surfactant. For the pristine the two band between 2000 and 2300 cm^{-1} are due to aromatic stretching C=C.

To detect the amount of defects present on the surface of CNTs, Raman spectroscopy can be used. In figure 37 the Raman analysis of pristine and thermally oxidized nanotubes are presented.

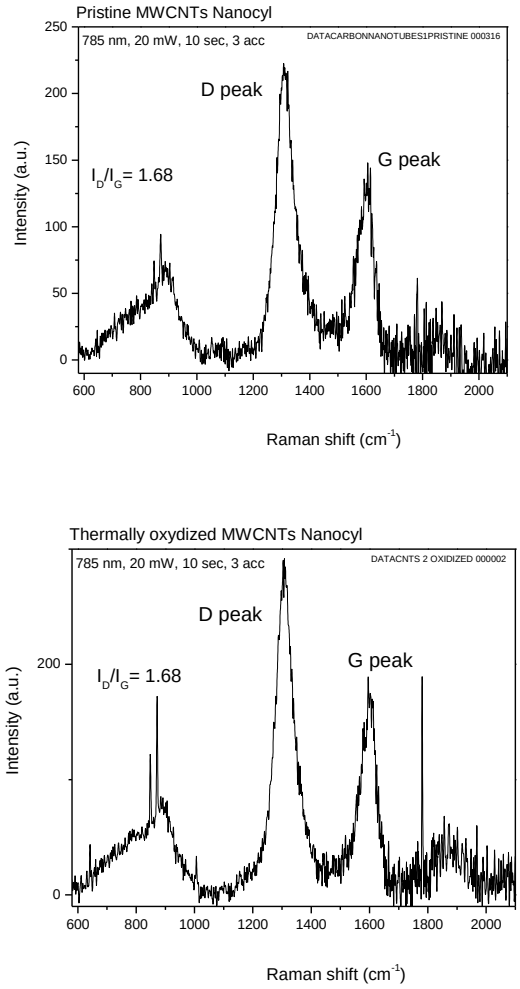

Figure 37: Average ID/IG on 3 spots of the pristine MWCNTs Top figure: 1.66 Average ID/IG on 4 spots of the thermally oxydized MWCNTs: 1.64

Each spectrum is characterized by two characteristic bands, namely the D-band at around 1300 cm^{-1}, arising from the disorder-induced phonon mode (A_{1g}-band), and the G-band at circa 1600 cm^{-1}, assigned to the Raman-allowed phonon mode (E_{2g}-band) (Melanitis et al. 1996). From this analysis there not seem to be any substantial difference between the two samples, even if a slight reduction of the I_D/I_G ratio is observed after oxidation. This reduction indicates that the temperature partially recombine the external lattice of MWCNTs, reducing the defectless of pristine one as shown by some work in literature (Andrews et al. 2001; Park et al. 2001; Huang et al. 2003). In any case these results suggest that CNTs were not significantly damaged from the oxidation.

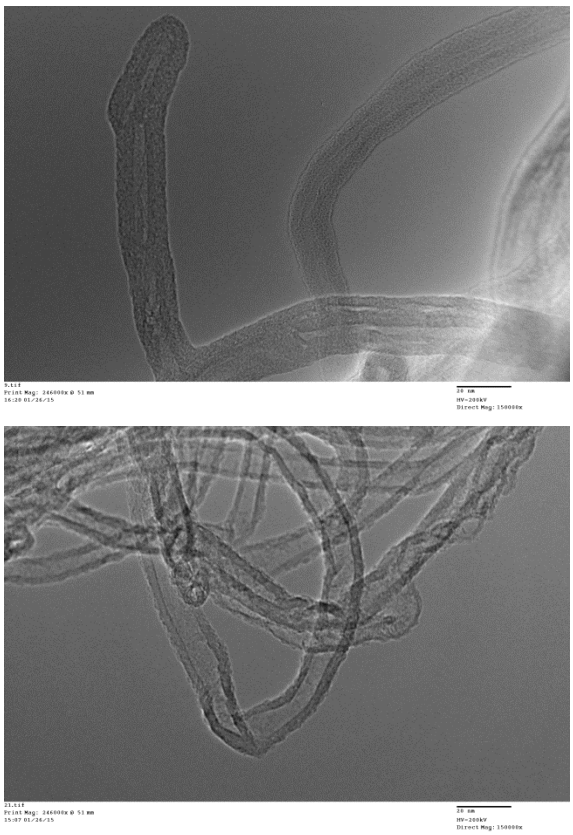

Figure 38: TEM images of pristine CNTS (top) and functionalized (bottom)

In addition, TEM images do not show any change in the structure of CNTs. The surface shows no obvious defect, and the nanotubes structure after oxidation is similar to the one of pristine CNTs. This fact suggests that, since no significant change of the structure of CNTs is observed, the chemical modification is limited to the surface. Since 350 °C is a rather low temperature for the reaction between the graphitic carbon of the carbon nanotubes and oxygen, it is probable that only amorphous carbon reacts, and not graphitic carbon. This would explain the substantially stable I_D/I_G ratio observed in Raman analysis. This hypothesis was partially confirmed by the oxidation at 350 °C in 2% oxygen atmosphere of carbon nanotubes treated at high temperature (1700 °C) in vacuum. These nanotubes were completely graphitized, and no amorphous carbon was present. After oxidation, no dispersion was observed, suggesting that the graphitic carbon of the nanotubes is not oxidized in these conditions, while the amorphous carbon present in significant quantity in commercial carbon nanotubes can instead undergo the functionalization reaction.

Finally, a stability comparison between pristine and oxidized CNTs was performed by TGA. The results, shown in figure 39, show that the degradation of

oxidized CNTs start before the one of pristine CNTs, suggesting that a low content of less stable oxygen containing groups was effectively grafted on the surface of the nanotubes. The presence of a low quantitative of oxygen helps the acceleration of the degradation and, in fact, the complete oxidation of nanotubes happens at lower temperature for the oxidized ones than for the pristine ones.

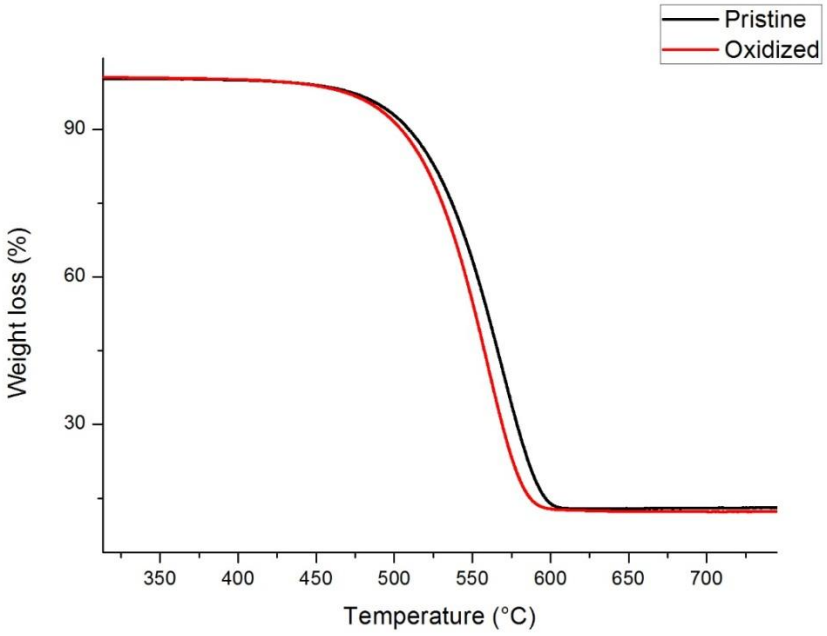

Figure 39: TGA analysis of pristine CNTs (black line) and functionalized (red line) carbon nanotubes at temperature ramp of 10 °C/min in air

5.2 Preparation of hierarchical material by chemical grafting carbon nanotubes onto carbon fibers

Part of the work described in this chapter was previously published in "Lavagna L, Massella D, Pavese M (2017) Preparation of hierarchical material by chemical grafting of carbon nanotubes onto carbon fibers. Diam Relat Mater 80:118–124." (Lavagna et al. 2017)

5.2.1 Oxidation of CFs and CNTs.

For the oxidation of CFs 2.0 g of carbon fibers were accurately weighted and placed in a 100 ml beaker. The acidic functionalization was performed by soaking the CFs in 80 ml sulfonitric acid solution (1 HNO_3 : 3 H_2SO_4) prepared by adding firstly 20 ml of nitric acid and then 60 ml into the beaker where CFs were placed.

In order to promote the oxidation process the solution was sonicated in an ultrasonic bath (SONICA 2400 MH series 40KHz of frequencies) for 30 minutes.

At the end of the treatment, the solution was neutralized in a basic solution of 1 M NaOH until pH 7 was reached. Functionalized carbon fibers were then recovered via filtration with a fritted glass filter class G3 Pyrex (pore size 15-40 μm). Fibers and nanotubes were washed several times with distilled water and dried overnight in an oven at 80 °C.

The same procedure was used to chemically oxidize 0.5 g of the carbon nanotubes; in this case, a filter with a fritted glass filter class G4 Pyrex (pore size 0.5-15 μm) was used.

5.2.2 Grafting of CNTs onto CFs.

For the grafting, 0.2 g of the oxidized CFs were split over a glass plate in order to maximize the contact area, while different quantities of the treated carbon nanotubes were dispersed in acetone using an ultrasonic probe at 100 W (40% of amplitude) power. The CNTs dispersion was poured, drop-by-drop, over the carbon fibers waiting for the solvent evaporation. To avoid the tendency of CNTs to aggregate in bundles, extra sonication steps were repeated in the ultrasonic bath for 5 minutes every 10 minutes, in order to maintain an effective dispersion.

After all of the CNTs dispersion was poured over the CFs, the CF-CNT system was put in oven at 200 °C for 5 hours in order to create the chemical bonding, as suggested in literature (Abdelghani Laachachi et al. 2008).

After the thermal treatment, the carbon fibers functionalized with carbon nanotubes were washed with pure water and dried in an oven at 60 °C.

The different amount of CNTs poured over the fibers and the sample nomenclature are listed in Table 8. The CNTs/CFs ratio was multiplied by100 in order to let it correspond to the percentage of CNTs with respect to CFs.

Table 8: Composition of the fibers grafted with carbon nanotubes

Sample number	100*CNT/CF ratio b.w.	CFs weight [g]	CNTs weight [g]
MS 50	50	0.3	0.15
MS 33	33	0.3	0.1
MS 20	20	0.2	0.04
MS 5	5	0.2	0.01
MS 2	2	0.2	0.004

5.2.3 Characterization of the grafted samples.

TGA was used to compare the behavior of the grafted fibers with the behavior of pristine and oxidized fibers and nanotubes. The sample of grafted fibers was prepared by taking some of the fibers and accurately washing them, in order to avoid errors in the analysis due to the presence of free CNTs powder. The analysis was performed in air atmosphere in order to observe the possible interactions among the oxygen containing surface groups and the air. Samples of CFs and CNTs both in the as received (pristine) and oxidized state were also submitted to TGA characterization. The samples were heated from 25 °C to 1000 °C with a constant heating rate of 10 °C/min, the air was supplied with a constant flow rate of 50 ml/min.

The morphology of the samples was inquired by means of a Zeiss Merlin FESEM. Samples were prepared for each grafted fibers batch. Various photos have been taken at different magnifications and in different areas of the samples in order to observe the average morphology.

5.2.4 Oxidation of the species.

The FT-IR spectra of pristine and oxidized CNTs have been collected and represented in figure 40.

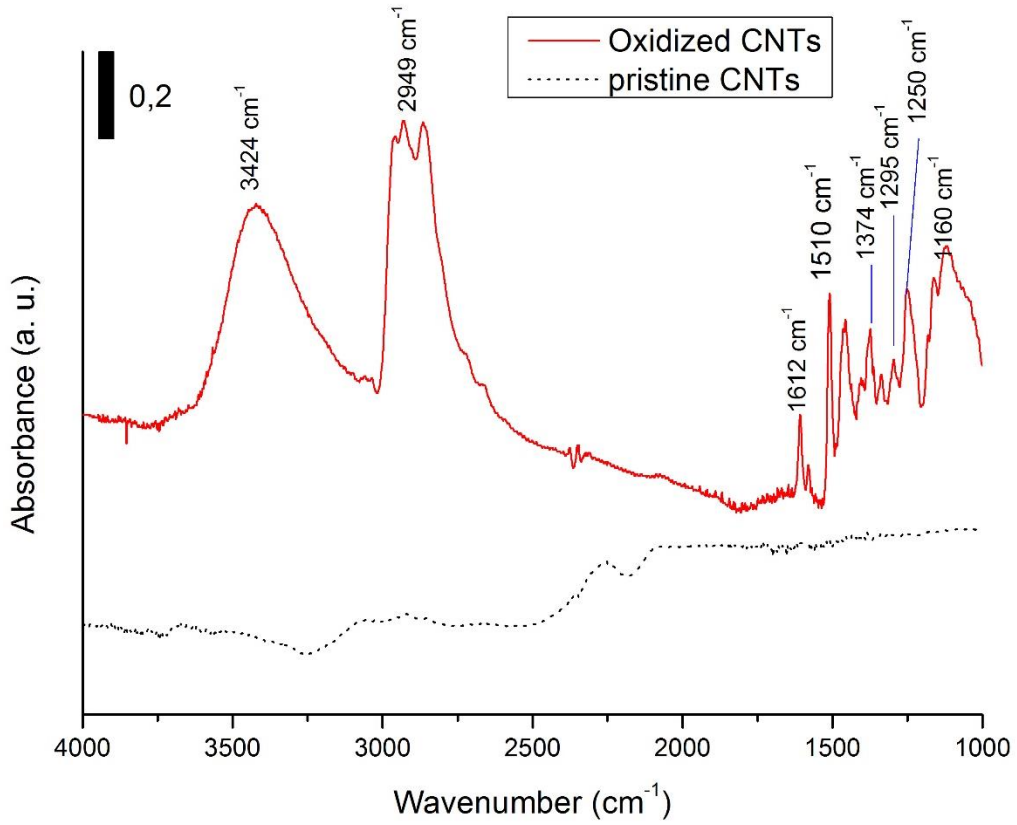

Figure 40: FT-IR spectrum of pristine and oxidized CNTs by sulfonitric acid

In the case of pristine CNTs, as expceted, there are no significant bands on the IR spectrum, since there is no IR-active species in pure CNTs; the only small signal observed around 2000 and 2200 cm^{-1} is due to the stretching of C=C bond. The presence of new chemical groups on the surface of oxidized CNTs is instead very clear. An absorption band at 3424 cm^{-1} is observed, related to both the –OH functionality and the absorbed water. The peak at 1374 cm^{-1} is due to the -OH bending deformation in –COOH. The band around 2949 cm^{-1} corresponds to the symmetric stretching of C-H bonds in carbonaceous material. The bands between 1750-1550 cm^{-1} can be assigned to C=O groups in different enviroments (carboxylic acid, ketone/quinone), whereas the peak at 1510 cm^{-1} is due to the stretching of C=C bond in aromatic rings (Socrates and Socrates 2001; Gómez et al. 2016). The peaks at 1295 cm^{-1}, 1250 cm^{-1} and 1160 cm^{-1} correspond to the C–O stretching vibrations of the carboxylic groups (–COOH) (Kathi and Rhee 2008). All these observations indicate that the surface of the nanotubes was functionalized by oxidation and hence confirm the formation of –COOH groups on MWCNTs.

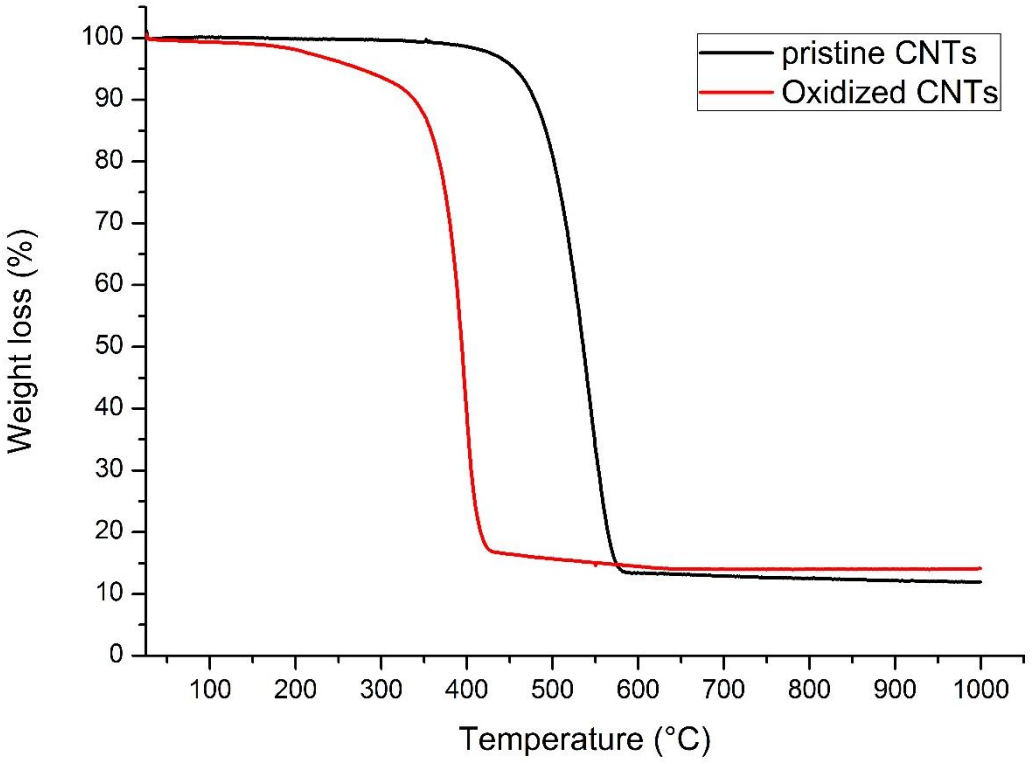

Figure 41: TGA profiles of pristine CNTs (black line) and of CNTs after oxidation with sulfonitric acid (red line)

Figure 41 shows that weight loss curves of pristine (red) and sulfonitric-treated samples (red curves) are very different. The oxidized nanotubes have a much lower thermal stability, with complete oxidation starting below 400 °C. This kind of behavior is due to the treatment. In fact, the sulfonitric treatment introduces a great amount of reactive and temperature sensitive chemical groups as confirmed by FT-IR analysis. The profile of the curve after the treatment suggests a very high damage to CNTs. The first small step of weight loss, up to a temperature of 150 °C, corresponds to the evaporation of the adsorbed water (Datsyuk et al. 2008). The second stage – from 150 to 300 °C – is attributed to the decarboxylation of the carboxylic groups present on the MWCNT walls (Tang et al. 2006). Thermal degradation in the range between the 300 °C and 350 °C may be explained by the elimination of hydroxyl functionalities, attached to the MWCNT walls (Grandi et al. 2006). Finally, at temperature higher than 400 °C, the observed degradation corresponds to the thermal oxidation of the remaining carbon (Hou et al. 2001).

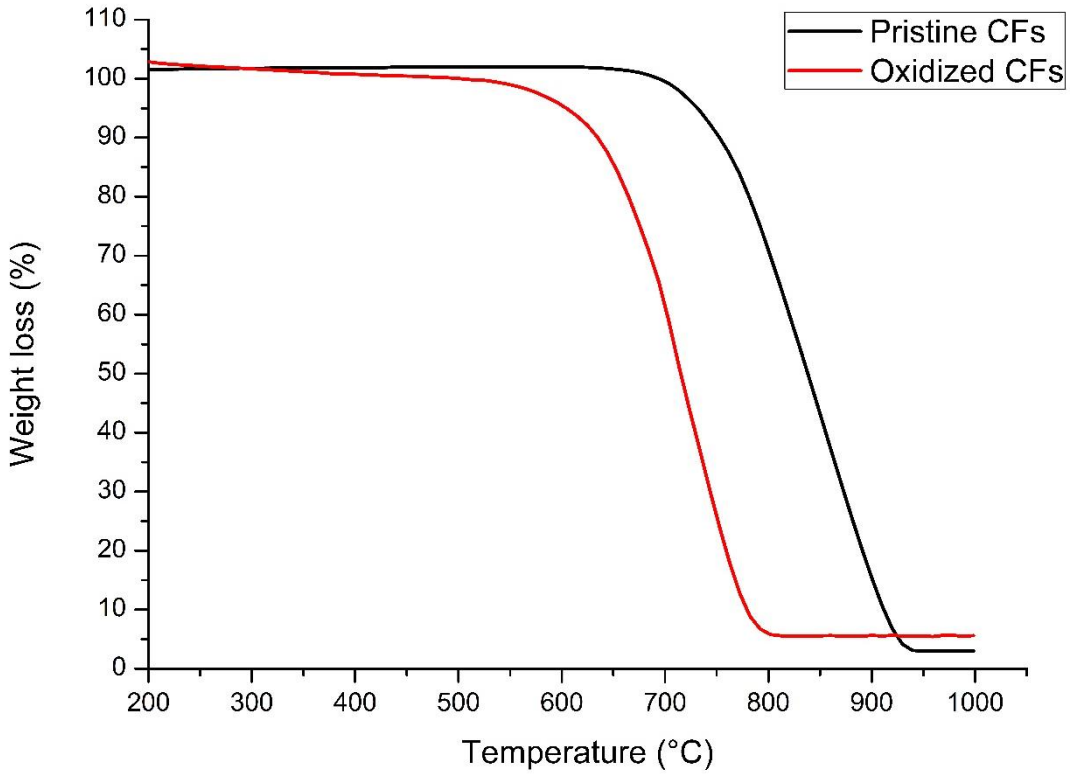

Figure 42: TGA profiles of pristine CFs (black line) and of CFs after oxidation with sulfonitric acid (red line)

Figure 42 shows that a similar behavior is observed also for carbon fibers: the TGA weight loss curves of pristine and sulfonitric-treated CFs are very different. The sulfonitric-treated sample exhibits a lower thermal stability, and starts to oxidize well below 700 °C. The origin of the behavior can be easily found in the fact that the sulfonitric treatment, introduces, as explained for CNTs, a greater amount of reactive and temperature sensitive chemical groups. The residuum at high temperature is slightly different in the case of pristine and oxidized CNTs and CFs, probably due to some residual salt formed during the neutralization of the acid, that could not be completely washed away during the washing and rinsing process.

5.2.5 Effectiveness of the grafting treatments.

The effectiveness of the grafting treatment was confirmed by mean of the thermogravimetric analysis. The results of the analyses made on the three samples of oxidized CNTs, oxidized CFs, and grafted fibers are plotted in figure 41.

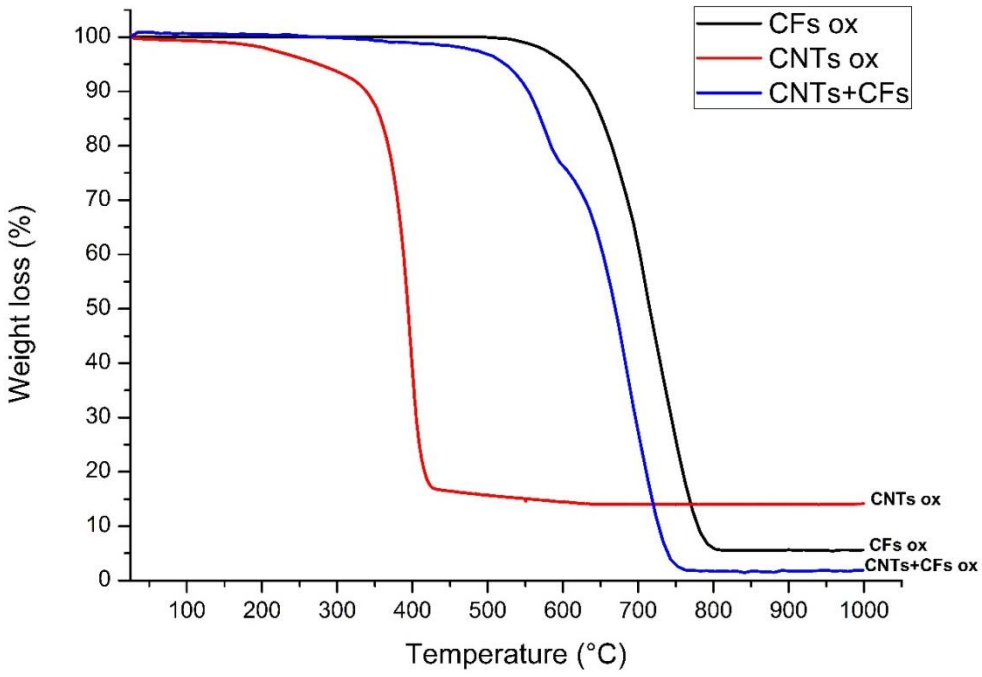

Figure 43: TGA profiles of oxidized CFs and CNTs compared with the grafted MS 20 sample

The TGA profiles show how the three samples started to be thermally degraded at different temperatures; the grafted fibers showed a curve, which is in between the one of pure CFs and CNTs. Referring to figure 43 it is observed that CFs and CNTs curves present a unique inflection point. A different behavior was instead observed for the grafted fibers curve, where two inflections can be observed. The presence of two inflection points suggests that different species are thermally degraded at different temperatures; the two peaks can be associated to a first degradation of CNTs and a subsequent degradation of the fibers. Moreover, it is observed that in the grafted fibers the thermal degradation of CNTs starts at a higher temperature (above 500 °C) with respect to the one at which the oxidized CNTs are typically degraded, which is below 400 °C. This phenomenon is caused by the fact that oxygen-containing groups are not present anymore on the CNTs surface, since they were used in the esterification reaction to form the chemical bond with the carbon fibers. Since such groups starts their degradation at lower temperature, in their absence the degradation started at higher temperature.

5.2.6 Morphological observation of the different batches

The samples were observed by mean of field emission scanning electron microscopy with the aim of observing the morphology of the grafted fibers at

different CNTs concentrations. In fact, the SEM analysis gave an ulterior confirmation of the success of the grafting treatment. In figure 44 the MS 2 is observed at increasing magnifications. Looking at the fibers at low magnification, in the top-left picture, it seems that the carbon nanotubes have not covered all the fibers. Moreover it is possible to notice the presence of big CNTs aggregates on the fiber surface, that could be due to the use of acetone to promote the reaction between CFs and CNTs, since acetone is not an effective dispersant for the nanotubes. Getting closer to a single fiber, however, (pictures c) and d)) is possible to observe that where the carbon nanotubes are present, they uniformly cover the surface. They lie prevalently flat on the surface, with a random orientation respect to the fiber axis.

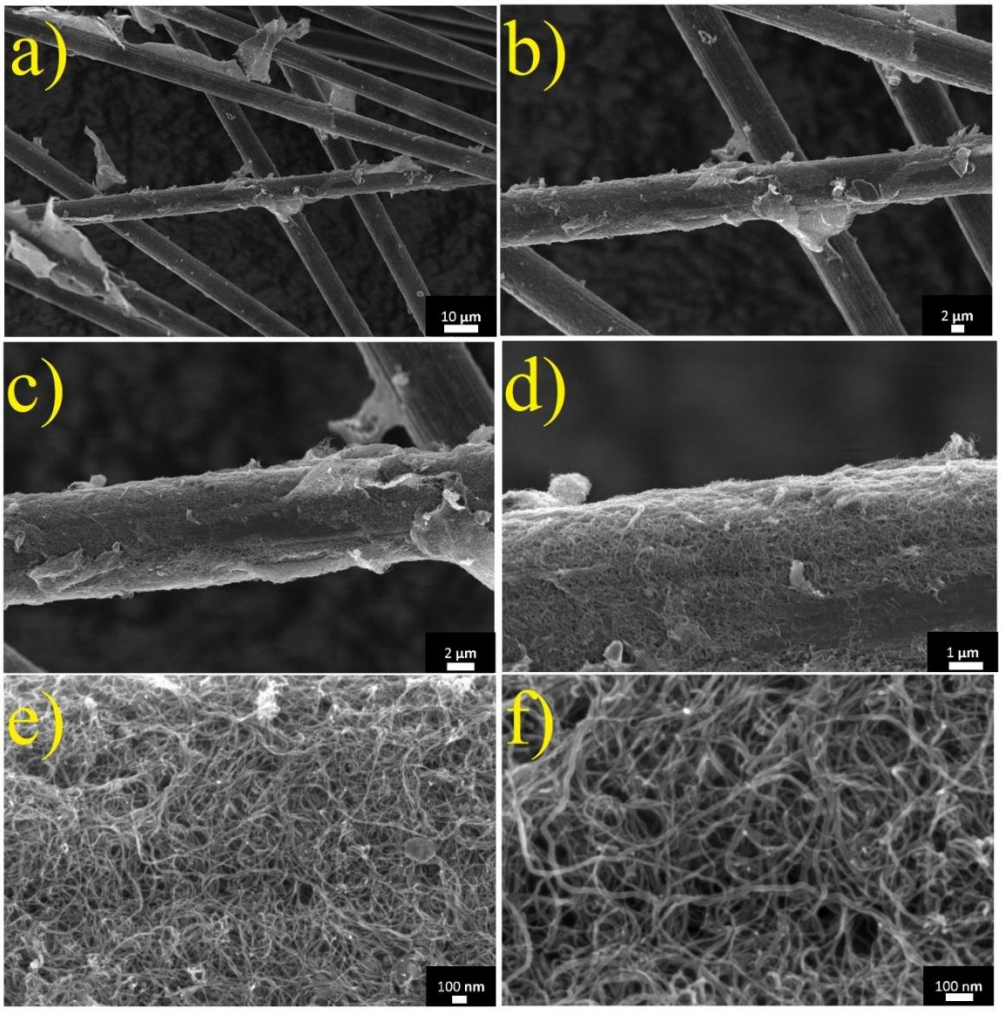

Figure 44: SEM images of a MS 2 sample at different magnifications: a) 2500 X b) 5000 Xc) 10000 X d) 25000 X e) 100000 X f) 200000 X

The not uniform coverage can be attributed to the small amount of CNTs used in the grafting treatment, which did not allow the entire fibers surface to come in contact with the carbon nanotubes. In figure 45 the case of a MS 5 is studied. It is

not possible to observe a significant change in the morphology between the two samples.

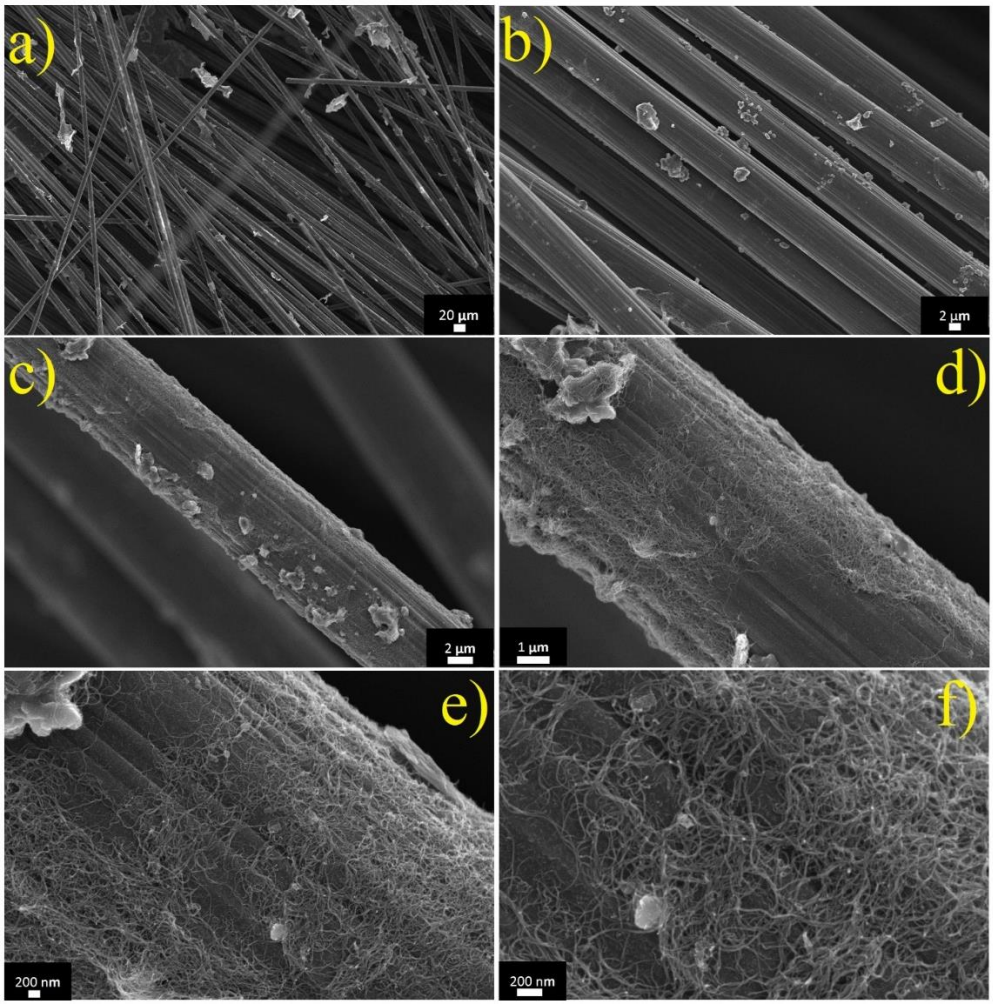

Figure 45: SEM images of a MS 5 sample at different magnifications: a) 500 X b) 5000 c) 10000 X d) 25000 X e) 50000 X f) 100000 X

In the case of MS 20 a great morphological change is observed. In figure 46 it is possible to see some carbon fibers that are uniformly covered by some nanoscale species, looking closely it is possible to understand that these species have a spherical geometry.

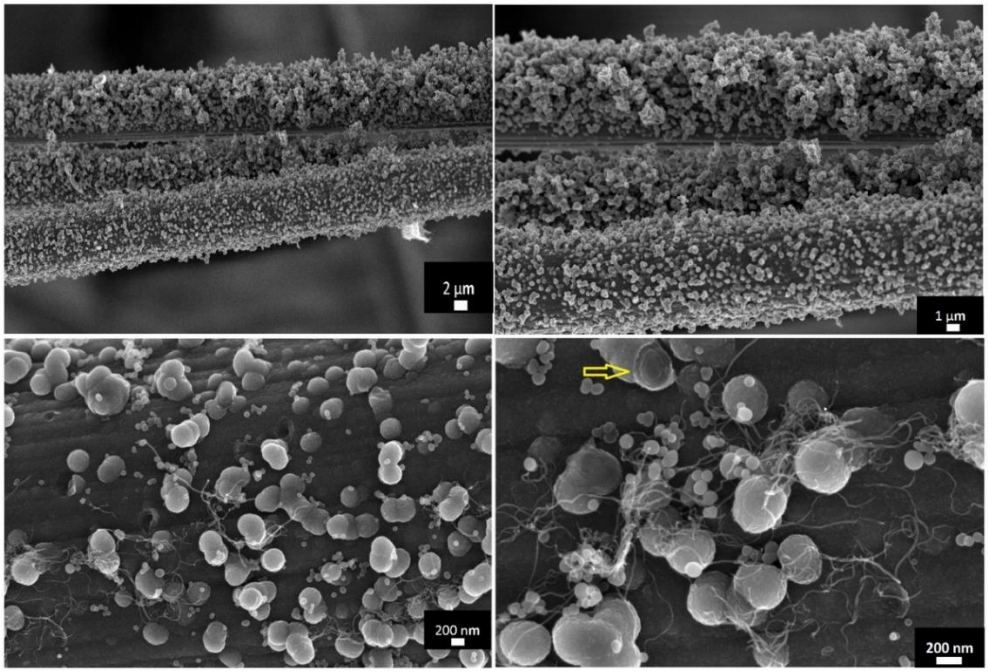

Figure 46: SEM images of a MS 20 sample at different magnifications: A) 5000 X B) 10000 X C) 50000 X D) 100000 X. The arrow indicates a particle showing inner concentric layers, that allowed the identification of the spherical particles as CNOs

Looking at figure 46C it is possible to observe in a clearer way the morphology of the fiber surface. The species covering the fiber present spherical geometry with a diameter ranging roughly from 20 nm to 250 nm. On the fiber surface, some holes are present. In figure 46D, a section of a spherical particle was observed showing a structure made of several concentric layers. The carbon nanotubes appear to interact with these spheroids.

The nanosphere can be identified as the carbonaceous materials called Carbon Nano Onions (CNOs) (Zeiger et al. 2016). The CNOs spheroidal structure can be synthetized from carbon fibers, the strong acid treatment probably weakens the bonds between differently oriented carbon structures in the fibers, and CNOs emerge out of the surface of the CFs from the liquid phase during the grafting process (Fan et al. 2012).

The correlation between the obtained morphology and the increased concentration of CNTs can be explained giving to the CNTs the role of nanometric ropes that keep the onions bound to the fibers and this required a higher CNTs concentration than in the case of MS 2 and MS 5. Further studies will be required to define the conditions under which it is possible to obtain the morphology described above. The hierarchical porosity and increased roughness may turn out to be crucial properties in the development of advanced composites.

For what concerns the samples containing the highest amount of carbon nanotubes i.e. MS 33 and MS 50, issues related to CNTs dispersion occurred. As a matter of facts, the high amount of nanotubes tended to aggregate in acetone, and this fact was reflected in the obtained fibers. The CNTs covered the fibers with a thick layer as shown in figures 47 and 48; this is very different from the case of MS 5 and MS 2 where a sort of CNTs monolayer was formed.

In this case, the higher amount of CNTs deposited on the fiber grants the complete coverage of the fiber surface: the large amount of CNTs available for bonding saturated all the available reacting sites, generating and increased bonding among nanotubes and subsequently agglomeration. In fact, the SEM images clearly show how the hierarchical structure was achieved; as a matter of fact, once the first CNTs layer is formed on the fiber surface, nanotubes continue to deposit over other nanotubes, giving rise to a multilayer hierarchical structure with increased surface area.

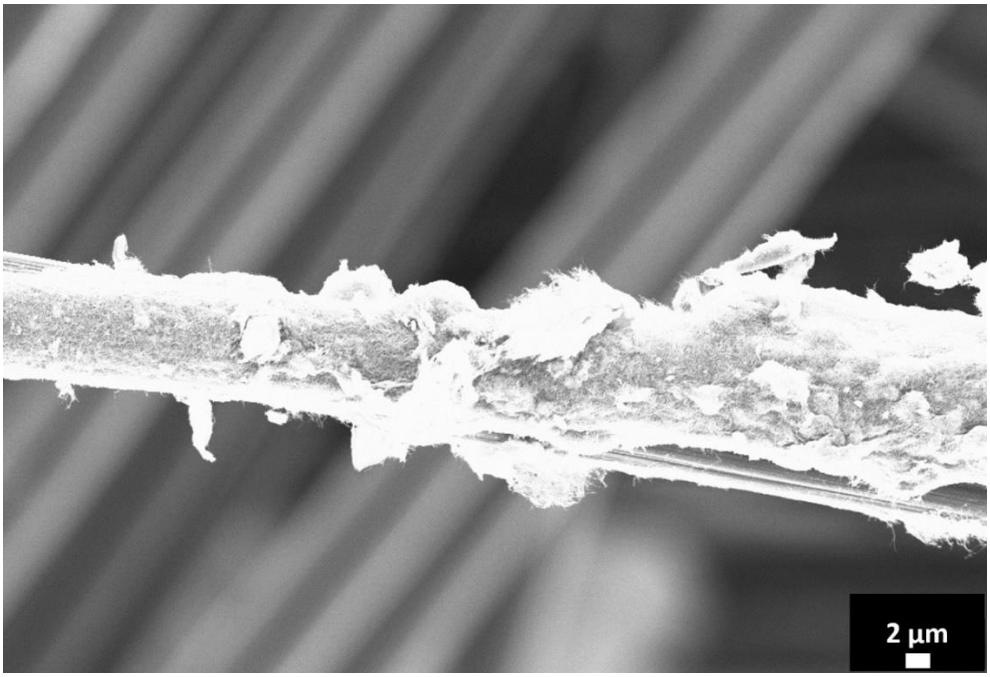

Figure 47: SEM image of a MS 33 sample at a 5000 X magnification

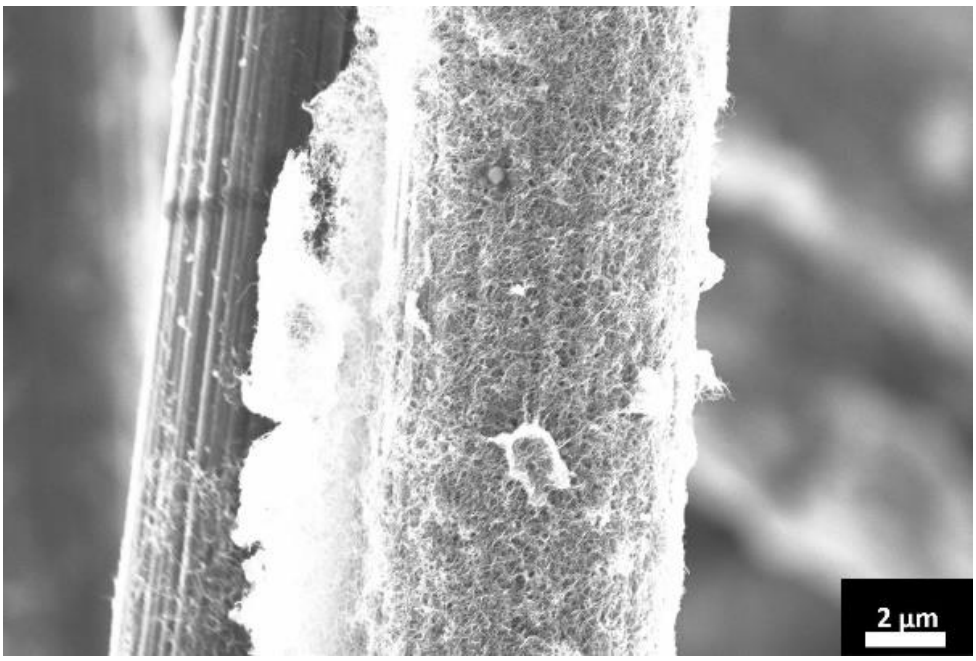

Figure 48: SEM image of a MS 50 sample at a 15000 X magnification

5.2.7 Conclusions

In this paragraph, a coating technique for the easy preparation of carbon fibers grafted with CNTs is presented.

The proposed chemical process allows to graft carbon nanotubes onto a carbon fiber surface without using neither catalysts nor coupling agents. The same oxidation process was used for both CFs and CNTs, thus simplifying the overall production process.

TGA, FT-IR and SEM analysis confirmed the success of both the oxidation and the grafting processes.

Different CNTs/CFs ratios were tested and the related variations of the overall morphology of the multiscale composite were observed by FESEM.

It was shown that grafting with a higher concentration of CNTs in acetone gives the best results in terms of coverage of CNTs around the fibers and improves the surface area by forming a hierarchical 3D network.

A novel multiscale structure was observed in the intermediate CNTs/CFs ratio case, where CFs and CNTs interlinking with carbon nano onions were observed and a synthesis mechanism was hypothesized. Further studies will be required to deeply define the conditions under which it is possible obtain carbon nano onions (CNOs) bonded on the surface of the fibers. The synthesis of the CF-CNO-CNT

structures gives rise to an ulterior level of hierarchy and the assessment of the properties of such a structure is something to be deeply investigated.

5.3 Cement matrix composites

In all works about cement matrix composite, it has to be underlined that we took care to provide a repeatable and reproducible preparation and curing of the cement.

5.3.1 Cement-base composites containing carbon nanotubes

The objective of this work was to improve the dispersibility of carbon nanotubes in water, in order to be able to disperse them efficiently in cement paste. Generally, the dispersion of CNTs can be improved by guaranteeing the presence of polar groups on the surface on CNTs, either by oxidation or by using a surfactant (see paragraph 2.2). In this work, the oxidation route was chosen, in order to avoid the presence of molecules on the surface of nanotubes, which could reduce electrical conductivity of the final cement-based composite.

For this reason, the first step of this work was to select the best acid mixture to guarantee a stable dispersion of oxidized carbon nanotubes in water. Even if sulfonitric oxidation is the most used for the formation of surface polar groups (Gómez et al. 2016), a first step was performed with different acid mixtures, in order to verify the effect of other acid attacks on the dispersibility of carbon nanotubes. Four oxidative acid mixtures were compared: a) 1 HNO_3 : 3 HCl (aqua regia); b) HNO_3 (nitric acid); c) 3 H_2SO_4 : 1 H_2O_2 (piranha solution); d) 1 HNO_3 : 3 H_2SO_4 (sulfonitric acid). A small amount (0.1 g) of pristine CNTs was soaked in each acid at 30 °C for 30 minutes. During the reaction, the CNTs suspension was continuously mixed by sonication, using an ultrasonic bath (SONICA 2400 MH series 40KHz of frequencies). At the end of the treatment, the acid solutions were neutralized with a basic solution of NaOH 1M up to pH 7. The functionalized CNTs were then recovered via filtration with a fritted glass filter (G4 class Pyrex). The CNTs were then washed several times with ultrapure water and dried overnight at 80 °C. The dried CNTs were dispersed in water with an ultrasonic tip (Vibra-cellTM, power 100 W, 40% of ampliude for 15 minutes) and poured in a test tube for observing the possible sedimentation of badly dispersed specimens.

As shown in figure 47, the evaluation of the dispersion was made by comparing the behavior of the CNTs suspension in each test tube after different periods of time (in figure are shown the images after 1 hour and 24 hours from the insertion of the solution in the test tube). Badly dispersed carbon nanotubes (cases *a*, *b*, *c* in figure 47, corresponding to oxidation with aqua regia, nitric acid and piranha solution) form large bundles that start to precipitate after only 1 hour. The CNTs are then fully precipitated at the bottom of the test tube within 24 hours. On the other hand, in the test tube containing CNTs treated with sulfonitric acid (case *d* in figure 47) a significant amount of the material remains suspended in the solution after 24 hours. To determine the real extent of dispersion it is however necessary to observe a very dilute suspension, otherwise the dark color of the concentrated suspension will not allow to discriminate between nanotubes completely dispersed and small bundles of agglomerated nanotubes remaining in the water due to the small size. After 1:9 dilution of the supernatant, it is possible to observed an uniform, light grey color, that guarantees that the suspension is made of individual nanotubes and stable over time (Bystrzejewski et al. 2010).

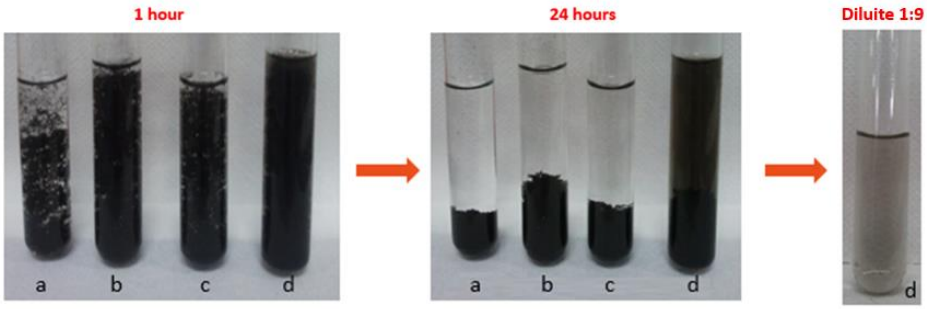

Figure 49: Test tubes used to evaluate the dispersion in water of CNTs treated with: a) aqua regia, b) nitric acid, c) piranha solution, d) sulfonitric acid. The images show, from left to right, the evaluation of the aqueous suspension after 1 hour, after 24 hour, and the test tube d solution diluted 1:9. The dilution was performed to better appreciate the successful dispersion of sulfonitric treated CNTs

This first step confirmed that aqua regia, nitric acid and piranha solution were not effective in the oxidation of carbon nanotubes, and thus that only sulfonitric acid could give a suspension suitable for the preparation of cement-CNT composites. Then, the effect of the duration of the treatment with sulfonitric acid on carbon nanotubes was assessed, by preparing multiple samples, considering oxidation times of 15, 30 and 120 minutes. The oxidized carbon nanotubes obtained with these treatments were used to prepare cement-based composites,

containing 0.1% by weight of cement (BWOC) CNTs. Also non-functionalized CNTs were used, for comparison, and samples of pure cement.

The procedure to prepare cement consists in the re-dispersion of the oxidized carbon nanotubes in water with an ultrasonic tip for 15 minutes at 100 W power, 40% of amplitude. The suspension of CNTs and water was then mechanical stirred for several minutes, while cement powder was slowly added. The slurry, prepared at water-to-cement (W/C) ratio of 0.45, and containing 0.1% bwoc of CNTs, was then poured into suitable molds and cured for 24 h at 85 °C in a controlled environment, at 100% of relative humidity. Prismatic molds of size 20x20x75 mm were used for the cement composites, that were then mechanically tested to obtain flexural strength (MOR) and toughness.

Characterization of carbon nanotubes after acidic treatment

Oxidized CNTs are better wetted by water than pristine ones (Pavese et al. 2008), thanks to the presence of polar groups on their surface, generally carboxilic groups in large amounts. Since for the application in a cementitious matrix it is important to introduce the right amount of chemical groups, while avoiding an excessive number of defects, the presence of new chemical groups on the surface of CNTs was investigated by FT-IR analysis. Avoiding defect formation is important not to reduce the extraordinary chemo-physical properties exhibited by pristine and defect free CNTs (Saito et al. 2002).

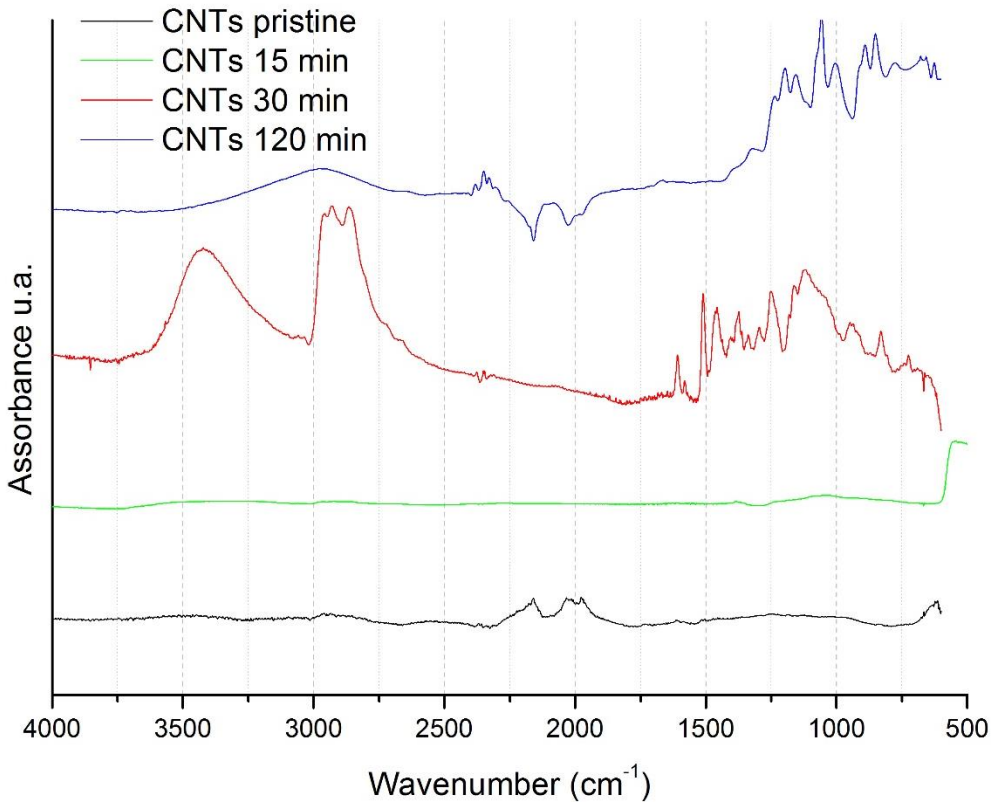

Figure 50: FT-IR spectrum of CNTs, pristine and oxidized by sulfonitric acid

The FT-IR spectrum of pristine and oxidized CNTs is shown in figure 50. For CNTs oxidized for 15 min, it has no substatial differences in comparison to the spectrum of pristine CNTs. After oxidation for 30 min, an absorption band centered at 3424 cm^{-1} is observed for the –OH functionality and a peak at 1374 cm^{-1} is due to the –OH bending deformation in –COOH. The band around 2949 cm^{-1} corresponds to the symmetric stretching of C–H bonds in carbonaceous material. The bands between 1750-1550 cm^{-1} can be assigned to C=O groups in different enviroments (carboxylic acid, ketone/quinone), whereas the peak at 1510 cm^{-1} is due to the stretching of C=C bond in aromatic rings (Socrates and Socrates 2001; Gómez et al. 2016).The peaks at 1295 cm^{-1}, 1250 cm^{-1} and 1160 cm^{-1} correspond to the C–O stretching vibrations of the carboxylic groups (–COOH) (Kathi and Rhee 2008). All these observations indicate a strong functionalization of the surface of the CNTs, with the formation of –COOH and other oxygen-containing groups. The spectrum of CNTs oxidized for 120 min is instead substantially different. A strong reduction of the band of –OH in the 3600-3250 cm^{-1} range is observed, suggesting these functionalities are reduced for long times of treatment. Moreover, the reduction of the bands in the 3000-2750 cm^{-1} range suggests that the structure of the lattice of CNTs is partially destroyed and that a

high amount of amorphous carbon is formed in the solution (Wepasnick et al. 2011; Sahebian et al. 2015). In fact, also the band at 2750 cm^{-1}, related to the stretching of C–H bonds, is reduced due to the elimination of these defective sites on the surface. On the low frequency part of the spectrum, the two peaks around 1100 cm^{-1} and 620 cm^{-1} indicate the presence of sulfonated groups, while the second peak in the 620 cm^{-1} region indicates a bending vibration of C–H bonding (Osorio et al. 2008); finally, the absence of bands in the 1550 cm^{-1} region demonstrates a reduction in term of –COOH funtionalities. On the whole, FT-IR analysis suggests a lower amount of oxygen-containing groups for the CNT samples oxidized for 120 min, that is consistent with the data shown further below in Table 9, where a reduction of mechanical properties is observed for long oxidation time: if less polar groups are present on the surface, both dispersibility in water and interaction with cement will decrease.

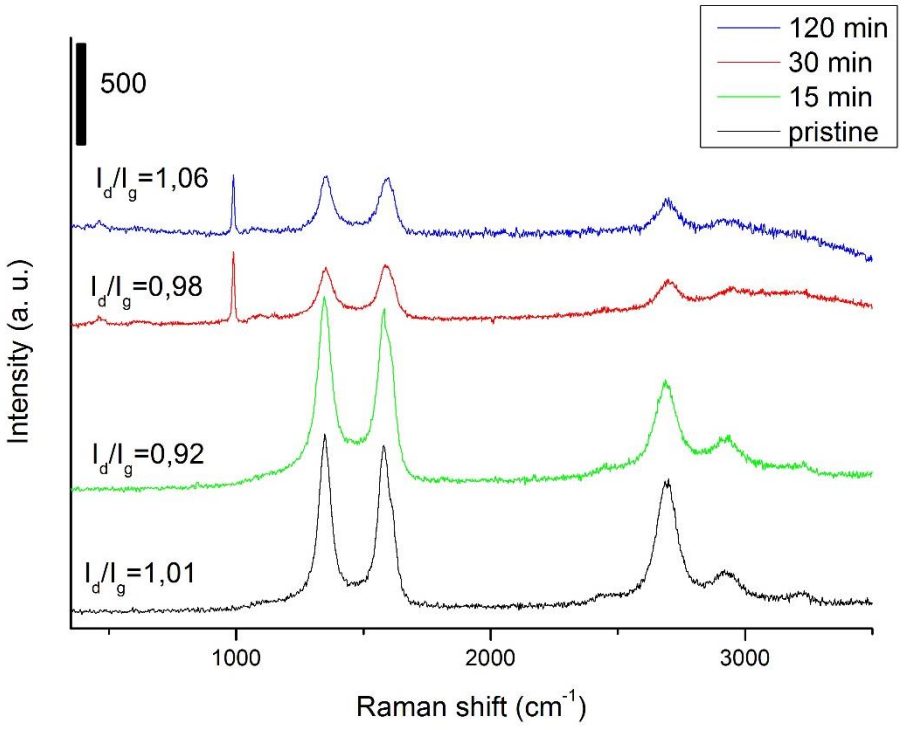

Figure 51: Raman spectrum of CNTs, pristine and oxidized y sulfonitric acid

Raman spectroscopy was employed to characterize the quality of the graphitic nature of the carbon nanotubes surface, before and after oxidation. The Raman spectra of pristine and sulfonitric treated CNTs are shown in figure 51. Interestingly, the acid treatment initially provokes a decrease in the I_D/I_G ratio consequent, as suggested by some studies (Dillon et al. 1999; Park et al. 2001), to the elimination of amorphous carbon from the CNTs. From IR analysis, however,

it was noted that after 15 minutes of treatment the surface is not still functionalized, since only samples treated for 30 min show a significant degree of oxygen-containing groups. Moreover, for longer reaction times, figure 51 suggests that the structure of the lattice of CNTs is partially destroyed as demonstrated by the reduction of the Raman peaks, in particular around 2700 cm^{-1}, that defines the lattice order. It is thus probable that after a first step of removal of amorphous carbon, the CNTs surface starts to be functionalized, with at the same time a reduction of crystallinity. For long reaction times (120 min), the damage to the surface becomes prevalent with respect to the functionalization, leading to a decrease both of IR bands related to oxygen-containing functionalities and of the Raman bands, in particular around 2700 cm^{-1}. Confirming this hypothesis, the I_D/I_G ratio increases again due to the formation of new defects.

The sharp peak around 993 cm^{-1} is due to the presence of Na_2SO_4 that is formed during the neutralization of the acidic solution after the oxidation process (Ben Mabrouk et al. 2013).

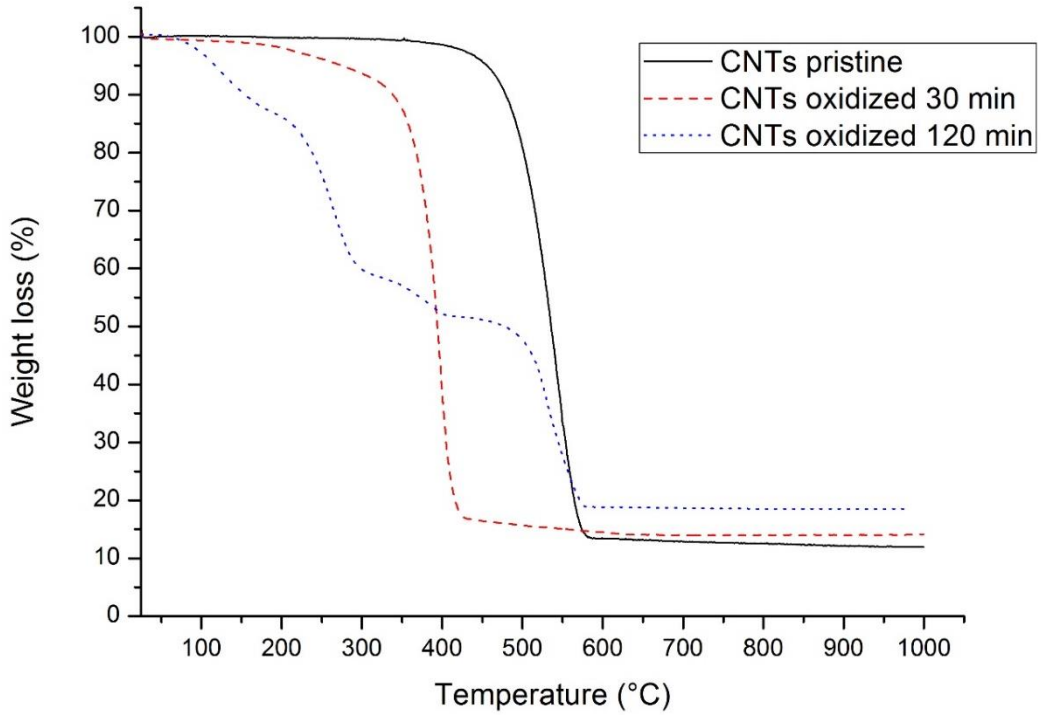

Figure 52: Thermal gravimetric analysis of pristine CNTs pristine (black line) and after oxidation with sulfonitric acid for 30 min (red line) and 120 min (blue line)

Figure 52 shows the weight loss curves of pristine (black) and sulfonitric-treated CNTs (red and blue curves) when heated under flowing air. The curves are very different, in particular both the curves of oxidized CNTs present much lower thermal stability than the pristine ones. This behavior is not unexpected since the

sulfonitric treatment introduces a great amount of reactive and thermal sensitive chemical groups as shown by FT-IR spectroscopy.

The curve of the sample treated for 30 minutes shows a significant weight loss starting at around 200 °C. This phenomenon can be attributed to the decarboxylation of the carboxylic groups present on the CNT (Tang et al. 2006). Then, at 350 °C, the fast and complete oxidation of carbon nanotubes start, leaving a 13% residuum at 1000 °C. In the case of the sample treated for 120 minutes the behavior is even more complex. There is a first weight loss phenomenon between 100 and 200 °C, which probably corresponds to the degradation of the residual fragments derived from the destruction of the external lattice from acidic treatment. Then a second step is observed between 200 and 300 °C, like in the curve of 30 min sample, due to the decarboxylation of functional groups present on the surface of CNTs. A small weight loss is observed between 300 and 400 °C, but the final oxidation occurs in the same temperature range of pristine CNTs. The decomposition at 300 °C is probably due to the degradation of functionalized and damaged CNTs (Grandi et al. 2006). It is however remarkable that a significant fraction of the material is oxidized in air in the same conditions of the pristine CNTs.

Since the FT-IR analysis suggests that a rather large amount of amorphous carbon forms in the case of long time oxidation, it is probable that several effects occur during the oxidation of CNTs in sulfonitric acid. Firstly, for short oxidation time the amorphous carbon present on the surface is removed by acidic treatment. Then, carbon nanotubes start to be functionalized. Finally for very long oxidation time the acidic treatment start to destroy the structure of CNTs creating a lot of amorphous carbon and unzipped nanotubes with a low quantity of functionalized CNTs. In fact, the literature confirms that very long treatments in sulfonitric acid lead to the opening of the tube caps or to the formation of holes in the sidewalls, that would then be followed by oxidative etching along the walls with the concomitant release of carbon dioxide (Zhang et al. 2003).

Scanning electron microscopy was used to investigate the possible CNTs fragmentation occurring during the acid oxidation treatment. figure 53 shows the SEM images of pristine CNTs and CNTs after the 30 and 120 minutes oxidation treatment. The samples treated for 30 minutes show no significant damage, the appearance of CNTs is similar in both cases. Instead, the CNTs treated 120 min

shows a high level of damage, in particular shortening and unzipping phenomena, with the presence of carbon particles of different shape.

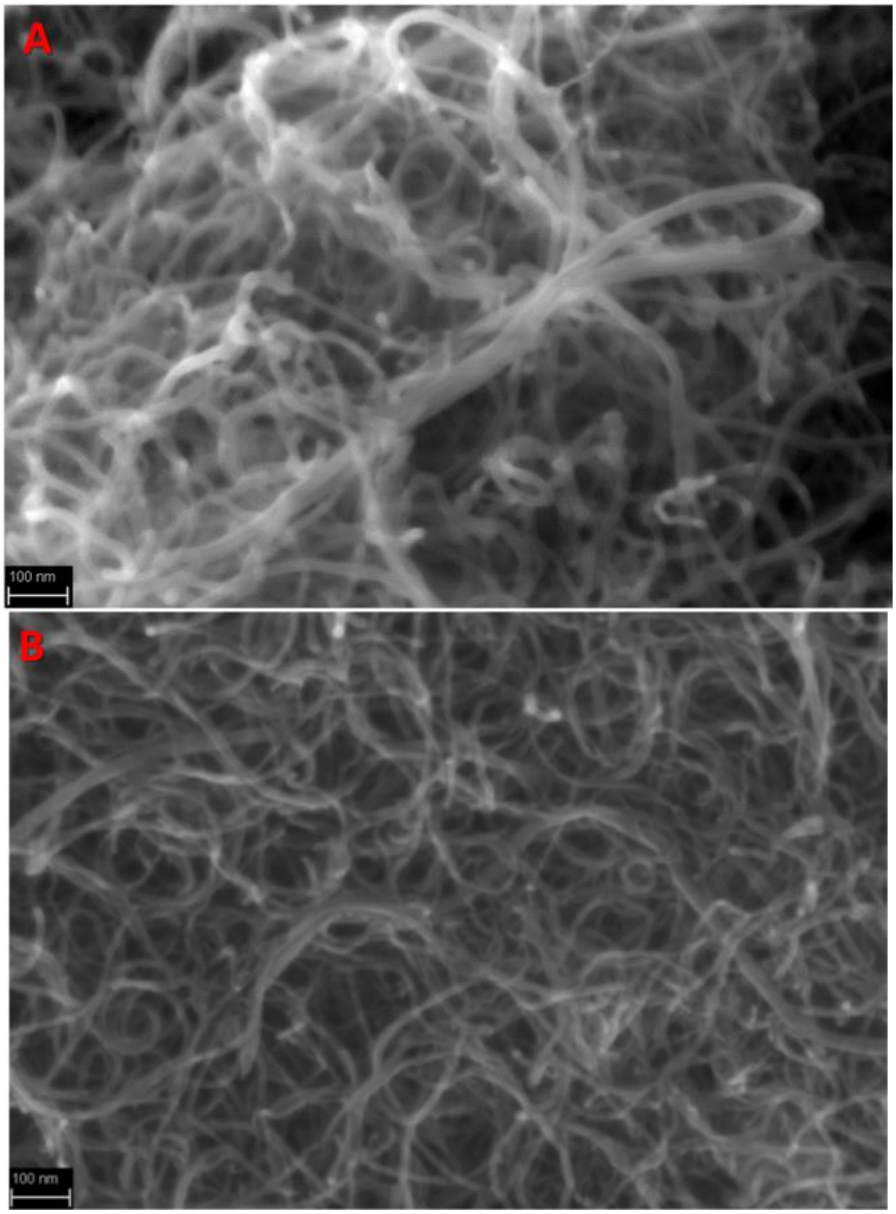

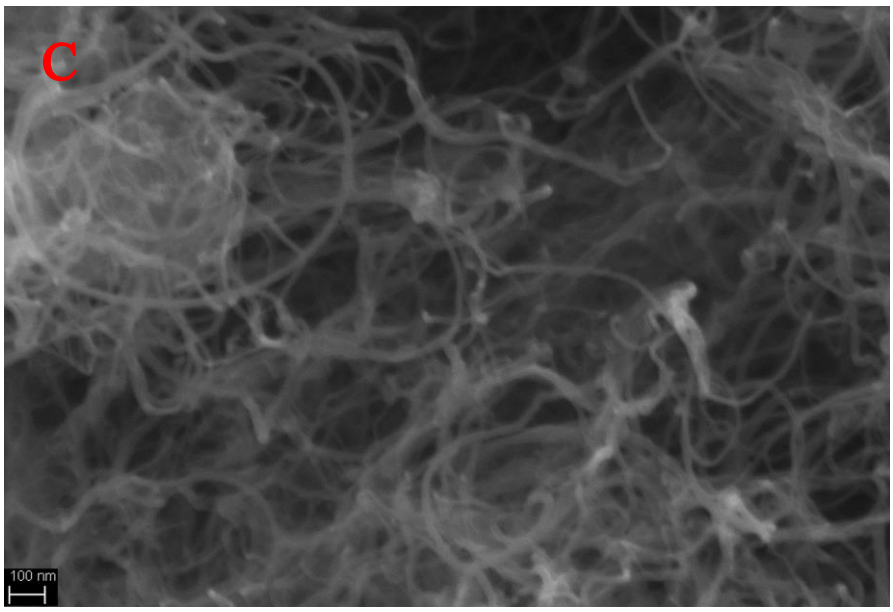

Figure 53: SEM images of pristine CNTs (A) and CNTs oxidized with sulfonitric acid for 30 min (B) and for 120 min (C)

Mechanical tests:

The mechanical testing of CNTs-containing cement allows the evaluation of the real reinforcing effect of pristine and modified carbon nanotubes. In figure 54 and Table 9 are presented the results of the flexural tests (in CMOD mode), giving both the strength (modulus of rupture, MOR) and the toughness (as the integral of the stress-displacement curve) for pure cement, cement reinforced with pristine CNT and cement reinforced with oxidized CNTs.

Table 9: In the columns are reported, from left to right, the code of the sample (treatment/time/temperature), the time of acid treatment, and the mechanical performance of cement and cement composites containing 0.1% bwoc of the pristine and oxidized CNTs resulting from each test

Sample name (treatment/time)	Time [min]	MOR (MPa)	Toughness (J)
cement	-	1.23 ± 0.14	1.33 ± 0.14
CNTs pristine	0	1.47 ± 0.03	1.78 ± 0.54
SN/15	15	1.47 ± 0.01	3.86 ± 1.84
SN/30	30	2.22 ± 0.05	4.94 ± 1.63
SN/120	120	1.99 ± 0.41	2.44 ± 0.04

The results show that the mechanical properties increase with the addition of carbon nanotubes to cement, and increase further and dramatically at a medium oxidation level of the carbon nanotubes. If the oxidation is limited (15 minutes), the toughness of the sample is doubled, even if the MOR is not increasing. The treatment of CNTs for 30 minutes in sulfonitric acid, though, allows to increase the MOR by 50% and the toughness by almost 200%. Finally, the longer treatment (120 minutes) results less effective, since while MOR increases significantly (30%), the toughness is reduced down to one half of the sample treated for 30 min.

Thus, the best condition is a limited oxidation of carbon nanotubes, that is sufficient to create a good amount of polar group on the surface of CNTs but that is not sufficient to damage the structure of the tubes, allowing the CNTs to maintain their reinforcing properties. Indeed, it is evident that an optimal number of polar functionalities on the surface has a very positive effect on the mechanical properties of cement, but also that the oxidation treatment must be tailored to find the best compromise between the generation of oxygen-containing functionalities and the damaging of the nanotubes due to intense acid reaction.

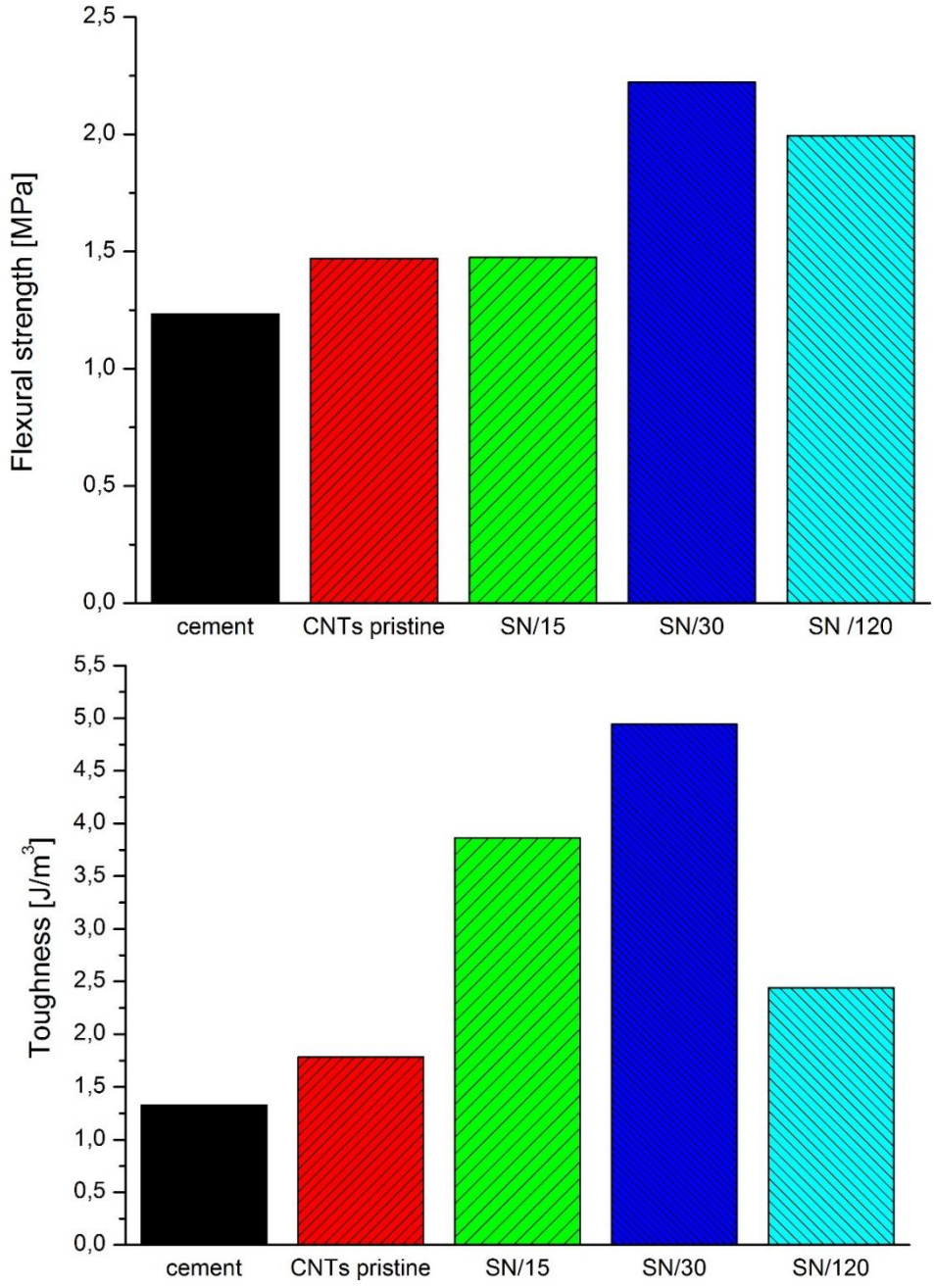

Figure 54: Flexural strength and toughness of cement (black), cement with 0.1 %bwoc of CNTs pristine (red) and 0.1 %bwoc of sulfonitric functionalized CNTs for 15 min (green), 30 min (blue) and 120 min (light blue)

Conclusion

This paragraph shows that proper oxidation of carbon nanotubes can improve significantly their dispersibility in water and their reinforcing effect in cement-based materials. Firstly, different acids were tested to find the most effective one for the proper oxidation of CNTs surface, and it was confirmed that sulfonitric acid gives the best results for the dispersion of functionalized CNTs in water. The time of the reaction resulted extremely important to guarantee the optimal amount

of polar functional groups on the surface of the oxidized CNTs. From FT-IR, Raman, TGA and SEM analysis it was determined that proper oxidation times are not damaging significantly the CNTs, while producing many –COOH groups and several other oxygen-containing functionalities on the surface. A too long oxidation time instead severely modifies both morphology and thermal stability of the CNTs. The mechanical testing of CNTs-containing cement showed that there is an optimum oxidation time (30 minutes) that allows to optimize both strength and toughness of the samples, bringing to 50% and 300% increase respectively with respect to samples containing untreated nanotubes and 300% and 400% increase respectively with respect to pure cement.

5.3.2 Cement-base composites containing graphene

After observing that the oxidation of carbon nanotubes must be brought only up to a certain extent, in order to optimize the mechanical properties of CNTs-containing cement, it was decided to analyze the same effect on a different material, in particular on graphene-reinforced cement. In fact, it is well-known in the literature (Choi et al. 2010) that the so-called graphene often contains some oxygen, depending on the preparation step. In this case it was decided to test commercial graphene-based materials with different oxygen content, and the choice was to use pure graphene nanoplatelets (GNPs), functionalized GNPs (GNP-COOH), reduced graphene oxide (RGO) and graphene oxide (GO).

The specimens for mechanical testing were prepared following three phases. The GNPs, GNP-COOH, RGO and GO were dispersed in water, to have a homogenous solution, with an ultrasonic tip (Vibra-cellTM 40 KHz of frequencies) for 15 minutes at 100 W. The solutions of different graphenes and water were mechanical stirred for several minutes, and then the cement powder was slowly added to the continuously stirred solutions. The graphene quantity was chosen as 0.1% bwoc for all the samples tested. The slurries, prepared at water-to-cement (W/C) ratio of 0.45, were then poured into suitable molds and cured for 24 h at 85 °C and 100% relative humidity. Prismatic molds of size 75x20x20 mm were used for the cement composites that had to be mechanically tested.

Characterization of graphene and mechanical results:

In figure 55 the results relative to the flexural tests are shown. The samples containing GNPs exhibit improved flexural strength with respect to pure cement, and the best performance is obtained when GNPs functionalized with –COOH are used. This behavior suggests that the presence of a nano-dispersed platelet-shaped second phase is useful to improve the flexural strength of the composites but also that the GNPs dispersion and their interaction with the cementitious matrix can be further improved by the presence of carboxyl groups on the surface of the nanomaterial. It can be also observed that when the oxygen content grows significantly (i.e. in the case of RGO and GO), the flexural strength is again similar to the pure cement. This suggests that nanoplatelets with a very high oxygen concentration are not effective in improving mechanical properties of cement.

Similar considerations can be made regarding the compressive strength (figure 55). The samples containing GNPs and –COOH functionalized GNPs exhibit a higher strength than pure cement, while samples containing RGO and GO have similar properties to pure cement.

Regarding toughness (figure 55), an increase is observed only with the functionalized GNP, while pristine GNPs are slightly detrimental to overall toughness. RGO-containing samples have similar properties to pure cement, while if GO is present, the toughness is reduced.

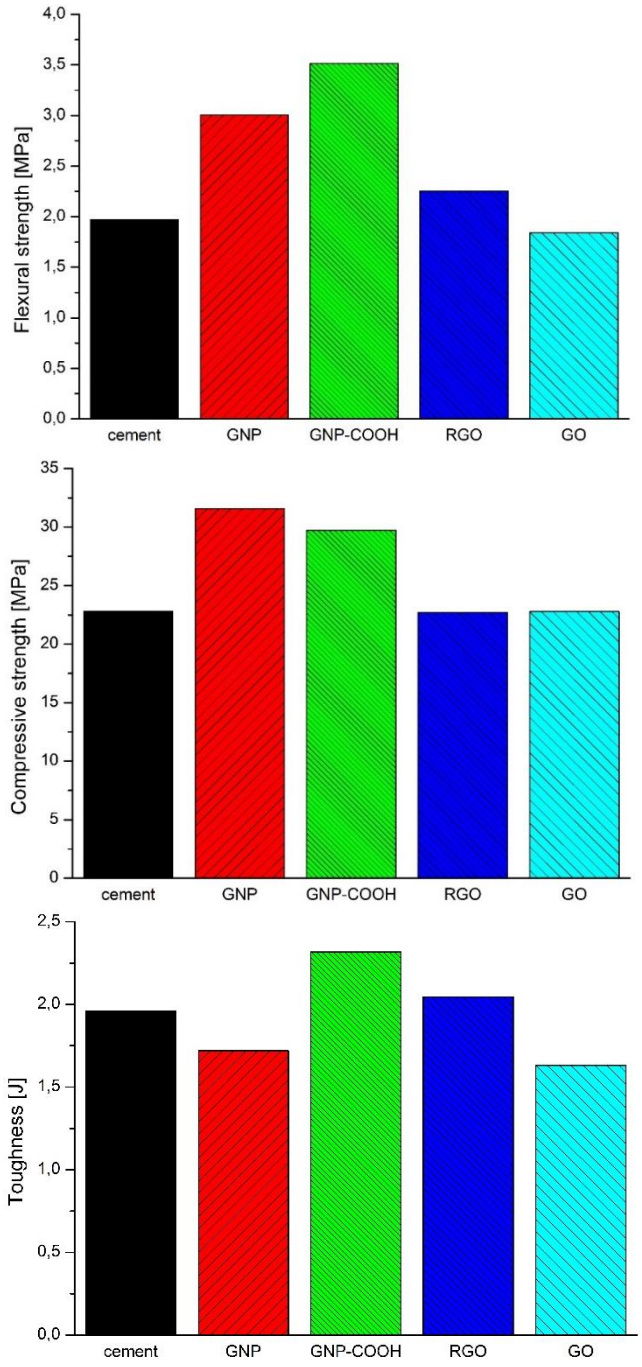

Figure 55: Flexural stress, compressive stress and toughness of pure cement (black), cement with 0.1 % bwoc of GNP (red), GNP-COOH (green), RGO (blue) and GO (light blue)

Raman spectroscopy was employed to characterize the different graphene structures. The Raman spectra of GNP, GNP-COOH, RGO and GO are shown in figure 56. The extent of the defects in the graphitic structure can be evaluated by the ratio of the D and G band intensities (I_D/I_G) (Tuinstra and Koenig 1970): the higher is the ratio the greater is the amount of lattice defects and amorphous carbon. After baseline correction and peak deconvolution, achieved with Origin software, for each sample the average I_D/I_G ratio has been calculated. The I_D/I_G

ratio is minimum for GNP and GNP-COOH, and is much higher for RGO and GO. This suggests that the functionalization of GNP to obtain a surface carboxylation does not modify the graphitic structure of the graphene. It is interesting to note that the RGO present a higher I_D/I_G ratio with respect to the GO, while it could be expected the inverse behavior(Kumar et al. 2013).

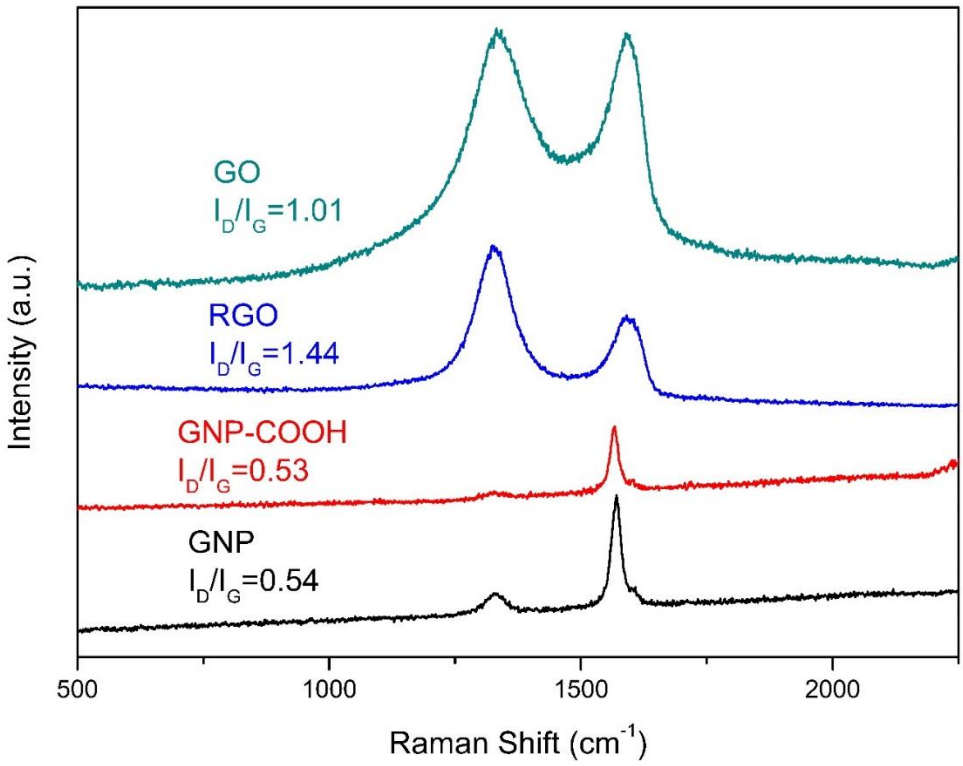

Figure 56: Comparison of Raman spectra collected for different graphene used. For each sample, the average ID/IG ratio is calculated

The values of the average size of the flakes and of the zeta potential are summarized in Table 10

Table 10: Average size and zeta potential of the nano-reinforcements

Sample	Size (nm)	Zeta potential (mV)
GO	2076	-28.8
RGO	2240	-16.3
GNP-COOH	2162	-21.5
GNP	2508	-12.9

All samples presented a mono modal size distribution and the data reported are the average of the distribution by intensity. Zeta potential (*Zp*) data give a description of the superficial charge of the nano species; it is possible to observe that oxygen containing species display a more negative *Zp*. Generally speaking *Zp* with values ranging lower than -20 mV are index of a good stability of a colloidal system in water (White et al. 2007; Kim et al. 2018), so the data collected suggest that GO and GNP-COOH can be well dispersed. The low value of GNPs is due to the very low polarity of its surface, while the RGO value is also unexpectedly low, suggesting a lower dispersing ability of this nanomaterial in water.

A higher percentage of oxygen in the nanoplatelets promotes a higher interaction between graphene and hydrated cement, by the formation of hydrogen bridge bonds. Nevertheless, this interaction does not always reflect in an improvement of strength, which is higher either with pure GNPs or with slightly oxidized graphene.

Evidently, a too strong interaction between graphene platelets and cement is detrimental to the mechanical properties. This is explainable taking into account that RGO and GO are so hydrophilic that they can absorb part of the water contained in the cement mixture, hence hampering the proper hydration of the cement paste, as already observed in the literature (Musso et al. 2009; Lavagna et al. 2018c). On the other hand, a limited presence of oxygen on the surface of the graphene can produce an improvement in the mechanical performance of the GNPs-reinforced composites. Several effects play a role in the different mechanical behaviors of the various composites.

1) With respect to the composites containing GNPs, it is evident that the graphene improves the strength of the material but, on the other hand, reduces the toughness (Wang et al. 2016). The mechanical strength improvement is probably due to the platelet shape of the nanomaterials, and to the fact that nano-sized powders have generally a positive effect on cement strength, as

demonstrated for example by Khushnood et al. (Khushnood et al. 2016). However, the bad dispersion of graphene in water, and as a consequence in the cement matrix, together with the absence of adhesion between filler and cement, limit the properties improvement, and in particular decrease the toughness. The presence of agglomerates is in fact a source of crack propagation, as shown by Ranjbar et al. (Ranjbar et al. 2015).

2) In the case of GNP-COOH, the shape factor of the nanofiller is the same as in the case of GNPs. Here, however, a role is also played by the interfacial interaction between graphene and cement. The presence of carboxylic acid groups on the surface of GNPs leads to a chemical reaction between the carboxylic acid groups and the hydrated calcium silicate (C–S–H) or the portlandite, $Ca(OH)_2$, as demonstrated by Pan and coworkers (Pan et al. 2015). This interaction, in turn, leads to a strong bond at the interface between the reinforcement and matrix in the composites, and therefore increases the load-transfer efficiency from cement matrix to GNP-COOH. As a result, the mechanical properties of the composites are improved.
3) Concerning GO, this filler is extremely hydrophilic and thus absorbs part of the water contained in the cement mixture, hence hampering the proper hydration of the cement paste (Musso et al. 2009; Lavagna et al. 2018c). The high content of functional groups is demonstrated by the high oxygen content and by the *Zp* analysis.
4) In the case of RGO, the content of functional groups on the surface is lower than in the case of GO, due to the thermal annealing that provokes a partial reduction of the structure. However the oxygen content is still very high, and a partial absorption of the hydration water is expected also in this case. The Raman spectroscopy shows a very high defectivity of this structure, that could be due to the presence of some amorphous carbon forming during the low temperature annealing process (Gómez-Navarro et al. 2010; Bagri et al. 2010). This is also confirmed by the rather low value of *Zp*, that suggests a low dispersibility in water of this nanomaterial. Thus the reduced mechanical properties of RGO-containing cement could be ascribed to a combination of water sequestration, defectivity of the structure, and imperfect adhesion to the matrix in correspondence of the amorphous carbon region.

Conclusions

This paragraph confirms the results of the previous paragraph: a well-tailored presence of oxygen on the surface of graphene plays a crucial role to obtain improved mechanical properties for graphene-containing cement matrix composites. In particular, it was demonstrated that flexural strength, compression strength and toughness are improved by the addition of slightly oxidized graphene, while pure GNPs provide a small increase in flexural and compressive strength but not on toughness. The use of GO or RGO, characterized by a high oxygen content, brings to mechanical properties similar to the pure cement, notwithstanding the presence of a strong nano-particle. This is probably due to a combination of water segregation that impedes the correct hydration of cement, and defectivity of the structure as suggested by Yang and coworkers (Yang et al. 2017). Thus, only a low oxygen content allows a proper cement-GNP interaction while not modifying the water accessibility to the cement itself, giving rise to an effective improvement of the properties of cement even at very low second phase content (0.1% bwoc).

5.3.3 Cement-base composite containing carbon fibers

Part of the work described in this chapter is to also previously published in Lavagna L, Musso S, Ferro G, Pavese M (2018b) Cement-based composites containing functionalized carbon fibers. Cem Concr Compos 88:165–171. (Lavagna et al. 2018c)

In this paragraph it was considered worthy to try to verify what happens when a micro-sized reinforcement is used instead of a nano-sized one. In fact, the cost of carbon nanotubes and graphene is rather high, while nowadays carbon fibers have reached a rather low cost. Moreover, the electrical properties of cement containing nano-sized reinforcement could be marred by the fact that a very high number of interfaces must be crossed by the electrons in their path through the material.

The use of fibers as reinforcement of cement is something well-established in the literature, but the chemical state of the surface of the fibers was not deemed in the past very important for the improvement of the composite properties. In this paragraph the effect of the treatment of fibers was studied to understand if further improvement of properties could be possible. In this case, both mechanical and

electrical properties of cement-based composites were studied, with the aim of finding the best compromise between the improvement of mechanical properties and the reduction of electrical resistance.

Experimental procedure

In the acidic functionalization of carbon fibers, three control factors (oxidation parameters) with three levels were examined, leading to nine experiments organized in a L9 Taguchi matrix design. The three investigated oxidation parameters were the acidic mixture (nitric acid: HNO_3; sulphonitric acid: 1 HNO_3 : 3 H_2SO_4; piranha solution: 3 H_2SO_4 : 1 H_2O_2), the reaction time (5, 30, 60 min), and the temperature (0, 30, 60 °C). During the functionalization, the solution was sonicated in an ultrasonic bath (SONICA 2400 MH series 40 KHz of frequencies). At the end of the treatment, the solution was neutralized in a basic solution of 1 M NaOH. The functionalized fibers were then recovered via filtration with a fritted glass filter class G4 Pyrex. The fibers were washed several times with distilled water and dried overnight at 80 °C.

In order to calculate the S/N ratios, we chose as output responses both the mechanical and electrical properties of the cement composite containing 0.1% BWOC of functionalized fibers. The larger-is-better response (1) was adopted for the S/N analysis of the mechanical performances (compressive strength, module of rupture, and toughness (Kackar 1989a, b)), whereas the smaller-is-better response (2) was used to analyze the electrical resistivity:

$$S/N_{larger-is-better} = -10\log_{10}\left[\frac{1}{n}\sum_{i=1}^{n}\frac{1}{Y_i^2}\right], \quad (1)$$

$$S/N_{smaller-is-better} = -10\log_{10}\left[\frac{1}{n}\sum_{i=1}^{n}Y_i^2\right], \quad (2)$$

where S/N indicates the signal to noise ratio statistic used in the Taguchi factors analysis, n is the number of levels in which each factor was investigated and Y_i the i^{th} value of the output response used for the evaluation of the oxidative treatment. The L9 orthogonal array, along with the output responses of the

electro-mechanical performance of the cement composites containing the functionalized fibers, is exhibited in Table 11. Samples containing no fibers or untreated fibers were also produced and tested.

After the functionalization, the carbon fibers were dispersed in water with an ultrasonic tip (Vibra-cellTM) for 15 minutes at 100 W, 40 % of amplitude. The suspension of carbon fibers and water was mechanical stirred for several minutes, and then the cement powder was slowly added to the continuously stirred solution. No dispersant agent or other additive was added. The slurry, composed only by cement and carbon fibers, prepared at water-to-cement (W/C) ratio of 0.45, was then poured into suitable molds and cured for 24 h at 85 °C and at 100% relative humidity. Prismatic molds of size 20x20x75 mm were used for the cement composites that had to be mechanically tested, whereas cylindrical molds having diameter Ø = 20 mm and height = 40 mm were employed for the samples undergoing electrical testing.

Table 11: L9 orthogonal array used for the design of experiments. The three different oxidation factors (three levels each) are shown, together with the mechanical and electrical results

Test	Time [min]	Tempertature [°C]	Acidic mixture	Compressive strength (MPa)	Flexural strength (MPa)	Toughness (J)	Electrical resistivity (Ω m)
1	5	0	HNO_3	23.4 ± 3.8	3.43 ± 0.85	12.7 ± 9.0	26.3 ± 2.9
2	5	30	1 HNO_3 : 3 H_2SO_4	33.2 ± 4.5	4.13 ± 0.76	12.7 ± 2.5	11.4 ± 1.4
3	5	60	3 H_2SO_4 : 1 H_2O_2	32.7 ± 2.4	4.87 ± 0.20	13.3 ± 1.4	15.7 ± 0.8
4	30	0	1 HNO_3 : 3 H_2SO_4	28.8 ± 0.5	4.51 ± 0.35	8.6 ± 0.9	74.9 ± 7.2
5	30	30	3 H_2SO_4 : 1 H_2O_2	29.7 ± 5.2	3.99 ± 0.31	10.6 ± 3.6	4.9 ± 0.4
6	30	60	HNO_3	29.7 ± 1.8	3.40 ± 0.49	11.0 ± 0.5	26.8 ± 3.5
7	60	0	3 H_2SO_4 : 1 H_2O_2	25.4 ± 2.2	5.36 ± 0.39	15.9 ± 3.9	21.3 ± 2.2
8	60	30	HNO_3	30.5 ± 4.5	4.27 ± 0.71	6.4 ± 1.8	44.6± 3.1
9	60	60	1 HNO_3 : 3 H_2SO_4	25.7 ± 3.4	2.89 ± 0.69	2.1 ± 0.7	146 ± 7

Mechanical and electrical tests:

The electrical resistance of the samples was measured applying 300 mV with a two-probe technique using alternating current (AC) at 200 kHz. Alternating current is recommended because it resolves technical difficulties and problems (e.g. polarization effects) related with direct current (DC) measurements (Wen and Chung 2001; Polder 2001; Lee and Wang 2010). Although some polarization may occur even when applying alternating current signals, if the frequency is high enough the polarization effect is narrowed to a tolerable range (Wen and Chung

2001; Azhari and Banthia 2012). The electrical tests were performed by clamping two flat copper electrodes to the ends of the cylindrical samples (figure 57). A conductive gel was used to improve the electrical contact between electrodes and sample. All the electrical measurements were performed after drying the cement samples at 80 °C overnight to eliminate all the free water.

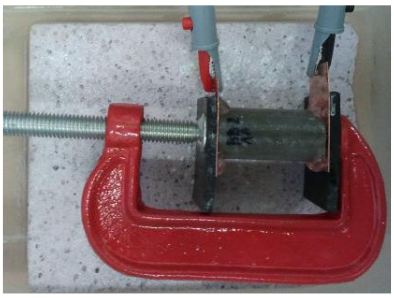

Figure 57: System adopted for electrical tests

The mechanical properties of the cement composites were measured through a three point bending test (ASTM C348) controlled by crack mouth opening displacement (CMOD) on notched specimens with size 75x20x20 mm. The specimens were tested with a single-column Zwick-Line z050 flexural testing machine with a load cell having a maximum capacity of 1 kN. As described in the literature (Jenq and Shah 1986; Shah 1990), this measurement requires the samples to be notched in the middle, the notch having a width of 2 mm and a depth of 5 mm, equal to one fourth of the width of specimen. CMOD was controlled at a fixed displacement rate of 0.003 mm/min by placing an extensometer on the two sides of the notch (figure 28). The distance between the supports was 65 mm and for every test at least three specimens were analyzed. The flexural strength was calculated by using the standard formula for un-notched bending tests, using the thickness in the notched area. The toughness was calculated by integrating the load-displacement curve. The compressive strength tests were conducted on at least three cubic specimens per sample of size 20x20x20 mm and was controlled at a fixed displacement rate of 0.2 mm/min.

Results and Discussion

As shown in figure 58, the results reported in Table 11 were used to calculate the response graphs of S/N ratios for the larger-is-better analysis of the mechanical performances (figure 58a-c) and for the smaller-is-better analysis of

the electrical resistivity (figure 58d) of the cement composite containing 0.1% bwoc of treated carbon fibers.

From these graphs, it can clearly see that best electrical and mechanical performance (best S/N ratio) was obtained when the carbon fibers were treated in piranha solution at 30 °C. As for time, both 5 and 30 minutes treatment show a similar optimal S/N ratios. On the other hand, the cement composite showing the worst electro-mechanical performance was the one containing CFs treated with sulphonitric acid for 60 minutes at 60 °C. When functionalization occurs for a long period at high temperature, oxidized CFs are obviously going to contain a greater number of functional groups. However, as it was observed in the precious paragraphs, for the final application in a cementitious matrix, it is important to introduce the right amount and right typology of chemical groups. For instance, as reported in the literature, the piranha solution is expected to eliminate amorphous carbon while it generates a limited amount of hydroxyl and carboxylic groups on the fiber surface (Dillon et al. 1999; Park et al. 2001; Pan and Yapici 2015). Instead, the sulphonitric acid treatment (60 min, 60 °C) generates a greater amount of chemical groups than piranha treatment (30 min, 30 °C), and mainly carboxylic and hydroxyl groups (Osorio et al. 2008). This is confirmed by the comparison of the oxidative stability of these two functionalized samples with pristine carbon fibers (figure 51). The stability of the fibers is greatly reduced after the stronger functionalization treatment.

In fact, figure 59 shows that, whereas the TGA weight loss curves of pristine and piranha-treated CFs are very similar, the sulphonitric-treated sample exhibits a lower thermal stability, and starts to oxidize well below 700 °C. The origin of the behavior can be easily found in the fact that the sulphonitric treatment, at higher temperature and for a longer period, introduces a greater amount of reactive and temperature sensitive chemical groups.

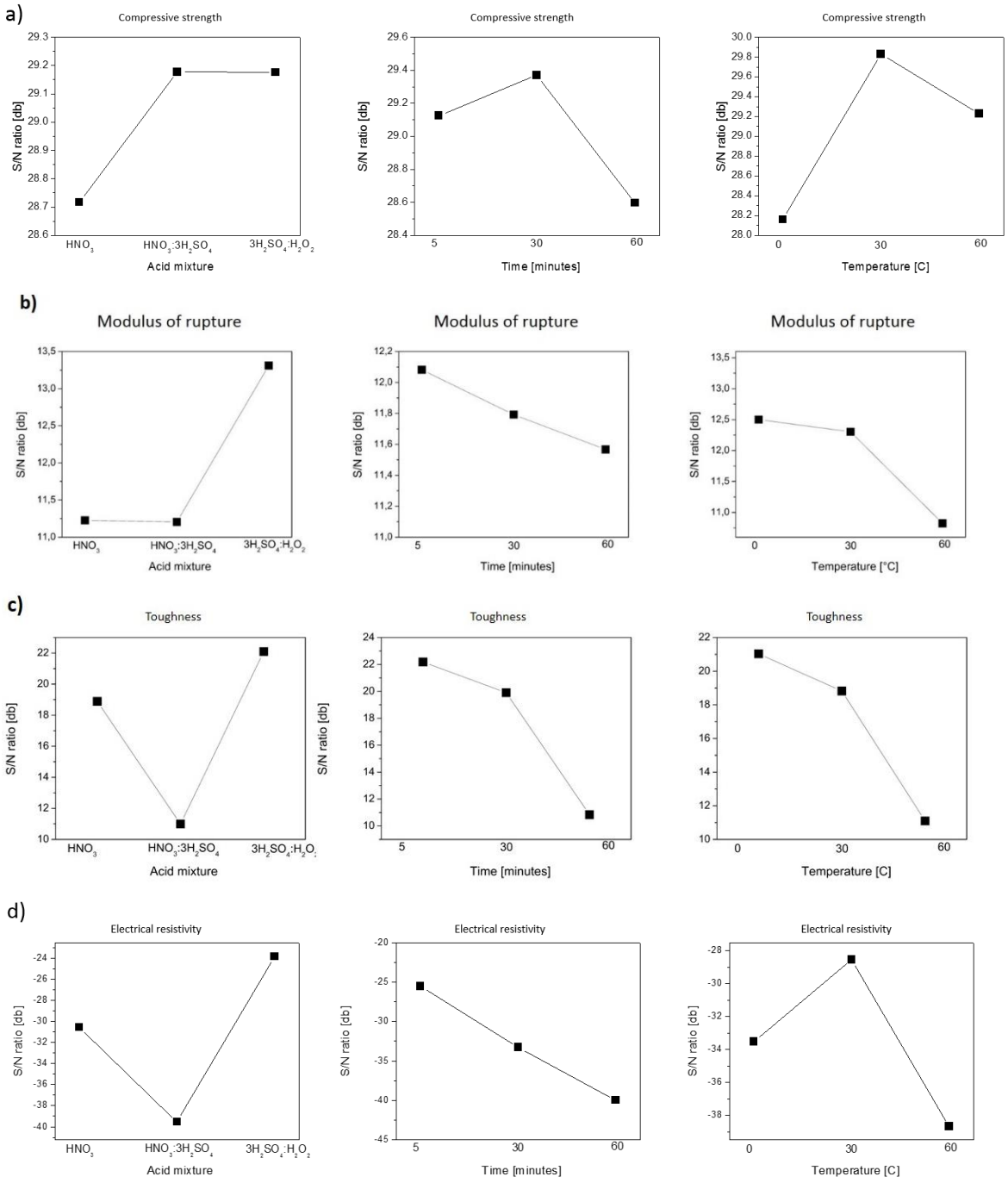

Figure 58: Response graphs of S/N ratios for: larger-is-better analysis (eq. 1) of compressive strength (a), modulus of rupture (b), toughness (c); smaller-is-better analysis (eq. 2) of electrical resistivity (d) of cement (0.1% BWOC of oxydized carbon fibers)

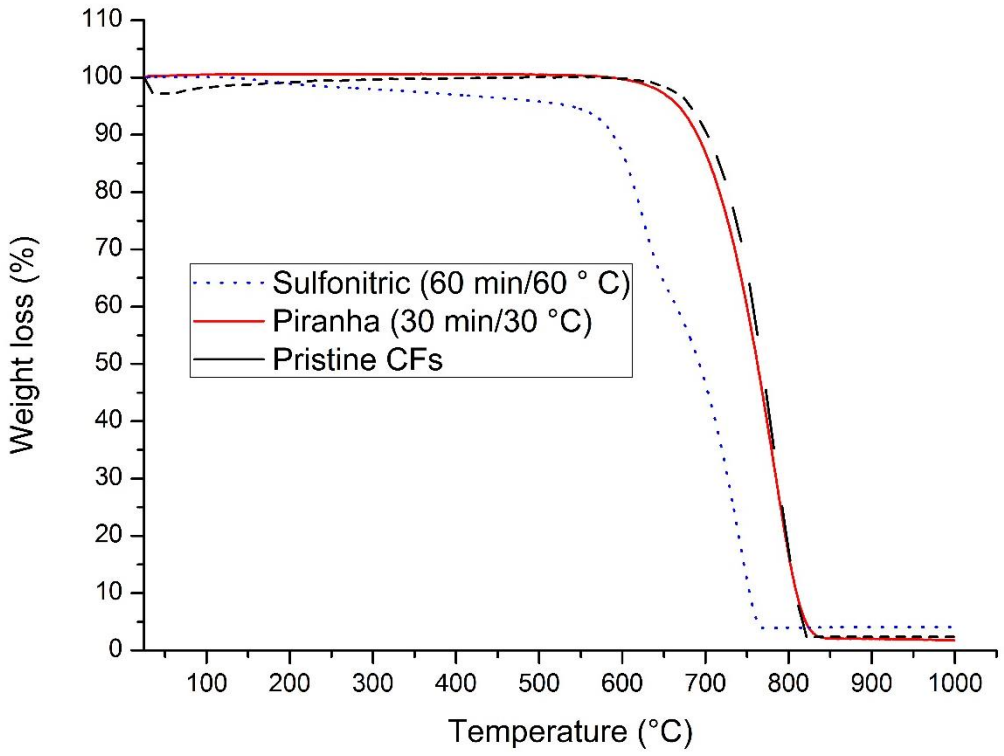

Figure 59: Thermal gravimetric analysis in 50 ml/min of air at 10 °C/min of CFs before (black-dash line) and after oxidation with piranha solutions (red line) and sulphonitric acid (blue-dotted line)

Raman spectroscopy was employed to characterize the quality of the graphitic nature of the carbon fibers surface, before and after functionalization. The Raman spectra of pristine, piranha treated and sulphonitric treated CFs are shown in figure 60. Interestingly, the acid treatments provoke a decrease in the I_D/I_G ratio consequent, as suggested by some studies (Dillon et al. 1999; Park et al. 2001), to the elimination of amorphous carbon from the fibers. In particular, a significant reduction of amorphous carbon is exhibited by the piranha treated (30 °C for 30 min) sample as proved by the lowest I_D/I_G.

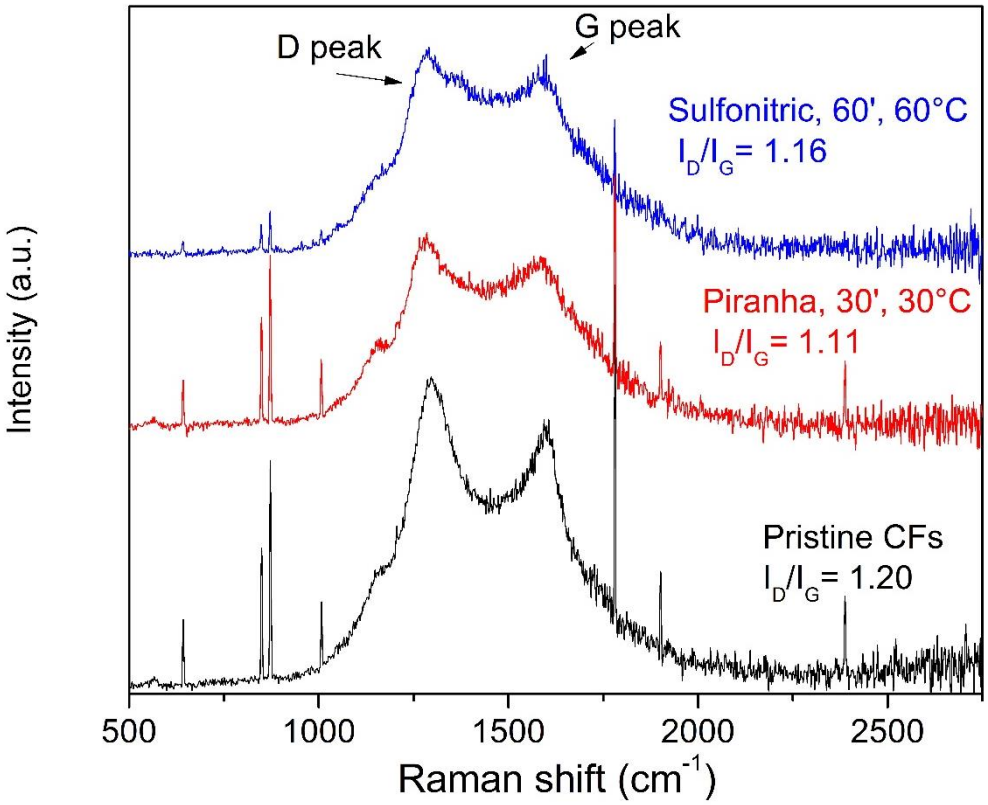

Figure 60: Comparison of Raman spectra collected before (black) and after oxidation with piranha solutions (red) and sulphonitric acid (blue)

Hence, given the response obtained with the Taguchi robust design approach, and the change in fiber properties caused by the different functionalization, we decided to focus our investigation mainly on the properties of the cement composite obtained by using carbon fibers oxidized in piranha solution for 30 minutes at 30 °C.

Electrical results

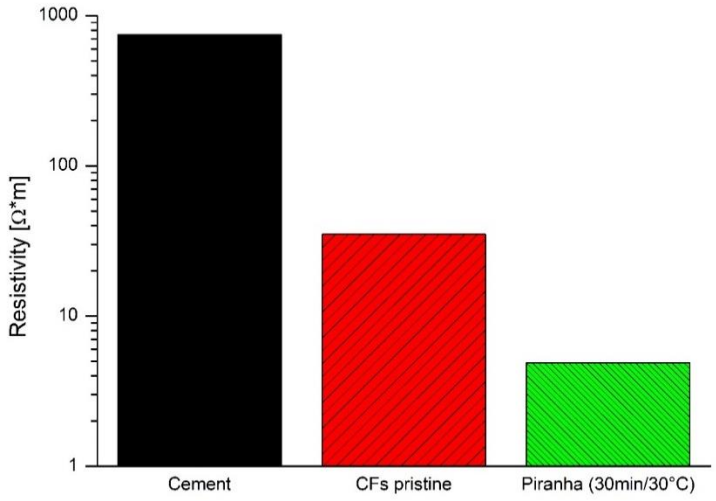

Figure 61: Electrical resistivity (logarithmic scale) of dry cement (black), cement with 0.1% BWOC of CFs pristine (red), and 0.1% BWOC of piranha functionalized CFs (green)

In figure 61, it is possible to observe the electrical resistivity of the cement samples with and without CFs. All the measurements were performed after completely drying the cement at 80 °C overnight, in order to eliminate the conductivity contribution of the saturated aqueous solution present in the cement pores.

The unreinforced cement, after drying, has a very low free water content and thus it has a very high electrical resistivity (748 Ω m). Since pristine carbon fibers are highly conductive, the electrical resistivity of the cement nanocomposite becomes one order of magnitude lower (35 Ω m). However, the electrical resistivity can be decreased even further when piranha solution is used to oxidize the fibers. In particular, cement with CFs treated with piranha solution for 30 minutes at 30 °C exhibits the best (5 Ω m) electrical resistivity. This behavior suggests that both the CFs dispersion in the cementitious matrix and their interaction with the cement were improved by the hydroxyl groups created during the piranha treatments (Pan et al. 2015).

Mechanical results

Similar considerations can be made regarding the mechanical properties. figure 62 and 63 show the results of flexural tests. The samples containing pristine carbon fibers exhibit improved flexural strength and toughness with respect to unreinforced cement. Then again, when piranha functionalized fibers are used,

both the flexural strength (figure 62A), the toughness (figure 62B) are remarkably enhanced. As described before, this mechanical enhancement is generated by the presence of new functional groups, which increase the dispersion of the functionalized CFs and their chemical bonding with the cement.

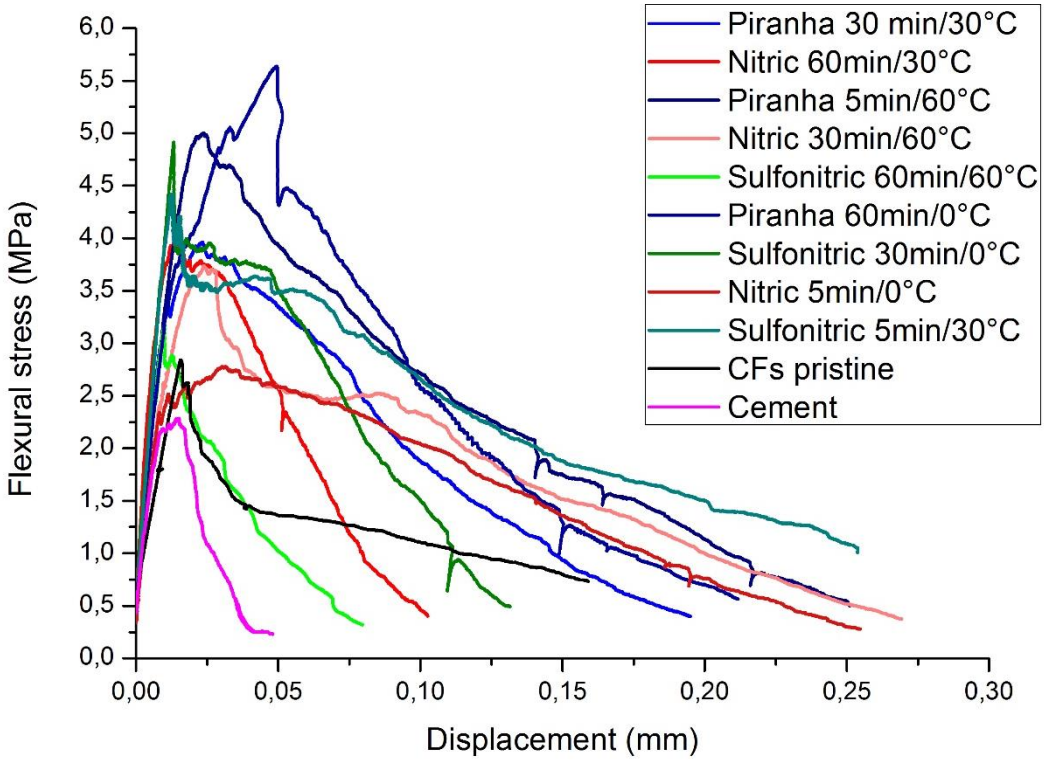

Figure 62: Typical load–displacement curves for flexural strength of the 11 typology of cement composite containing 0.1% BWOC of CFs functionalized in different way

A deeper analysis of figure 62 or Table 11 can give further information regarding the effect of the functionalization on the final mechanical properties of the composites. Evidently, the type of acid is of the foremost importance, since all the piranha solution-treated samples present good mechanical performance. But also the intensity of the treatment has a significant influence, since too high temperature and/or time are particularly detrimental to the flexural strength and/or toughness of the composite, as demonstrated by the sulphonitric 60 min/60 °C or by the nitric 60 min/30 °C samples. It can be thus concluded that only a limited and proper modification of the surface of the fibers can produce a remarkable improvement of strength and toughness in the CFs-reinforced composite.

In the case of compressive strength (figure 62 C) the behavior is rather similar to the flexural strength case. The samples containing pristine fibers have the same strength than the pure cement, while the use of functionalized fibers allows a significant increase of the compressive strength.

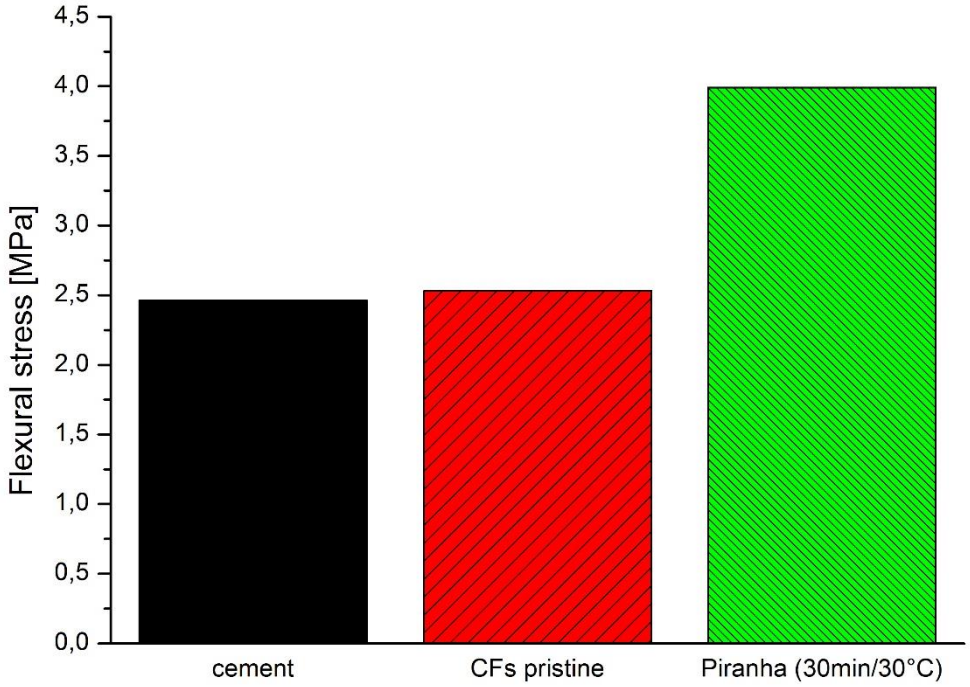
Flexural stress [MPa]
4,5
4,0
3,5
3,0
2,5
2,0
1,5
1,0
0,5
0,0
cement
CFs pristine
Piranha (30min/30°C)

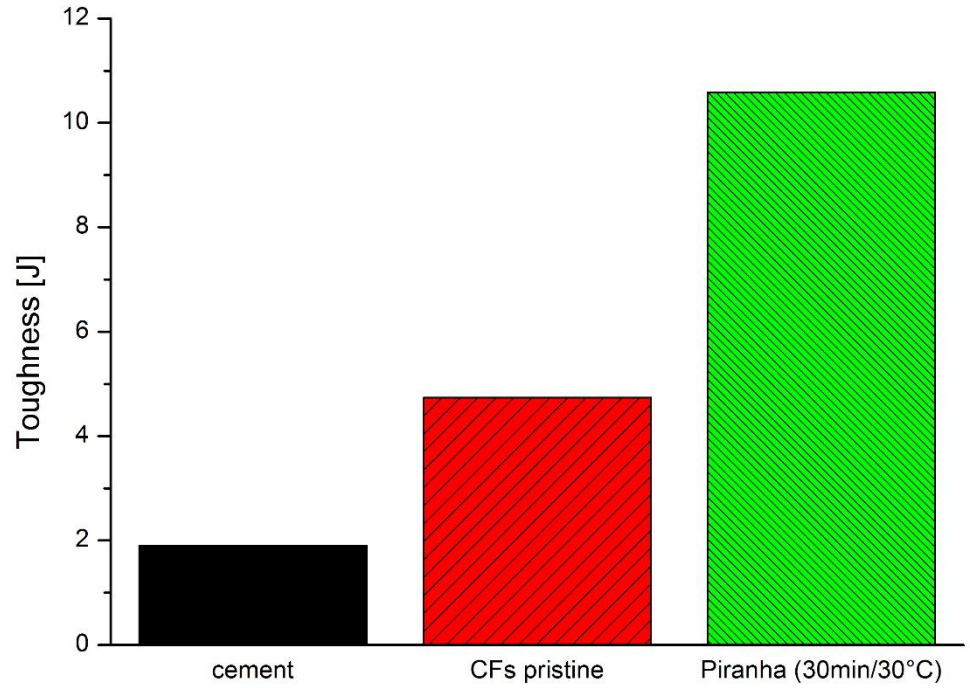
Toughness [J]
12
10
8
6
4
2
0
cement
CFs pristine
Piranha (30min/30°C)

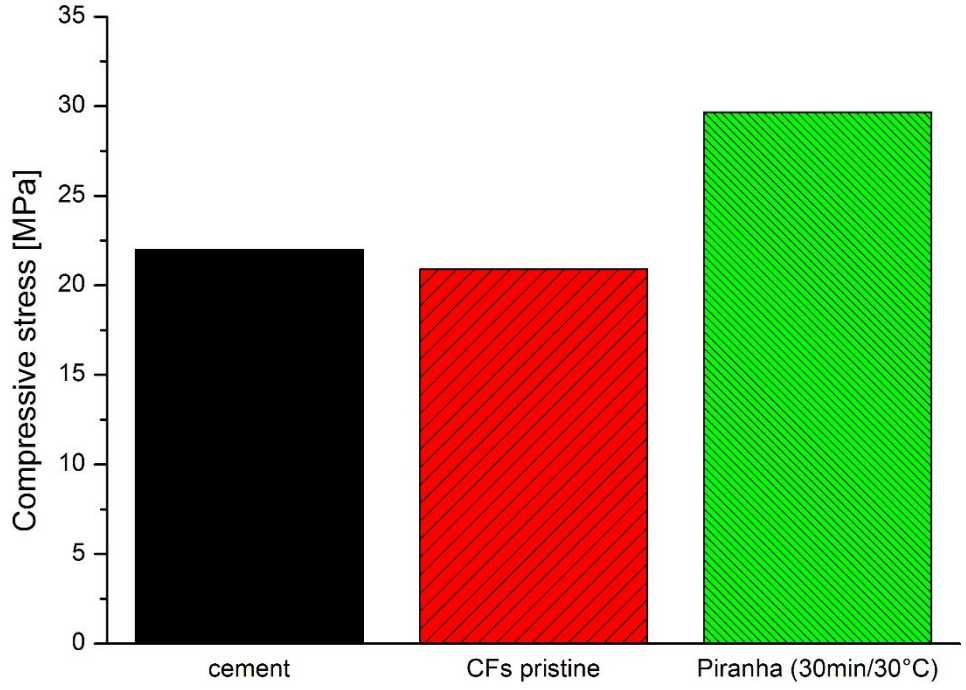

Figure 63: Flexural strength, toughness and compressive strength of pure cement (black), cement with 0.1 % BWOC of pristine CFs (red) and 0.1 % BWOC of functionalized CFs (green)

Conclusion

This paragraph shows that a well-tailored and limited functionalization of CFs plays a crucial role to obtain the best CFs dispersion in water and the best interaction with cementitious matrix. This behavior confirms what was observed in the previous paragraphs for carbon nanotubes and graphene, but in this case the combined improvement of mechanical and electrical properties is observed:

- A Taguchi approach allowed to determine the best conditions for the acidic oxidation of carbon fibers. The best results were obtained by using a piranha solution for 30 min at 30 °C.
- The electrical properties of samples containing properly treated CFs are greatly enhanced not only with respect to pure cement but also with respect to the samples containing untreated fibers. This effect is probably due to the improvement of the fibers dispersion in the cement paste and of the electrical connectivity between filler and cementitious matrix.
- The composites containing treated CFs exhibit as well improved mechanical properties. Flexural strength, compression strength and

toughness all increase when carbon fibers are surface treated. In particular, very high toughness results when using properly functionalized fibers.

Overall, the results confirm that the optimization of the oxidative treatment had a strong effect on the interaction and adhesion of the fibers with cement, resulting in better electrical and mechanical properties. These results are interesting for a wide range of applications where the variation of electrical conductivity of cement can be used to monitor the structural integrity of cementitious structures.

5.4 Polymer matrix composites

Part of the work described in this chapter is to also previously published in "Lavagna L, Massella D, Pantano MF, et al (2018a) Grafting carbon nanotubes onto carbon fibres doubles their effective strength and the toughness of the composite. Compos Sci Technol. (Lavagna et al. 2018a)

5.4.1 Polymer matrix composites

In literature it well-known that the addition of carbon micro- and nano-reinforcement improves the properties of a polymeric matrix. Since in this thesis carbon fibers were covered with grafted nanotubes, the question arose about the possibility of an improvement of mechanical properties by using grafted carbon fibers with respect to standard ones. In fact, the nanotubes could enhance the interfacial bond between carbon fibers and the polymer matrix, guaranteeing an improved strength and/or toughness to the composite.

To verify this assumption it was decided to use a model system to understand the effect of grating carbon nanotubes on the surface of carbon fibers. The chosen polymer was polyvinyl butyral, because it is a good dispersant for carbon-based materials, it is easily cast in tapes by the tape casting technique, it is transparent and its T_g is higher than room temperature, allowing toughening effects to be easily seen during mechanical testing. To produce composites, first a slurry must be produced containing PVB, ethanol and the dispersed reinforcement, and then the slurry must be cast by tape casting to produce composite sheets. The composites were produced with nanotubes, fibers and grafted fibers, in order to try to verify the effect of the different fillers, individually or coupled together, on the final properties.

The slurry for tape casting was prepared by dispersing different fillers i.e. CFs, CNTs and grafted CFs in a solution of PVB in ethanol. An amount of 40 g of ethanol was weighed in a beaker, the same was done with 10 g of PVB; the fillers were then prepared in the required amounts and mixed with the ethanol; a small portion of PVB (0.6-0.8 g) was then added to the ethanol-based system, which was then mixed with a magnetic stirrer. When the solution became transparent, it was ultra-sonicated with an ultrasonic tip for 10 minutes with a power of 100 W, 40% of amplitude. In the cases in which the dispersion was not sufficiently uniform, an additional sonication time of 5 minutes was necessary.

The aim of the ultrasounds treatment was to disperse the reinforcement, in particular CNTs, in the matrix. A small amount of PVB was added before the treatment in order to improve the dispersion and prevent the fillers from re-aggregating in bundles at the end of ultrasound treatment.

The system was then placed on a magnetic stirrer that provided a mild but continuous agitation, and the remaining PVB added slowly (about 2 g/h). During the processing, the beaker was kept covered in order to prevent solvent evaporation. The solution was stirred overnight before being processed.

In Table 12, the different slurries prepared are listed; the filler fraction values are percentage by weight of the PVB, and are also used to define the nomenclature of the samples.

After the stirring was completed, the slurry was degassed by mean of a vacuum pump in order to remove the air bubbles that would act as defects in the final composite. The resulting slurries were poured by tape casting on a movable mylar support (advance speed 100 mm/min); the doctor blade was adjusted to a height of 1 mm. By slow evaporation of the solvent, occurring at room temperature in air for 12 h, composite tapes with a thickness of 200–250 μm and without macroscopic defects were obtained.

Table 12: Sample labels and corresponding slurry composition

Sample	CF weight fraction [%]	CNT weight fraction [%]
PVB	0	0
CF 0.1	0.1	0
CF 0.5	0.5	0
CF 1	1	0
CNT 0.025	0	0.025
CNT 0.1	0	0.1
CNT 0.5	0	0.5
CNT 1	0	1
CF 0.1 CNT 0.1	0.1	0.1
CF 0.5 CNT 0.01	0.5	0.01
CF 0.5 CNT 0.025	0.5	0.025
CF 0.5 CNT 0.1	0.5	0.1
CF 1 CNT 0.1	1	0.1
MS 0.5-0.01	0.5*	0.01*
MS 0.5-0.025	0.5*	0.025*
MS 0.5-0.1	0.5*	0.1*

*Multiscale samples with grafted CNTs

5.4.2 Mechanical testing

Tensile tests were performed on the samples using a ZwickLine z050 testing machine with a 50 kN load cell. The test was conducted at room temperature in displacement control at a velocity of 0.5 mm/min and applying a preload of 5 N. All measurements were also subsequently repeated and verified using a universal testing machine MIDI 10 by Messphysik Materials Testing, at a velocity of 0.6 mm/min, corresponding to a strain rate of about 0.025%s^{-1}. The samples were rectangular specimens, cut from the fabricated tapes, 57 x 9 or 40 x 9 mm^2 in size with variable thickness, as reported in Table 13. The unreinforced polymer is indicated with “PVB”, while the thickness variation among the samples depends on the viscosity of the slurry before casting and on the rate of solvent evaporation, thus on the quantity of CNTs or CF present in the composites. For most of the samples, a thickness of approximately 100 μm was obtained. Adhesive pads were

glued on the specimen ends in order to fit the testing machine grips and avoid slippage during loading. The tests allowed to determine stress-strain curves for the various specimens in the quasi-static regime, and to derive the quantities of interest such as stiffness, yield stress, strength, ultimate strain.

Table 13: Geometrical dimension of the specimens

Sample label	Length [mm]	Width [mm]	Thickness [mm]	Section [mm^2]
PVB	57 (40)	9	0.04	0.32
CF 0.1	57 (40)	9	0.05	0.45
CF 0.5	57 (40)	9	0.09	0.81
CF 1	57 (40)	9	0.09	0.81
CNT 0.025	57 (40)	9	0.10	0.90
CNT 0.1	57 (40)	9	0.11	0.95
CNT 0.5	57 (40)	9	0.10	0.90
CNT 1	57 (40)	9	0.10	0.90
CF 0.1 CNT 0.1	57 (40)	9	0.09	0.77
CF 0.5 CNT 0.1	57 (40)	9	0.11	0.99
CF 0.5 CNT 0.025	57 (40)	9	0.10	0.9
CF 0.5 CNT 0.01	57 (40)	9	0.09	0.81
CF 1 CNT 0.1	57 (40)	9	0.09	0.81
MS 0.5-0.1	57 (40)	9	0.08	0.72
MS 0.5-0.025	57 (40)	9	0.09	0.81

The tests were performed on every composite by loading up to failure several specimens (from 5 to 16) for each type. The onset of damage occurs typically at both sides of the tape, followed by specimen tearing which induces torsion. Some examples of fractured specimens are shown in figure 64.

In order to observe how the addition of CFs and CNTs affects the mechanical behavior, in the following a comparison will be provided for the different families of composites produced.

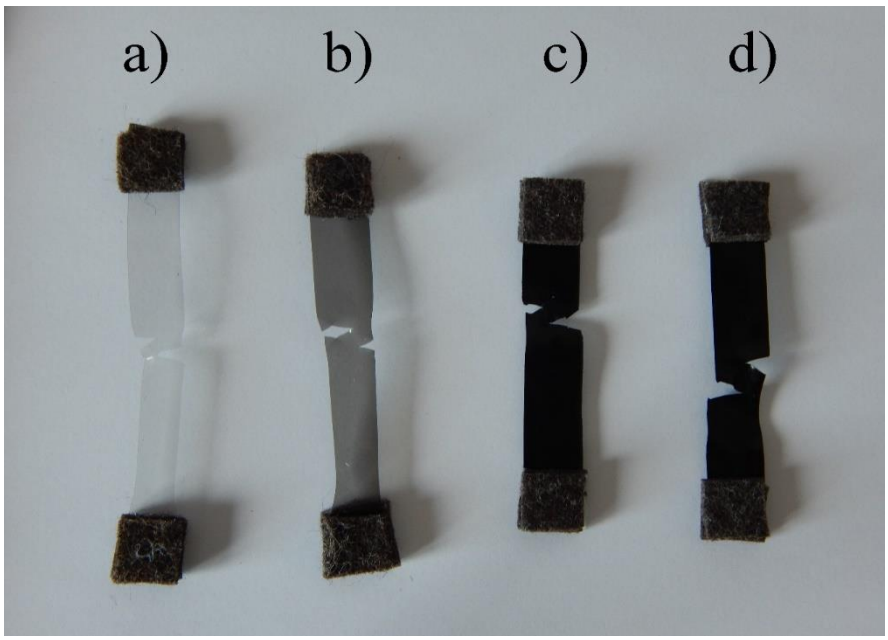

Figure 64: Fractured specimens of different types: a) CNT 0.025 b) CNT 0.1 c) CNT 0.5 d) CNT 1

5.4.3 CF and CNT-reinforced composites.

A typical stress-strain curve for various samples is shown in figure 65. It is apparent that the addition of CFs leads to a 30% increase in strength and promotes brittle fracture. The further addition of CNTs provides a small additional increase in strength, but also a considerable toughening of the composite, with a transition from brittle to ductile fracture, an increase in the ultimate strain, and the corresponding increase of over 10 times in the dissipated energy, per unit mass *E/m*. The latter is taken as a measure of material toughness and is calculated as:

$$\frac{E}{m} = \frac{1}{\rho}\int_0^{\varepsilon_f} \sigma d\varepsilon \qquad (1)$$

where σ is the stress, ε the strain, ρ the material density, and ε_f the ultimate strain (Timoshenko 1956). Large simultaneous strength and toughness values are distinctive of biological materials, which can conjugate these two mutually exclusive properties through hierarchical structures and multiscale damage mechanisms (Wegst et al. 2014). Therefore, these are extremely important properties to be achieved in the development of bioinspired materials.

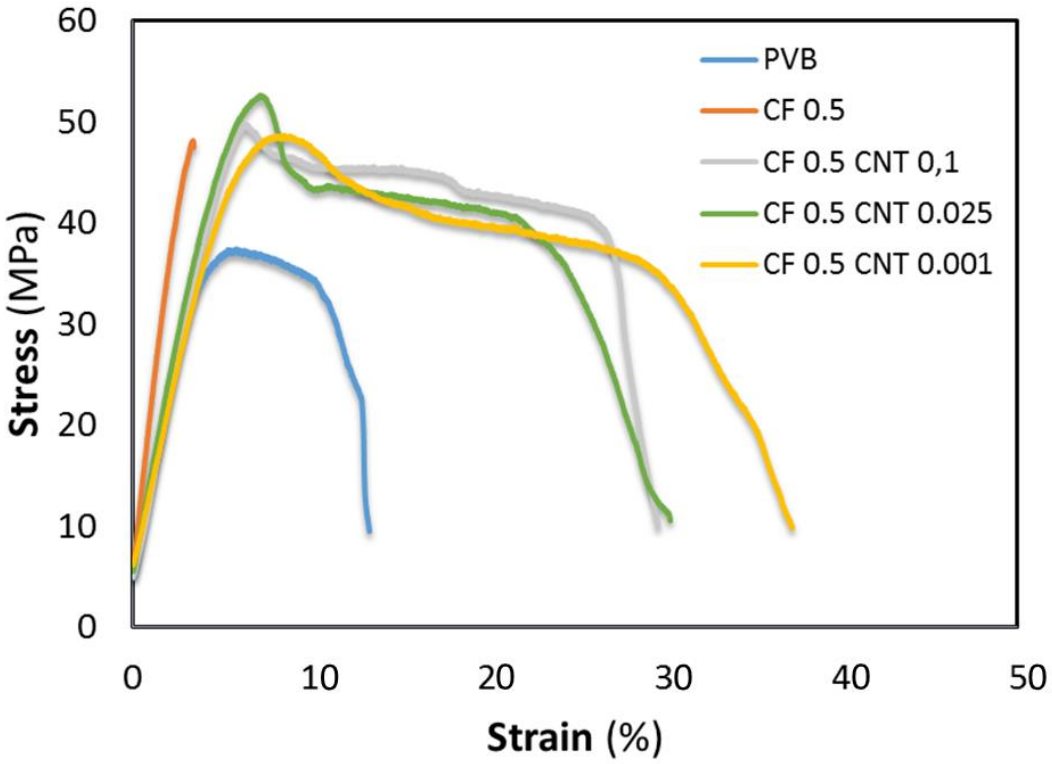

Figure 65: Examples of stress vs. strain for different CF/CNT reinforced PVB composites

To evaluate the reinforcing effect of CFs and CNTs separately, average mechanical properties of (non-hierarchical) composites with only a single reinforcement type (CFs or CNTs) are initially analysed (figure 66 and Table 14). Predictions using a direct and inverse Rule of Mixtures (RM) are included as lines in the plots for comparison (Alger 1997), using the data in Table 15 for the matrix and fibre properties.

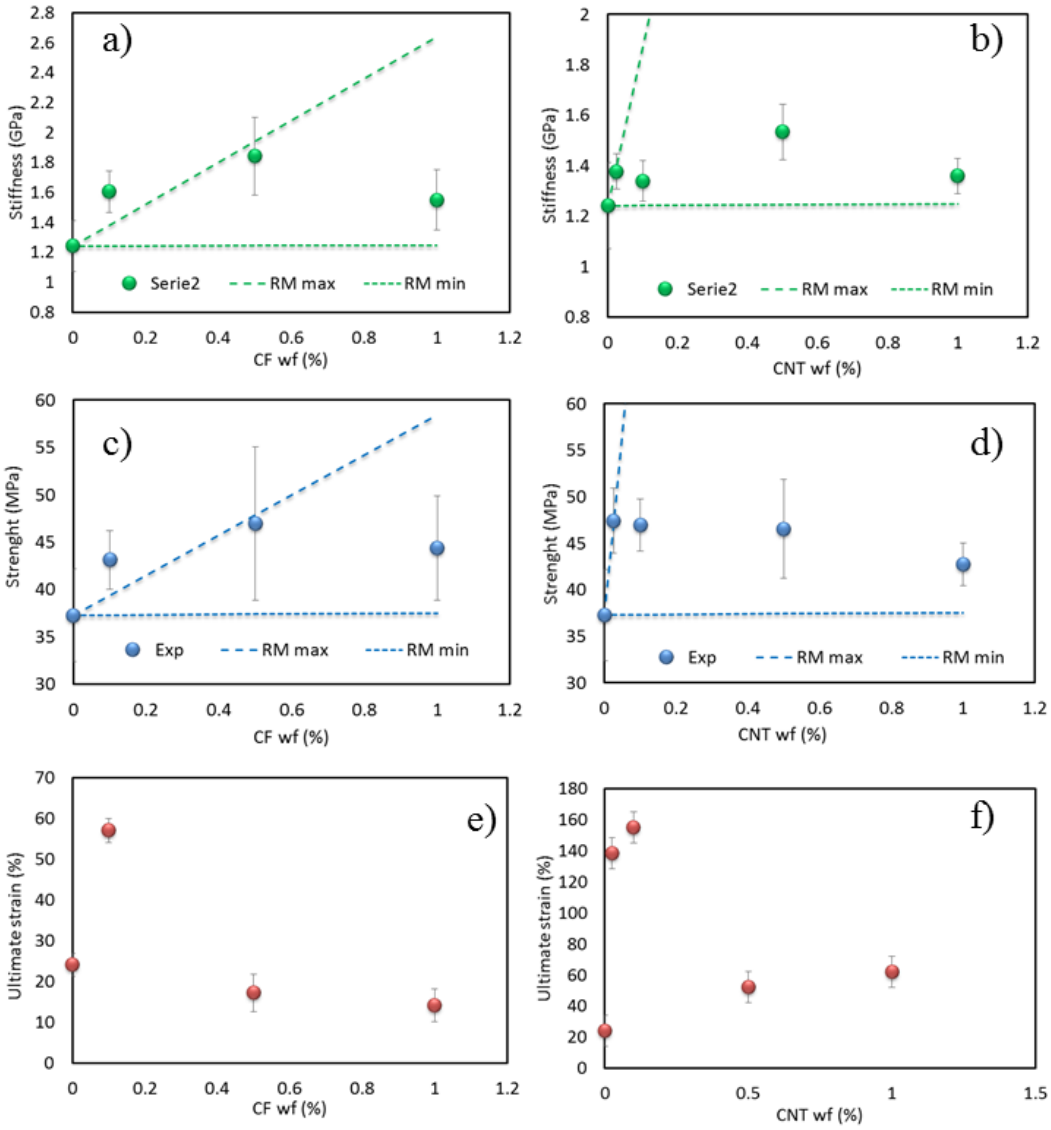

Figure 66: Average stiffness, strength, and ultimate strain values for CF-reinforced PVB (left column) and CNT-reinforced PVB (right column) composites. Dotted lines display direct ("RM max") and inverse ("RM min") rule of mixtures predictions

Table 14: Average mechanical properties of CF and CNT composite tapes measured in tensile testing

Sample	Stiffness (GPa)	Strength (MPa)	Ultimate Strain (%)	Toughness (J/g)
PVB	1.24±0.17	37.3±4.9	24.2±2.8	150±36
CF 0.1	1.84±0.02	43.1±3.1	57.1±1.4	122±14
CF 0.5	1.55±0.06	46.9±8.1	17.2±4.6	92±32
CF 1	1.36±0.07	44.4±5.5	14.1±5.3	135±40
CNT 0.025	1.38±0.07	47.4±3.5	138.4±1.1	222±47
CNT 0.1	1.22±0.02	47.0±2.8	154.9±2.5	164±16
CNT 0.5	1.53±0.11	46.6±5.3	52.2±4.7	146±49
CNT 1	1.55±0.20	42.7±2.3	61.9±10.3	139±15

Results show that the composites reinforced with CFs achieve an increase in stiffness and strength with increasing CF weight fraction, up to a maximum for 0.5% CFs. This increase is consistent with RM predictions, indicating that the fibres are well aligned. For larger fibre contents, the effects of imperfect dispersion become non negligible, since the CFs agglomerate in bundles that behave as brittle inclusions, leading to a decrease in the overall strength of the composites. The ultimate strain increases with respect to pure PVB in the case of the sample containing 0.1% CFs while at 0.5% CFs the fracture becomes brittle. This effect is again related to the size of the reinforcements: for 0.1% CFs there is sufficient space between the fibres to guarantee the deformation of the samples, while in the case of a higher CF content, the effect of local stiffening of the polymer induced by the fibres prevails and fracture becomes brittle.

Table 15: Material properties used in direct and inverse RM

Property	PVB	CF	CNT
Density (kg/m^3)	1070	1760	1350
Young's modulus (GPa)	1.24	230	800
Strength (MPa)	37.3	3500	50000

SEM analysis of fracture surfaces of CF-reinforced samples (figure 67) shows that as expected fibres are mainly oriented along the tape direction due to the

shear stresses acting during the tape casting process. Partial debonding and pull-out from the matrix is observed (figure 67). This suggests a relatively weak interface between the polymer and the fibres, which leads to limited toughness values, consistently with observed ultimate strain values.

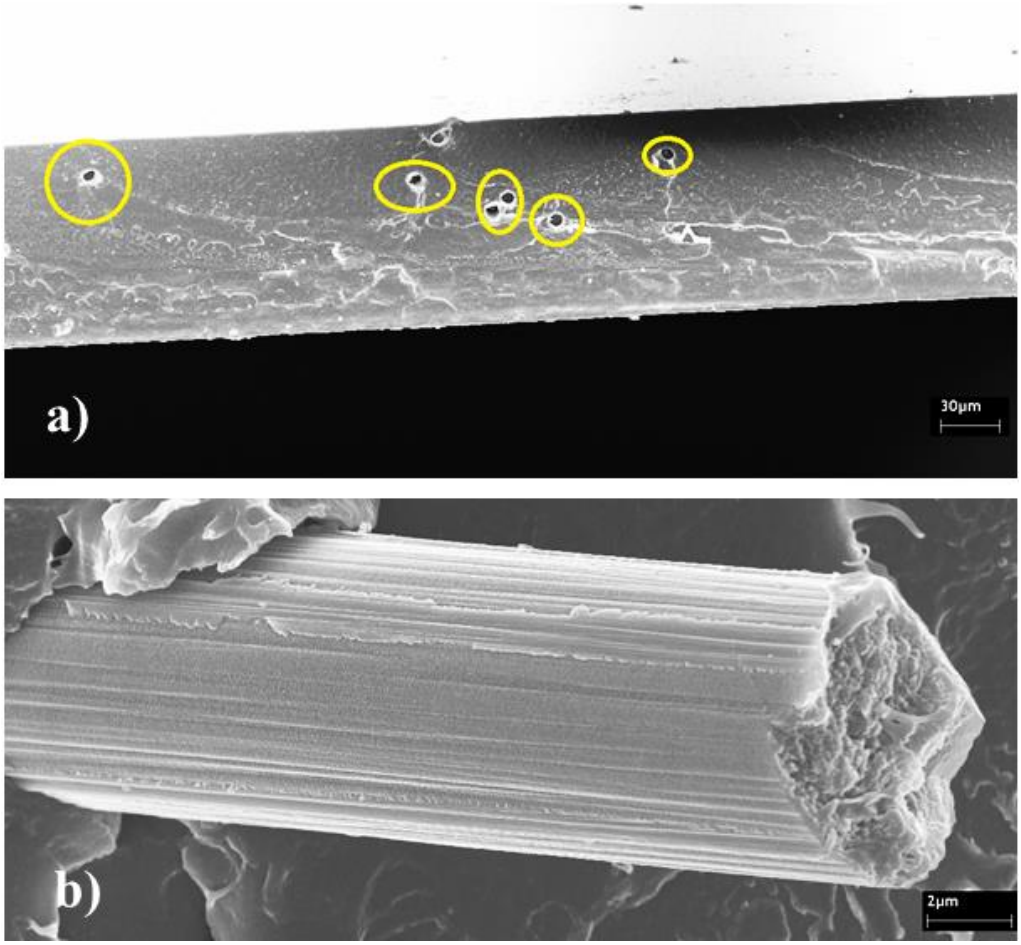

Figure 67: SEM image of a CF 0.5 sample at (a) 700X magnification (b) 15000X magnification, highlighting fibre pull-out

The stiffness and strength data indicate that 0.5% is the optimal CF weight fraction to provide the best mechanical properties. This is because this concentration allows a good dispersion of CFs during composite manufacturing with limited fibre aggregation. Analysis of the fracture surfaces suggests that an improvement in the interface could significantly change the mode of fracture of these composites, and lead to further toughness improvements.

The addition of CNTs also significantly improves mechanical properties in terms of stiffness and tensile strength, as expected. However, the best mechanical performance, comparable with RM predictions, is obtained at a very low weight fractions (0.025% wf for tensile strength and 0.1% wf for ultimate strain), while higher percentages lead to a degradation of the mechanical properties, with

properties considerably below direct RM predictions. This is due to the fact that low CNT concentrations allow a uniform dispersion of the filler in the matrix and a better exploitation of the exceptional mechanical properties of the single CNTs. When the CNT concentration is increased, nanotube bundles tend to form behaving as structural defects, counterbalancing the positive effect of the increased CNT concentration in the matrix (figure 68). The smaller amount of filler needed to reach the optimal stiffness and strength with respect to the case of CF-reinforced composites is related to the higher CNT stiffness and strength values, making them more effective in providing reinforcement effects at lower weight fractions. In addition, some nanoscale-related effects can occur, leading to a change in the local properties of the polymer matrix due to the high CNT surface area and the vicinity between CNTs even at low weight fractions. Additionally, CNTs can potentially interact with surrounding polymer chains and modify the crystalline morphology of the matrix (Paul and Robeson 2008).

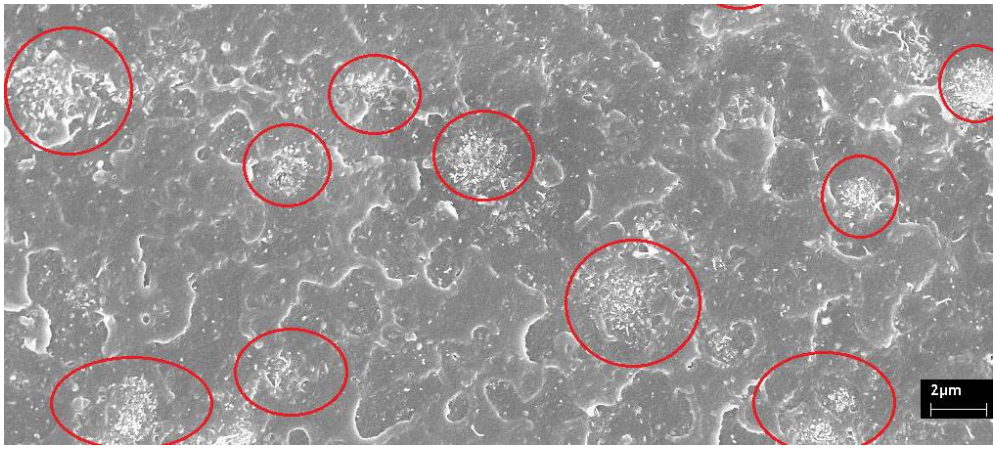

Figure 68: SEM image of a CNT 1 sample at 10000X magnification. Red circles indicate CNT agglomeration in bundles

The latter effects are responsible for the observed increase in ultimate strain for CNT-reinforced samples, leading to a higher toughness composite. Necking and unfolding of polymer chains is improved by the addition of a small amount of CNTs, while it is hindered by the presence of CNT agglomerates. In the case of PVB-CNTs composites, a chain-wrapping phenomenon is hypothesized at the interface between CNTs and PVB (Yang et al. 2005). When a tensile stress is applied, the chains start to unfold, sliding along the nanotubes, giving rise to an improved elongation at break with respect to the pure polymer.

5.4.4 Multiscale composites

To evaluate the influence of multiscale hierarchical structure on the mechanical behaviour of the considered CF-CNT composites, a comparison is made between samples with CNTs grafted on the CF surfaces (MS samples), and samples where the CFs and CNTs are simply mixed in the matrix. The measured stiffness and strength values for the same CF and CNT content for the two types of composite are reported in figure 69 and in Table 16. As discussed in the previous section, the CF weight fraction for which best results are obtained in the case of a single-reinforcement composite is kept constant (0.5 %) and CNT content varies between 0.01 % and 0.1%. Results show an improvement in both stiffness and strength of the composites containing both CFs and CNTs with respect to the case of the composites with only single reinforcement types (Fig.66). A further improvement is observed in the case of MS samples compared to the samples obtained by mixing together non-grafted fibres and CNTs. In the best case, a stiffness and strength increase of 45% and 47% is obtained compared to PVB, of 18% and 23% compared to the CF 0.5 specimens, and of 24% and 28% compared to the non-grafted CNT case. Writing the direct RM for strength as:

$$\sigma_{CF} = \frac{\sigma_C - \sigma_{PVB}(1 - f_{CF})}{f_{CF}} \quad (2)$$

where σ_{CF} is the CF strength, σ_C is the composite strength, σ_{PVB} is the matrix strength, and f_{CF} the CF volume fraction, one can derive that the effect of adding grafted CNTs is equivalent to using CFs that are twice as strong as conventional ones (7.7 GPa instead of 3.5 GPa).

Table 16: Average mechanical properties of Multiscale (MS) and conventional CF/CNT composite tapes measured in tensile testing

Sample	Stiffness (GPa)	Strength (MPa)	Ultimate Strain (%)	Toughness (J/g)
CF 0.5 CNT 0.01	1.7±0.1	47.5±1.2	29.6±15.5	251±51
CF 0.5 CNT 0.025	1.7±0.1	49.8±1.8	27.5±11.6	239±49
CF 0.5 CNT 0.1	1.7±0.1	49.3±3.9	31.6±23.9	227±53
MS 0.5 - 0.01	1.6±0.3	51.0±3.4	3.2±0.69	65±28
MS 0.5 - 0.025	1.8±0.1	52.7±6.0	35.6±18.7	218±23
MS 0.5 - 0.1	2.0±0.1	60.5±0.2	19.9±7.1	255±18

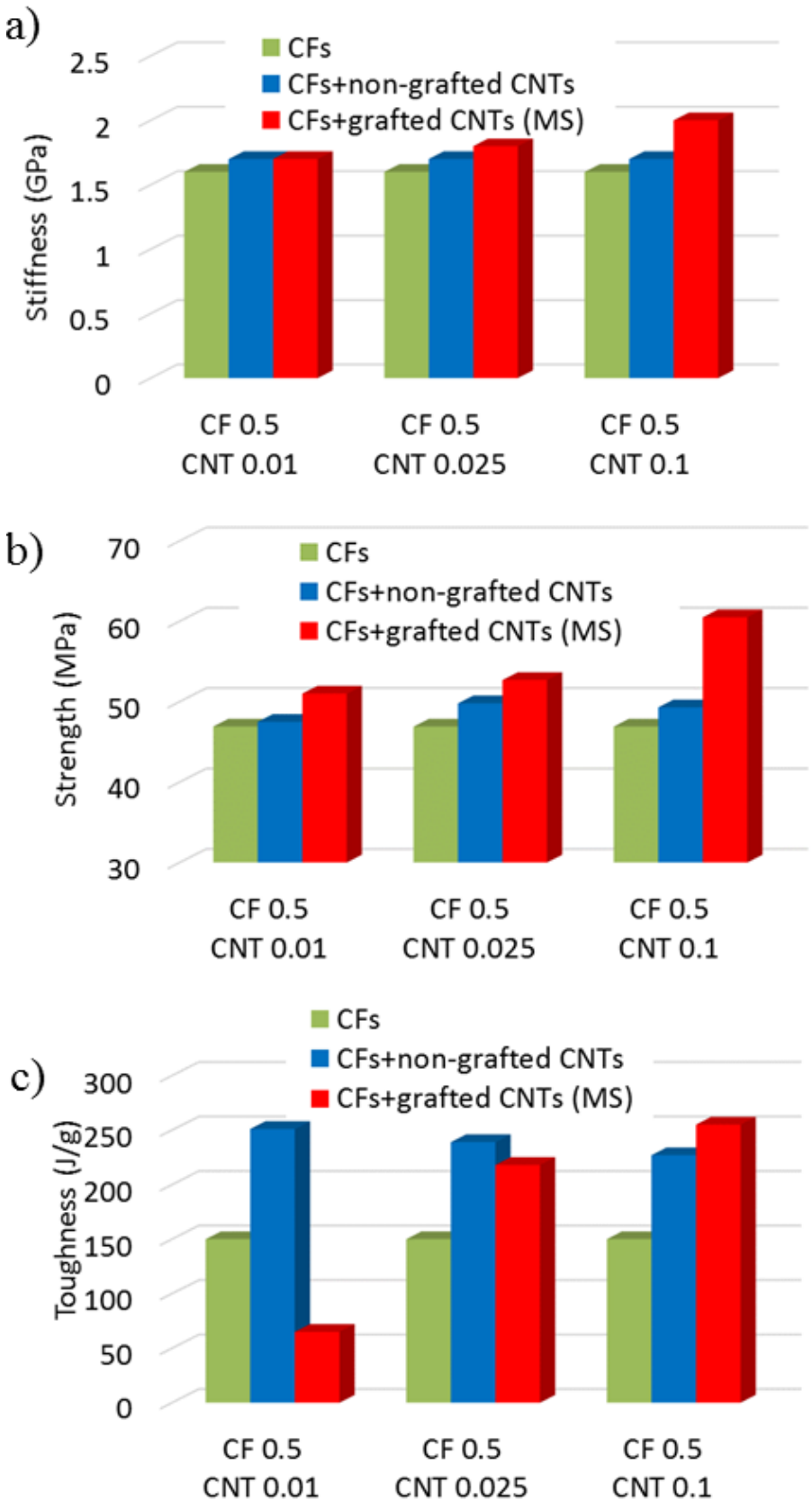

Figure 69: Stiffness, strength and toughness of multiscale (MS) composites with CNTs grafted on CFs compared with composites with non-grafted CNTs and with conventional CF composites. The MS composites optimize both strength and toughness

This behaviour is due to the hierarchical structure of the reinforcements in MS samples shown in figure 44, 45 and 46, which enhances the adhesion between fibre and matrix, giving rise to a strength increase. Moreover, a stronger interface between fibres and matrix allows the sliding of the polymer chains during damage evolution within the polymer itself, rather than at the interface with the carbon fibres. Thus, the overall fracture process becomes more ductile, with greater polymer deformation around the fibre rather than fibre pull-out from of the polymer. This leads to a simultaneously stronger and tougher material.

On the other hand, the properties of the mixed composites with non-grafted fibres lie between those of multiscale ones and single-fibre reinforced ones. The CNT content does not significantly alter the mechanical properties of CF 0.5 samples, confirming the indication that a good dispersion of CNTs is obtained for small weight fraction values, while agglomeration effects take place at greater concentrations. Consistently with previous observations, in most cases samples containing small amounts of CNTs show plasticization effects that lead to larger ultimate strain value and toughness.

5.4.5 Numerical analysis of CF-CNT interface properties

The improvement in mechanical properties identified in specimens with grafted CNTs discussed in the previous sections is attributed to the improvement in interface properties between CFs and matrix, which helps prevent fibre pull out during specimen failure. This improvement can be highlighted by analysing stress distributions at the interface for CFs with and without grafted CNTs. In particular, we qualitatively evaluate the distributions in the case of the presence of CNOs (Fig. 44) by means Finite Element (FE) simulations using COMSOL Multiphysics. An axisymmetric model of a single CF embedded in a PVB matrix with and without grafted CNOs is considered. The fibre is 50 μm in length and CNOs (200 nm in radius) are regularly spaced at 2 μm along its length. Material properties are taken from Table 15. figure 70 shows the shear stress concentrations in and around the embedded matrix when a unit pull-out force *P* is applied to the fibre end. The corresponding stresses at the interface highlight the mechanism responsible for the improvement of interface properties for

hierarchical fibres. In the case of a non-grafted fibre, the stress peaks occur at the fibre ends, giving rise to anticipated fibre-matrix debonding and fibre pull-out. Instead, the presence of CNOs along the fibre give rise to a redistribution of stresses, and a reduction in the stress peaks, thus leading to a greater load bearing capacity and improved overall composite strength, as observed experimentally.

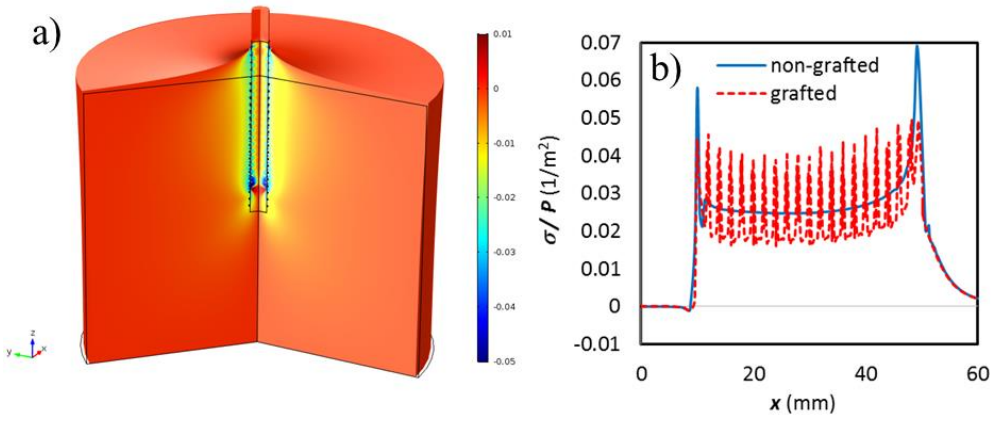

Figure 70: FE results of the pull-out from a PVB matrix of a CF with grafted CNOs: a) Stress σ (per unit pull-out load P) distribution in the matrix and fibre; b) Calculated stresses at the interface for grafted and non-grafted fibres

The increase in toughness between a CF-reinforced composite and a MS composite can be quantified using a recently-introduced "hierarchical shear lag" theory by some of the authors (Brely et al. 2017), according to which the increase of dissipated energy during fibre pull-out per unit contact area W_2/A_2 when adding a hierarchical level to a fibrillar system can be expressed as:

$$\frac{W_2}{A_2} = \frac{W_1}{A_1}\left(2 + \frac{l_d}{l_a}\right) \tag{3}$$

where W_1/A_1 is the dissipated energy per unit area for the non-hierarchical system, l_d is the average detached length of second-level fibrils (CNTs in this case) and l_a their attached length. Thus, the additional hierarchical level produces at least a doubling of toughness, which is compatible with the observed values, at least for sufficient CNT concentrations to ensure uniform coating of the CF. The l_a value is also inversely proportional to the linear density of grafted CNTs on the CF, so Eq.(3) correctly predicts an increase in toughness with increasing CNT concentration, at least until self-bunching effects set in.

5.4.6 Conclusions

In conclusion, our experimental results on CF/CNT reinforced PVB composite tapes show that it is possible to obtain a considerable increase in stiffness, strength and toughness with respect to the pure polymer by using relatively low reinforcement weight fractions. The addition of single fillers (either CFs or CNTs) leads to increments of up to 50% in stiffness, 30% in strength, and up to 500% in ultimate strain. Larger weight fractions lead to saturation effects given by dispersion difficulties. The mixture of CFs and CNTs produces a further improvement that can be ascribed to a synergic interaction of the two different fillers. The best results, however, are obtained when a hierarchical bioinspired structure is attained using surface-grafted CNTs on CF reinforcing fibres, since fibre-matrix interface properties are significantly improved and fibre pull-out effects are reduced, leading to a further 60% increase in stiffness and 20% increase in strength with respect to the non-hierarchical case. Morphological analysis and numerical simulations support the interpretation of the role of the grafted CNTs on the mechanical performance. These results provide useful indications for the manufacture of stronger and tougher polymer nanocomposites and could contribute in fully realizing the potential of nanocomposites in the field of advanced materials using the concepts provided a bioinspired approach.

Chapter 6

Final conclusions and remarks

As already seen in the literature, the use of carbon nanotubes, graphene and carbon fibers in composite materials can guarantee an increase of the properties of the matrix. What we can observe, however, is that the interaction between matrix and reinforcement is not always optimal. The aim of this thesis was to find a way to overcome this problem and thus to further increase the already good properties of the existing composite materials.

For what concerns the cement matrix composites, the two key roles for the improvement of the properties are played by: the dispersion in water and the matrix-reinforcement interaction. As shown in this work, a slight chemical functionalization of the surface can improve both of them. The presence of functional hydrophilic groups allows a better dispersion of the reinforcement in water and consequently in the final composite. The same functional groups also give an excellent interaction with the chemical structure of the cement, creating secondary bonds between reinforcement and matrix, thus obtaining an evident increase in properties. On the other hand, excessive functionalization of the surface has a negative effect on the properties of the final composite. This is because defects are created on the surface of the reinforcement, which worsen their intrinsic properties. An excessive presence of functional groups can also sequester the water needed for the hydration of cement, thus creating a low quality final product.

For what concerns the polymer matrix, we have shown how the use of carbon fibers or nanotubes greatly improve the mechanical properties of the polymer. However, a large quantity of reinforcement can be not homogeneously dispersed

in the matrix, creating areas with defects. Moreover, if there is a bad interaction with the matrix, a low toughness can be observed notwithstanding pull-out phenomena. It has been shown that the best solution is to create a multiscale reinforcement, thus improving the interfacial adhesion between matrix and reinforcement by increasing the surface area on which the interaction occurs. The numerical data show that grafting carbon nanotubes on the carbon fibers greatly improves the mechanical properties with respect to the not grafted case.

As a whole, functionalization of the reinforcement in cement- and polymer-based composite materials seems a very promising way to reduce problems related to interaction and dispersion, and to improve the properties of such composites over the current state-of-art.

References

A. Ferri (2015) High performance textile applications

A. Laachachi, A. Vivet, G. Nouet, et al (2007) A chemical method to graft carbon nanotubes onto carbon fiber. Materials Letters. 62:394–397

Abdelghani Laachachi, Alexandre Vivet, Gérard Nouet, et al (2008) A chemical method to graft carbon nanotubes onto a carbon fiber. Materials Letters. 62:394–397

Ajayan PM, Ebbesen TW, Ichihashi T, et al (1993) Opening carbon nanotubes with oxygen and implications for filling. Nature 362:522–525. doi: 10.1038/362522a0

Alan M. Cassell, J.A. Raymakers., J. Kong, H. Dai (1999) Large Scale CVD Synthesis of Single-Walled Carbon Nanotubes. The journal of physical chemistry B 103:6484–6492

Alfredo M. Morales, Charles M. Lieber (1998) A Laser Ablation Method for the Synthesis of Crystalline Semiconductor Nanowires. Science 279:208–221

Alger M (1997) Polymer Science Dictionary, 2nd edn. Springer Netherlands

Ando Y (1994) The Preparation of Carbon Nanotubes. Fullerene Science and Technology 2:173–180. doi: 10.1080/15363839408009542

Andrews R, Berkovich, Hower JC, et al (2002) FABRICATION OF CARBON MULTIWALL NANOTUBE / POLYMER COMPOSITES BY SHEAR MIXING. Macromol. Mater. Eng. 287

Andrews R, Jacques D, Qian D, Dickey EC (2001) Purification and structural annealing of multiwalled carbon nanotubes at graphitization temperatures. Carbon 39:1681–1687

Avilés F, Cauich-Rodríguez JV, Moo-Tah L, et al (2009) Evaluation of mild acid oxidation treatments for MWCNT functionalization. Carbon 47:2970–2975. doi: 10.1016/j.carbon.2009.06.044

Azhari F, Banthia N (2012) Cement-based sensors with carbon fibers and carbon nanotubes for piezoresistive sensing. Cement and Concrete Composites 34:866–873. doi: 10.1016/j.cemconcomp.2012.04.007

Bacon R, Moses CT (1986) Carbon Fibers, from Light Bulbs to Outer Space. In: Seymour RB, Kirshenbaum GS (eds) High Performance Polymers: Their Origin and Development. Springer Netherlands, pp 341–353

Badini CF, Caradonna DA, Pepe R Effetto di grafene e nanotubi di carbonio sulla conducibilità di compositi ibridi con matrice epossidica. 65

Bagri A, Mattevi C, Acik M, et al (2010) Structural evolution during the reduction of chemically derived graphene oxide. Nature Chemistry 2:581–587. doi: 10.1038/nchem.686

Balandin AA (2011) Thermal properties of graphene and nanostructured carbon materials. Nature Materials 10:569

Bethune DS, Klang CH, De Vries MS, et al (1993) Cobalt-catalysed growth of carbon nanotubes with single-atomic-layer walls. Nature 363:605–607. doi: 10.1038/363605a0

Brandt AM (2008) Fibre reinforced cement-based (FRC) composites after over 40 years of development in building and civil engineering. Composite Structures 86:3–9. doi: 10.1016/j.compstruct.2008.03.006

Brely L, Bosia F, Pugno NM (2017) Emergence of the interplay between hierarchy and contact splitting in biological adhesion highlighted through a hierarchical shear lag model. arXiv preprint arXiv:171009265

Brodie BC, F. R. S. (1859) XIII. On the atomic weight of graphite. Phil Trans R Soc Lond 149:249–259

Bundy FP (1996) The pressure-temperature phase and transformation diagram for carbon; updated through 1994. Carbon 34:141–153. doi: 10.1016/0008-6223(96)00170-4

Bystrzejewski M, Huczko A, Lange H, et al (2010) Dispersion and diameter separation of multi-wall carbon nanotubes in aqueous solutions. Journal of Colloid and Interface Science 345:138–142. doi: 10.1016/j.jcis.2010.01.081

Callister WD, Callister WD (2001) Fundamentals of materials science and engineering: an interactive etext. Wiley, New York

Castro Neto AH, Guinea F, Peres NMR, et al (2009) The electronic properties of graphene. Reviews of Modern Physics 81:109–162. doi: 10.1103/RevModPhys.81.109

Chen J, Yao B, Li C, Shi G (2013) An improved Hummers method for eco-friendly synthesis of graphene oxide. Carbon 64:225–229. doi: 10.1016/j.carbon.2013.07.055

Chiang IW, Brinson BE, Huang AY, et al (2001) Purification and Characterization of Single-Wall Carbon Nanotubes (SWNTs) Obtained from the Gas-Phase Decomposition of CO (HiPco Process). The Journal of Physical Chemistry B 105:8297–8301. doi: 10.1021/jp0114891

Chiang Y-C, Lin W-H, Chang Y-C (2011) The influence of treatment duration on multi-walled carbon nanotubes functionalized by H2SO4/HNO3 oxidation. Applied Surface Science 257:2401–2410. doi: 10.1016/j.apsusc.2010.09.110

Choi W, Lahiri I, Seelaboyina R, Kang YS (2010) Synthesis of Graphene and Its Applications: A Review. Critical Reviews in Solid State and Materials Sciences 35:52–71. doi: 10.1080/10408430903505036

Chuang W, Geng-sheng J, Bing-liang L, et al (2017) Dispersion of carbon fibers and conductivity of carbon fiber-reinforced cement-based composites. Ceramics International 43:15122–15132. doi: 10.1016/j.ceramint.2017.08.041

Cohen ML (1998) Pergamon. 107:589–596

Cohen ML (1994) Predicting properties and new materials. Solid State Communications 92:45–52

Coleman JN, Khan U, Blau WJ, Gun'ko YK (2006) Small but strong: A review of the mechanical properties of carbon nanotube–polymer composites. Carbon 44:1624–1652. doi: 10.1016/j.carbon.2006.02.038

Dai H, Wong EW, Lieber CM (1996) Probing Electrical Transport in Nanomaterials: Conductivity of Individual Carbon Nanotubes. Science 272:523. doi: 10.1126/science.272.5261.523

Dasgupta D, Demichelis F, Tagliaferro A (1991) Electrical conductivity of amorphous carbon and amorphous hydrogenated carbon. Philosophical Magazine B 63:1255–1266. doi: 10.1080/13642819108205558

Datsyuk V, Kalyva M, Papagelis K, et al (2008) Chemical oxidation of multiwalled carbon nanotubes. Carbon 46:833–840. doi: 10.1016/j.carbon.2008.02.012

de Pablo PJ, Graugnard E, Walsh B, et al (1999) A simple, reliable technique for making electrical contact to multiwalled carbon nanotubes. Applied Physics Letters 74:323–325. doi: 10.1063/1.123011

Dillon AC, Gennett T, Jones KM, et al (1999) A simple and complete purification of single-walled carbon nanotube materials. Advanced Materials 11:1354–1358

Donnet JB, Fousson E, Samirant M, et al (2000) Shock synthesis of nanodiamonds from carbon precursors: identification of carbynes. COMPTES RENDUS DE L ACADEMIE DES SCIENCES SERIE II FASCICULE CCHIMIE 3:359–364

Dresselhaus MS, Jorio A, Saito R (2010) Characterizing Graphene, Graphite, and Carbon Nanotubes by Raman Spectroscopy. Annu Rev Condens Matter Phys 1:89–108. doi: 10.1146/annurev-conmatphys-070909-103919

Eastman, Chemical Company (2013) Butvar® polyvinyl butyral resin Properties and uses

Ebbesen TW, Lezec HJ, Hiura H, et al (1996) Electrical conductivity of individual carbon nanotubes. Nature 382:54

Edie D.D., Dunham M.G. (1989) Melt spinning pitch based carbon fibres. Carbon 647–655

Fan J-C, Sung H-H, Lin C-R, Lai M-H (2012) The production of onion-like carbon nanoparticles by heating carbon in a liquid alcohol. Journal of Materials Chemistry 22:9794. doi: 10.1039/c2jm13273g

Geim AK, Novoselov KS (2007) The rise of graphene. Nature Materials 6:183

Gómez S, Rendtorff NM, Aglietti EF, et al (2016) Surface modification of multiwall carbon nanotubes by sulfonitric treatment. Applied Surface Science 379:264–269. doi: 10.1016/j.apsusc.2016.04.065

Gómez-Navarro C, Meyer JC, Sundaram RS, et al (2010) Atomic Structure of Reduced Graphene Oxide. Nano Letters 10:1144–1148. doi: 10.1021/nl9031617

Gong K, Pan Z, Korayem AH, et al (2015) Reinforcing Effects of Graphene Oxide on Portland Cement Paste. Journal of Materials in Civil Engineering 27:A4014010. doi: 10.1061/(ASCE)MT.1943-5533.0001125

Grandi S, Magistris A, Mustarelli P, et al (2006) Synthesis and characterization of SiO2–PEG hybrid materials. Journal of Non-Crystalline Solids 352:273–280. doi: 10.1016/j.jnoncrysol.2005.11.033

Hamada N, Sawada S, Oshiyama A (1992) New One-Dimensional Conductors: Graphitic Microtubuleles. Physical Review Letters 68:1579–1581. doi: 10.1176/appi.neuropsych.242259

Han MY, Özyilmaz B, Zhang Y, Kim P (2007) Energy Band-Gap Engineering of Graphene Nanoribbons. Physical Review Letters 98:. doi: 10.1103/PhysRevLett.98.206805

Hernandez Y, Nicolosi V, Lotya M, et al (2008) High-yield production of graphene by liquid-phase exfoliation of graphite. Nature Nanotechnology 3:563

Hertel T, Martel R, Avouris P (1998) Manipulation of individual carbon nanotubes and their interaction with surfaces. J Phys Chem 102:910–915. doi: 10.1021/jp9734686

Hone J, Llaguno MC, Nemes NM, et al (2000) Electrical and thermal transport properties of magnetically aligned single wall carbon nanotube films. Applied Physics Letters 77:666–668. doi: 10.1063/1.127079

Hou P, Liu C, Tong Y, et al (2001) Purification of single-walled carbon nanotubes synthesized by the hydrogen arc-discharge method. Journal of Materials Research 16:2526–2529. doi: 10.1557/JMR.2001.0346

Hou P-X, Liu C, Cheng H-M (2008) Purification of carbon nanotubes. Carbon 46:2003–2025. doi: 10.1016/j.carbon.2008.09.009

Huang W, Wang Y, Luo G, Wei F (2003) 99.9% purity multi-walled carbon nanotubes by vacuum high-temperature annealing. Carbon 41:2585–2590

Hummers Jr WS, Offeman RE (1958) Preparation of graphitic oxide. Journal of the American Chemical Society 80:1339–1339

Iijima S (1991) Helical microtubules of graphitic carbon. Nature 354:56–58

Iijima S, Ichihashi T (1993) SINGLE-SHELL CARBON NANOTUBES OF 1-NM DIAMETER (VOL 363, PG 603, 1993). Nature 364:737

Inam F, Bhat BR, Vo T, Daoush WM (2014) Structural health monitoring capabilities in ceramic–carbon nanocomposites. Ceramics International 40:3793–3798. doi: 10.1016/j.ceramint.2013.09.039

J. G. Lavin (2001) Carbon Fibres. In: High performance fibres. Woodhead pubblishing limited, pp 156–188

Jenq YS, Shah SP (1986) Crack propagation in fiber-reinforced concrete. Journal of Structural Engineering 112:19–34

John J, Gangadhar SA, Shah I (2001) Flexural strength of heat-polymerized polymethyl methacrylate denture resin reinforced with glass, aramid, or nylon fibers. The Journal of Prosthetic Dentistry 86:424–427. doi: 10.1067/mpr.2001.118564

Jorge FC, Pereira C, Ferreira JMF (2004) Wood-cement composites: a review. Holz als Roh- und Werkstoff 62:370–377. doi: 10.1007/s00107-004-0501-2

Junrong Yu, Nadia Grossiord, Cor E. Koning, Joachim Loos (2007) Controlling the dispersion of multi-wall carbon nanotubes in aqueous surfactant solution. Carbon 45:618–623

Kackar RN (1989a) Off-Line Quality Control, Parameter Design, and the Taguchi Method. In: Dehnad K (ed) Quality Control, Robust Design, and the Taguchi Method. Springer US, Boston, MA, pp 51–76

Kackar RN (1989b) Taguchi's Quality Philosophy: Analysis and Commentary. In: Dehnad K (ed) Quality Control, Robust Design, and the Taguchi Method. Springer US, Boston, MA, pp 3–21

Kathi J, Rhee KY (2008) Surface modification of multi-walled carbon nanotubes using 3-aminopropyltriethoxysilane. Journal of Materials Science 43:33–37. doi: 10.1007/s10853-007-2209-2

Khushnood RA, Ahmad S, Restuccia L, et al (2016) Carbonized nano/microparticles for enhanced mechanical properties and electromagnetic interference shielding of cementitious materials. Frontiers of Structural and Civil Engineering 10:209–213. doi: 10.1007/s11709-016-0330-5

Kim GM, Nam IW, Yoon HN, Lee HK (2018) Effect of superplasticizer type and siliceous materials on the dispersion of carbon nanotube in cementitious composites. Composite Structures 185:264–272. doi: 10.1016/j.compstruct.2017.11.011

Kim YJ, Shin TS, Choi HD, et al (2005) Electrical conductivity of chemically modified multiwalled carbon nanotube/epoxy composites. Carbon 43:23–30. doi: 10.1016/j.carbon.2004.08.015

Konsta-Gdoutos MS, Metaxa ZS, Shah SP (2010) Multi-scale mechanical and fracture characteristics and early-age strain capacity of high performance carbon nanotube/cement nanocomposites. Cement and Concrete Composites 32:110–115. doi: 10.1016/j.cemconcomp.2009.10.007

Kroto HW, Heath JR, O'Brien SC, et al (1985) 1985 Nature Publishing Group. Nature 318:162–163. doi: 10.1038/318162a0

Kumar PV, Bardhan NM, Tongay S, et al (2013) Scalable enhancement of graphene oxide properties by thermally driven phase transformation. Nature Chemistry 6:151–158. doi: 10.1038/nchem.1820

Laplaze D, Bernier P, Barbedette L, et al (1994) Production de fullerenes à partir de l'énergie solaire: L'expérience d'Odeillo. CR Acad Sci Paris 318:733–738

Laplaze D, Bernier P, Maser WK, et al (1998) Carbon nanotubes: The solar approach. Carbon 36:685–688. doi: 10.1016/S0008-6223(98)00025-6

Larson BK, Drzal LT, Sorousian P (1990) Carbon fibre-cement adhesion in carbon fibre reinforced cement composites. Composites 21:205–215

Lavagna L, Massella D, Pantano MF, et al (2018a) Grafting carbon nanotubes onto carbon fibres doubles their effective strength and the toughness of the composite. Composites Science and Technology. doi: 10.1016/j.compscitech.2018.03.015

Lavagna L, Massella D, Pavese M (2017) Preparation of hierarchical material by chemical grafting of carbon nanotubes onto carbon fibers. Diamond and Related Materials 80:118–124. doi: 10.1016/j.diamond.2017.10.013

Lavagna L, Musso S, Ferro G, Pavese M (2018b) Cement-based composites containing functionalized carbon fibers. Cement and Concrete Composites 88:165–171. doi: 10.1016/j.cemconcomp.2018.02.007

Lavagna L, Musso S, Ferro G, Pavese M (2018c) Cement-based composites containing functionalized carbon fibers. Cement and Concrete Composites 88:165–171. doi: 10.1016/j.cemconcomp.2018.02.007

Lavin J.G., Boyington D.R., Lahijani J., et al (1993) The correlation of thermal conductivity and electrical resistivity in pitch based carbon fibres. Carbon 1001–1002

Lee C, Wei X, Kysar JW, Hone J (2008) Measurement of the Elastic Properties and Intrinsic Strength of Monolayer Graphene. Science 321:385. doi: 10.1126/science.1157996

Lee C-Y, Wang S-R (2010) Application of Four-electrode Method to Analysis Resistance Characteristics of Conductive Concrete. World Academy of Science, Engineering and Technology 4:77–80

Lestari Y, Bahri S, Sugiarti E, et al (2013) Effect of different dispersants in compressive strength of carbon fiber cementitious composites. AIP Conference Proceedings 1555:67–69. doi: 10.1063/1.4820995

Li C, Wang D, Liang T, et al (2004) Oxidation of multiwalled carbon nanotubes by air: benefits for electric double layer capacitors. Powder Technology 142:175–179. doi: 10.1016/j.powtec.2004.04.037

Li G (2004) Properties of high-volume fly ash concrete incorporating nano-SiO2. Cement and Concrete Research 34:1043–1049. doi: 10.1016/j.cemconres.2003.11.013

Li M, Boggs M, Beebe TP, Huang CP (2008a) Oxidation of single-walled carbon nanotubes in dilute aqueous solutions by ozone as affected by ultrasound. Carbon 46:466–475. doi: 10.1016/j.carbon.2007.12.012

Li S-Y, Zhou H-H, Gu J-L, Zhu J (2000) Does carbyne really exist? — carbynes in expanded graphite. Carbon 38:934–937. doi: 10.1016/S0008-6223(00)00056-7

Li X, Wang X, Zhang L, et al (2008b) Chemically Derived, Ultrasmooth Graphene Nanoribbon Semiconductors. Science 319:1229. doi: 10.1126/science.1150878

Linda Vaisman, H. Daniel Wagner, Gad Marom (2006) The role of surfactants in dispersion of carbon nanotubes. Advances in Colloid and Interface Science 128:37–46

Loiseau A, Launois P, Petit P, et al (2006) Understanding Carbon Nanotubes. Elsevier Ltd

Lotya M, Hernandez Y, King PJ, et al (2009) Liquid Phase Production of Graphene by Exfoliation of Graphite in Surfactant/Water Solutions. J Am Chem Soc 131:3611–3620. doi: 10.1021/ja807449u

Lotya M, King PJ, Khan U, et al (2010) High-Concentration, Surfactant-Stabilized Graphene Dispersions. ACS Nano 4:3155–3162. doi: 10.1021/nn1005304

Lu X, Chen Z (2005) Curved Pi-Conjugation, Aromaticity, and the Related Chemistry of Small Fullerenes (<C_{60}) and Single-Walled Carbon Nanotubes. Chemical Reviews 105:3643–3696. doi: 10.1021/cr030093d

MACKAY AL, TERRONES H (1991) Diamond from graphite. Nature 352:762

Marchisio Silvia (2013) Composite Materials reinforced by Carbon Nanotubes. PhD thesis, Politecnico di Torino

Mawhinney DB, Naumenko V, Kuznetsova A, et al (2000) Infrared spectral evidence for the etching of carbon nanotubes: ozone oxidation at 298 K. Journal of the American Chemical Society 122:2383–2384

Melanitis N, Tetlow PL, Galiotis C (1996) Characterization of PAN-based carbon fibres with laser Raman spectroscopy. Journal of Materials Science 31:851–860. doi: 10.1007/BF00352882

Mendoza Reales OA, Dias Toledo Filho R (2017) A review on the chemical, mechanical and microstructural characterization of carbon nanotubes-cement based composites. Construction and Building Materials 154:697–710. doi: 10.1016/j.conbuildmat.2017.07.232

Mintmire JW, Dunlap BI, White CT (1992) Are fullerene tubules metallic? Physical Review Letters 68:631–634. doi: 10.1103/PhysRevLett.68.631

Mistler RE, Twiname ER (2000) Tape casting: theory and practice. American Ceramic Society, Westerville, OH

Monthioux M, Kuznetsov VL (2006) Who should be given the credit for the discovery of carbon nanotubes? Carbon 44:1621–1623. doi: 10.1016/j.carbon.2006.03.019

Moreno-Castilla C, Lopez-Ramon MV, Carrasco-Marın F (2000) Changes in surface chemistry of activated carbons by wet oxidation. Carbon 38:1995–2001

Musso S, Tulliani J-M, Ferro G, Tagliaferro A (2009) Influence of carbon nanotubes structure on the mechanical behavior of cement composites.

Composites Science and Technology 69:1985–1990. doi: 10.1016/j.compscitech.2009.05.002

Nasibulina LI, Anoshkin IV, Nasibulin AG, et al (2012) Effect of Carbon Nanotube Aqueous Dispersion Quality on Mechanical Properties of Cement Composite. Journal of Nanomaterials 2012:1–6. doi: 10.1155/2012/169262

Novoselov KS (2004) Electric Field Effect in Atomically Thin Carbon Films. Science 306:666–669. doi: 10.1126/science.1102896

Novoselov KS, Geim AK, Morozov SV, et al (2005) Two-dimensional gas of massless Dirac fermions in graphene. Nature 438:197

O. BREUER, UTTANDARAMAN SUNDARARAJ (2004) Big Returns From Small Fibers: A Review of Polymer/Carbon Nanotube Composites. Polymer composites 25:630–645

Osorio AG, Silveira ICL, Bueno VL, Bergmann CP (2008) H2SO4/HNO3/HCl—Functionalization and its effect on dispersion of carbon nanotubes in aqueous media. Applied Surface Science 255:2485–2489. doi: 10.1016/j.apsusc.2008.07.144

Pan L, Yapici U (2015) A comparative study on mechanical properties of carbon fiber/PEEK composites. Advanced Composite Materials 1–16. doi: 10.1080/09243046.2014.996961

Pan Z, He L, Qiu L, et al (2015) Mechanical properties and microstructure of a graphene oxide–cement composite. Cement and Concrete Composites 58:140–147. doi: 10.1016/j.cemconcomp.2015.02.001

Papageorgiou DG, Kinloch IA, Young RJ (2017) Mechanical properties of graphene and graphene-based nanocomposites. Progress in Materials Science 90:75–127. doi: 10.1016/j.pmatsci.2017.07.004

Park YS, Choi YC, Kim KS, et al (2001) High yield purification of multiwalled carbon nanotubes by selective oxidation during thermal annealing. Carbon 39:655–661

Paul DR, Robeson LM (2008) Polymer nanotechnology: Nanocomposites. Polymer 49:3187–3204. doi: 10.1016/j.polymer.2008.04.017

Pavese M, Musso S, Bianco S, et al (2008) An analysis of carbon nanotube structure wettability before and after oxidation treatment. Journal of

Physics: Condensed Matter 20:474206. doi: 10.1088/0953-8984/20/47/474206

Peng Y, Liu H (2006) Effects of Oxidation by Hydrogen Peroxide on the Structures of Multiwalled Carbon Nanotubes. Industrial & Engineering Chemistry Research 45:6483–6488. doi: 10.1021/ie0604627

Pierson HO (1993) 3 - Graphite Structure and Properties. In: Pierson HO (ed) Handbook of Carbon, Graphite, Diamonds and Fullerenes. William Andrew Publishing, Oxford, pp 43–69

Polder RB (2001) Test methods for on site measurement of resistivity of concrete — a RILEM TC-154 technical recommendation. Construction and Building Materials 15:125–131. doi: 10.1016/S0950-0618(00)00061-1

Ramanathan T, Fisher FT, Ruoff RS, Brinson LC (2005) Amino-Functionalized Carbon Nanotubes for Binding to Polymers and Biological Systems. Chemistry of Materials 17:1290–1295. doi: 10.1021/cm048357f

Ranjbar N, Mehrali M, Mehrali M, et al (2015) Graphene nanoplatelet-fly ash based geopolymer composites. Cement and Concrete Research 76:222–231. doi: 10.1016/j.cemconres.2015.06.003

Riley VR, Razl I (1974) Polymer additives for cement composites: a review. Composites 5:27–33. doi: 10.1016/0010-4361(74)90016-0

Robertson DH, Brenner DW, Mintmire JW (1992) Energetics of nanoscale graphitic tubules. Physical Review B 45:12592–12595

Rosca ID, Watari F, Uo M, Akasaka T (2005) Oxidation of multiwalled carbon nanotubes by nitric acid. Carbon 43:3124–3131. doi: 10.1016/j.carbon.2005.06.019

Sahebian S, Zebarjad SM, vahdati Khaki J, Lazzeri A (2015) A study on the dependence of structure of multi-walled carbon nanotubes on acid treatment. Journal of Nanostructure in Chemistry 5:287–293. doi: 10.1007/s40097-015-0160-3

Saito T, Matsushige K, Tanaka K (2002) Chemical treatment and modification of multi-walled carbon nanotubes. Physica B: Condensed Matter 323:280–283

Saleh TA (2011) The influence of treatment temperature on the acidity of MWCNT oxidized by HNO3 or a mixture of HNO3/H2SO4. Applied Surface Science 257:7746–7751. doi: 10.1016/j.apsusc.2011.04.020

Sathishkumar T, Satheeshkumar S, Naveen J (2014) Glass fiber-reinforced polymer composites – a review. Journal of Reinforced Plastics and Composites 33:1258–1275. doi: 10.1177/0731684414530790

Schwarz H (1890) Gesammelte mathematische Abhandlungen. 2 Bande. Berlin

Sen R, Rickard SM, Itkis ME, Haddon RC (2003) Controlled Purification of Single-Walled Carbon Nanotube Films by Use of Selective Oxidation and Near-IR Spectroscopy. Chemistry of Materials 15:4273–4279. doi: 10.1021/cm0342997

Shah SP (1990) Determination of fracture parameters (K Ic s and CTODc) of plain concrete using three-point bend tests. Materials and Structures 23:457–460. doi: 10.1007/BF02472029

Shah SP, Konsta-Gdoutos MS, Metaxa ZS, Mondal P (2009) Nanoscale Modification of Cementitious Materials. In: Bittnar Z, Bartos PM, Němeček J, et al. (eds) Nanotechnology in Construction 3. Springer Berlin Heidelberg, pp 125–130

Sham M-L, Kim J-K (2006) Surface functionalities of multi-wall carbon nanotubes after UV/Ozone and TETA treatments. Carbon 44:768–777. doi: 10.1016/j.carbon.2005.09.013

Sihai Wen and D. D. L. Chung (2005) Strain-Sensing Characteristics of Carbon Fiber-Reinforced Cement. Materials Journal 102:. doi: 10.14359/14617

Sines G., Yang Z., Vickers B.D. (1989) Creep of a carbon-carbon composite at high temperatures and high stresses. Carbon 27:403–415

Socrates G, Socrates G (2001) Infrared and Raman characteristic group frequencies: tables and charts, 3rd ed. Wiley, Chichester ; New York

Sofi A (2017) Effect of waste tyre rubber on mechanical and durability properties of concrete – A review. Ain Shams Engineering Journal. doi: 10.1016/j.asej.2017.08.007

Tang M, Dou H, Sun K (2006) One-step synthesis of dextran-based stable nanoparticles assisted by self-assembly. Polymer 47:728–734. doi: 10.1016/j.polymer.2005.11.091

Tchoul MN, Ford WT, Lolli G, et al (2007) Effect of Mild Nitric Acid Oxidation on Dispersability, Size, and Structure of Single-Walled Carbon Nanotubes. Chemistry of Materials 19:5765–5772. doi: 10.1021/cm071758l

Timoshenko SP (1956) Strength of materials : part II, advanced. Van Nostrand Reinhold, New York

Tuinstra F, Koenig JL (1970) Raman Spectrum of Graphite. The Journal of Chemical Physics 53:1126–1130. doi: 10.1063/1.1674108

Valentin N. Popov (2004) Carbon nanotubes: properties and application. Materials Science and Engineering: R: Reports 43:61–102

Vázquez E, Giacalone F, Prato M (2014) Non-conventional methods and media for the activation and manipulation of carbon nanoforms. Chemical Society Reviews 43:58. doi: 10.1039/c3cs60164a

Wang B, Jiang R, Wu Z (2016) Investigation of the Mechanical Properties and Microstructure of Graphene Nanoplatelet-Cement Composite. Nanomaterials 6:200. doi: 10.3390/nano6110200

Wang C, Li K-Z, Li H-J, et al (2008) Effect of carbon fiber dispersion on the mechanical properties of carbon fiber-reinforced cement-based composites. Materials Science and Engineering: A 487:52–57. doi: 10.1016/j.msea.2007.09.073

Wang X, Liu Y, Yu G, et al Anisotropic Electrical Transport Properties of Aligned Carbon Nanotube Films. 4

Wang Z, Gao J, Ai T, et al (2014) Quantitative evaluation of carbon fiber dispersion in cement based composites. Construction and Building Materials 68:26–30. doi: 10.1016/j.conbuildmat.2014.06.035

Wegst UGK, Bai H, Saiz E, et al (2014) Bioinspired structural materials. Nature Materials 14:23–36. doi: 10.1038/nmat4089

Wen S, Chung DDL (2001) Effect of stress on the electric polarization in cement. Cement and concrete research 31:291–295

Wepasnick KA, Smith BA, Schrote KE, et al (2011) Surface and structural characterization of multi-walled carbon nanotubes following different oxidative treatments. Carbon 49:24–36. doi: 10.1016/j.carbon.2010.08.034

White B, Banerjee S, O'Brien S, et al (2007) Zeta-Potential Measurements of Surfactant-Wrapped Individual Single-Walled Carbon Nanotubes. The Journal of Physical Chemistry C 111:13684–13690. doi: 10.1021/jp070853e

Wu Z, Pittman Jr CU, Gardner SD (1995) Nitric acid oxidation of carbon fibers and the effects of subsequent treatment in refluxing aqueous NaOH. Carbon 33:597–605

Xia W, Jin C, Kundu S, Muhler M (2009) A highly efficient gas-phase route for the oxygen functionalization of carbon nanotubes based on nitric acid vapor. Carbon 47:919–922. doi: 10.1016/j.carbon.2008.12.026

Xing Y, Li L, Chusuei CC, Hull RV (2005) Sonochemical Oxidation of Multiwalled Carbon Nanotubes. Langmuir 21:4185–4190. doi: 10.1021/la047268e

Yan J-A, Ruan WY, Chou MY (2009) Electron-phonon interactions for optical-phonon modes in few-layer graphene: First-principles calculations. Physical Review B 79:. doi: 10.1103/PhysRevB.79.115443

Yang H, Cui H, Tang W, et al (2017) A critical review on research progress of graphene/cement based composites. Composites Part A: Applied Science and Manufacturing 102:273–296. doi: 10.1016/j.compositesa.2017.07.019

Yang M, Koutsos V, Zaiser M (2005) Interactions between Polymers and Carbon Nanotubes: A Molecular Dynamics Study. The Journal of Physical Chemistry B 109:10009–10014. doi: 10.1021/jp0442403

Yang Y (2002) Methods study on dispersion of fibers in CFRC. Cement and Concrete Research 32:747–750

Yu M-F, Files BS, Arepalli S, Ruoff RS (2000a) Tensile loading of ropes of single wall carbon nanotubes and their mechanical properties. Physical review letters 84:5552

Yu M-F, Lourie O, Dyer MJ, et al (2000b) Strength and breaking mechanism of multiwalled carbon nanotubes under tensile load. Science 287:637–640

Yu X, Kwon E (2009) A carbon nanotube/cement composite with piezoresistive properties. Smart Materials and Structures 18:055010. doi: 10.1088/0964-1726/18/5/055010

Zandiatashbar A, Lee G-H, An SJ, et al (2014) Effect of defects on the intrinsic strength and stiffness of graphene. Nature Communications 5:3186

Zeiger M, Jäckel N, Mochalin VN, Presser V (2016) Review: carbon onions for electrochemical energy storage. J Mater Chem A 4:3172–3196. doi: 10.1039/C5TA08295A

Zhang G, Sun S, Yang D, et al (2008) The surface analytical characterization of carbon fibers functionalized by H2SO4/HNO3 treatment. Carbon 46:196–205. doi: 10.1016/j.carbon.2007.11.002

Zhang J, Zou H, Qing Q, et al (2003) Effect of Chemical Oxidation on the Structure of Single-Walled Carbon Nanotubes. The Journal of Physical Chemistry B 107:3712–3718. doi: 10.1021/jp027500u

Zhang Y, Tan Y-W, Stormer HL, Kim P (2005) Experimental observation of the quantum Hall effect and Berry's phase in graphene. Nature 438:201

Ziegler KJ, Gu Z, Peng H, et al (2005) Controlled Oxidative Cutting of Single-Walled Carbon Nanotubes. Journal of the American Chemical Society 127:1541–1547. doi: 10.1021/ja044537e

High Performance Carbon Fibers - National Historic Chemical Landmark. In: American Chemical Society. http://www.acs.org/content/acs/en/education/whatischemistry/landmarks/carbonfibers.html. Accessed 3 May 2016